

SENSORS & TRANSDUCERS

ISSN 1726-5479

vol. 218

12/17



Wireless Sensor Networks (WSN)

Sensors & Transducers

**International Official Open Access Journal of the
International Frequency Sensor Association (IFSA)
Devoted to Research and Development
of Sensors and Transducers**

Volume 218, Issue 12, December 2017

Editor-in-Chief

Prof., Dr. Sergey Y. YURISH



IFSA Publishing: Barcelona • Toronto

Sensors & Transducers is an open access journal which means that all content (article by article) is freely available without charge to the user or his/her institution. Users are allowed to read, download, copy, distribute, print, search, or link to the full texts of the articles, or use them for any other lawful purpose, without asking prior permission from the publisher or the author. This is in accordance with the BOAI definition of open access. Authors who publish articles in *Sensors & Transducers* journal retain the copyrights of their articles. The *Sensors & Transducers* journal operates under the Creative Commons License CC-BY.

Notice: No responsibility is assumed by the Publisher for any injury and/or damage to persons or property as a matter of products liability, negligence or otherwise, or from any use or operation of any methods, products, instructions or ideas contained in the material herein.

Published by International Frequency Sensor Association (IFSA) Publishing. Printed in the USA.





Editors-in-Chief: Professor, Dr. Sergey Y. Yurish, tel.: +34 696067716, e-mail: editor@sensorsportal.com

Editors for Western Europe

Meijer, Gerard C.M., Delft Univ. of Technology, The Netherlands
Ferrari, Vittorio, Università di Brescia, Italy
Mescheder, Ulrich, Univ. of Applied Sciences, Furtwangen, Germany

Editor for Eastern Europe

Sachenko, Anatoly, Ternopil National Economic University, Ukraine

Editors for North America

Katz, Evgeny, Clarkson University, USA
Datskos, Panos G., Oak Ridge National Laboratory, USA
Fabien, J. Josse, Marquette University, USA

Editor for Africa

Maki K., Habib, American University in Cairo, Egypt

Editors South America

Costa-Felix, Rodrigo, Inmetro, Brazil
Walsole de Reca, Noemi Elisabeth, CINSO-CITEDEF
UNIDEF (MINDEF-CONICET), Argentina

Editors for Asia

Ohyama, Shinji, Tokyo Institute of Technology, Japan
Zhengbing, Hu, Huazhong Univ. of Science and Technol., China
Li, Gongfa, Wuhan Univ. of Science and Technology, China

Editor for Asia-Pacific

Mukhopadhyay, Subhas, Massey University, New Zealand

Editorial Board

Abdul Rahim, Ruzairi, Universiti Teknologi, Malaysia
Abramchuk, George, Measur. Tech. & Advanced Applications, Canada
Aluri, Geetha S., Globalfoundries, USA
Ascoli, Giorgio, George Mason University, USA
Atalay, Selcuk, Inonu University, Turkey
Atghiaee, Ahmad, University of Tehran, Iran
Augutis, Vygtantas, Kaunas University of Technology, Lithuania
Ayesh, Aladdin, De Montfort University, UK
Baliga, Shankar, B., General Monitors, USA
Barlingay, Ravindra, Larsen & Toubro - Technology Services, India
Basu, Sukumar, Jadavpur University, India
Booranawong, Apidet, Prince of Songkla University, Thailand
Bousbia-Salah, Mounir, University of Annaba, Algeria
Bouvet, Marcel, University of Burgundy, France
Campanella, Luigi, University La Sapienza, Italy
Carvalho, Vitor, Minho University, Portugal
Changhai, Ru, Harbin Engineering University, China
Chen, Wei, Hefei University of Technology, China
Cheng-Ta, Chiang, National Chia-Yi University, Taiwan
Cherstvy, Andrey, University of Potsdam, Germany
Chung, Wen-Yaw, Chung Yuan Christian University, Taiwan
Cortes, Camilo A., Universidad Nacional de Colombia, Colombia
D'Amico, Arnaldo, Università di Tor Vergata, Italy
De Stefano, Luca, Institute for Microelectronics and Microsystem, Italy
Ding, Jianning, Changzhou University, China
Djordjevic, Alexandar, City University of Hong Kong, Hong Kong
Donato, Nicola, University of Messina, Italy
Dong, Feng, Tianjin University, China
Erkmen, Aydan M., Middle East Technical University, Turkey
Fezari, Mohamed, Badji Mokhtar Annaba University, Algeria
Gaura, Elena, Coventry University, UK
Gole, James, Georgia Institute of Technology, USA
Gong, Hao, National University of Singapore, Singapore
Gonzalez de la Rosa, Juan Jose, University of Cadiz, Spain
Goswami, Amarjyoti, Kaziranga University, India
Guillet, Bruno, University of Caen, France
Hadjiloucas, Sillas, The University of Reading, UK
Hao, Shiyang, Michigan State University, USA
Hui, David, University of New Orleans, USA
Jaffrezic-Renault, Nicole, Claude Bernard University Lyon 1, France
Jamil, Mohammad, Qatar University, Qatar
Kaniusas, Eugenijus, Vienna University of Technology, Austria
Kim, Min Young, Kyungpook National University, Korea
Kumar, Arun, University of Delaware, USA
Lay-Ekuakille, Aime, University of Lecce, Italy
Li, Fengyuan, HARMAN International, USA
Li, Jingsong, Anhui University, China
Li, Si, GE Global Research Center, USA
Lin, Paul, Cleveland State University, USA
Liu, Aihua, Chinese Academy of Sciences, China
Liu, Chenglian, Long Yan University, China
Liu, Fei, City College of New York, USA
Mahadi, Muhammad, University Tun Hussein Onn Malaysia, Malaysia

Mansor, Muhammad Naufal, University Malaysia Perlis, Malaysia
Marquez, Alfredo, Centro de Investigacion en Materiales Avanzados, Mexico
Mishra, Vivekanand, National Institute of Technology, India
Moghavvemi, Mahmoud, University of Malaya, Malaysia
Morello, Rosario, University "Mediterranea" of Reggio Calabria, Italy
Mulla, Imtiaz Sirajuddin, National Chemical Laboratory, Pune, India
Nabok, Aleksey, Sheffield Hallam University, UK
Neshkova, Milka, Bulgarian Academy of Sciences, Bulgaria
Passaro, Vittorio M. N., Politecnico di Bari, Italy
Patil, Devidas Ramrao, R. L. College, Parola, India
Penza, Michele, ENEA, Italy
Pereira, Jose Miguel, Instituto Politecnico de Seteбал, Portugal
Pillarsetti, Anand, Sensata Technologies Inc, USA
Pogacnik, Lea, University of Ljubljana, Slovenia
Pullini, Daniele, Centro Ricerche FIAT, Italy
Qiu, Liang, Avago Technologies, USA
Reig, Candid, University of Valencia, Spain
Restivo, Maria Teresa, University of Porto, Portugal
Rodríguez Martínez, Angel, Universidad Politécnica de Cataluña, Spain
Sadana, Ajit, University of Mississippi, USA
Sadeghian Marnani, Hamed, TU Delft, The Netherlands
Sapozhnikova, Ksenia, D. I. Mendeleyev Institute for Metrology, Russia
Singhal, Subodh Kumar, National Physical Laboratory, India
Shah, Kriyang, La Trobe University, Australia
Shi, Wendian, California Institute of Technology, USA
Shmaliy, Yuriy, Guanajuato University, Mexico
Song, Xu, An Yang Normal University, China
Srivastava, Arvind K., Systron Donner Inertial, USA
Stefanescu, Dan Mihai, Romanian Measurement Society, Romania
Sumridetchajorn, Sarun, Nat. Electr. & Comp. Tech. Center, Thailand
Sun, Zhiqiang, Central South University, China
Sysoev, Victor, Saratov State Technical University, Russia
Thirunavukkarasu, I., Manipal University Karnataka, India
Thomas, Sadiq, Heriot Watt University, Edinburgh, UK
Tian, Lei, Xidian University, China
Tianxing, Chu, Research Center for Surveying & Mapping, Beijing, China
Vanga, Kumar L., ePack, Inc., USA
Vazquez, Carmen, Universidad Carlos III Madrid, Spain
Wang, Jiangping, Xian Shiyou University, China
Wang, Peng, Qualcomm Technologies, USA
Wang, Zongbo, University of Kansas, USA
Xu, Han, Measurement Specialties, Inc., USA
Xu, Weihe, Brookhaven National Lab, USA
Xue, Ning, Agiltron, Inc., USA
Yang, Dongfang, National Research Council, Canada
Yang, Shuang-Hua, Loughborough University, UK
Yaping Dan, Harvard University, USA
Yue, Xiao-Guang, Shanxi University of Chinese Traditional Medicine, China
Xiao-Guang, Yue, Wuhan University of Technology, China
Zakaria, Zulkarnay, University Malaysia Perlis, Malaysia
Zhang, Weiping, Shanghai Jiao Tong University, China
Zhang, Wenming, Shanghai Jiao Tong University, China
Zhang, Yudong, Nanjing Normal University China

Contents

Volume 218
Issue 12
December 2017

www.sensorsportal.com

ISSN 2306-8515
e-ISSN 1726-5479

Research Articles

Robust Network Models for Mobility Analysis: Validation from an Unstable Mobility in a Maritime Setting <i>Ik-Hyun Youn, Abhilash Patella and Hesham H. Ali</i>	1
A Novel Routing Fault Tolerant Reliable Protocol for Wireless Sensor Networks <i>Islam Moursy, Mohamed Elderini and Magdy Ahmed</i>	10
A Modular Wireless Sensor Platform with a Sensor Identification Scheme <i>Yi-Jie Hsieh, Chih-Chyau Yang, Yi-Jun Liu, Wei-Lin Lai, Chien-Ming Wu and Chun-Ming Huang</i>	19
Repeater Protocol to Extend Signal Coverage <i>Eloísa Alexandre Nielsen Matthiesen, Omar Carvalho Branquinho, Guilherme Lopes da Silva and Paulo Cardieri</i>	27
A Fine-Grained Visible Light Communication Position Detection System <i>M. Vieira, M. A. Vieira, P. Louro, A. Fantoni and P. Vieira</i>	32
Vehicle-to-Vehicle and Infrastructure-to-Vehicle Communication in the Visible Range <i>M. A. Vieira, M. Vieira, P. Vieira, P. Louro</i>	40
A Wireless Sensor Networks Management Strategy for the Small and Medium Sized Manufacturing Enterprises <i>Pedro Chaves, Omar Branquinho and Fabiano Fruett</i>	49

Authors are encouraged to submit article in MS Word (doc) and Acrobat (pdf) formats
by e-mail: editor@sensorsportal.com. Please visit journal's webpage with preparation instructions:
<http://www.sensorsportal.com/HTML/DIGEST/Submission.htm>

Robust Network Models for Mobility Analysis: Validation from an Unstable Mobility in a Maritime Setting

Ik-Hyun Youn, Abhilash Patella and * Hesham H. Ali

College of Information Science and Technology, Omaha, NE 68182, USA

Tel.: +1 402 554 2380, fax: +1 402 554 3400

E-mail: hali@unomaha.edu

Received: 10 November 2017 /Accepted: 10 December 2017 /Published: 29 December 2017

Abstract: The importance of human mobility in maintaining physical health is of emerging interest in research and practice. Technological advances in wearable technology enable us to monitor human mobility in out-of-laboratory settings. Although a large amount of human mobility data is available from wearable sensors, there is a lack of systematic methodologies for extracting useful knowledge on human mobility from the collected data. The objective description of the different status of mobility patterns to interpret different physical health levels especially remains challenging. In this paper, robust network modeling from our preliminary study is validated in a real-world scenario with stable and unstable mobility conditions. The models based on population analysis utilize mobility data and extract distinctive mobility characteristics. Correlation networks and population-based analysis are utilized to efficiently examine the natural variability of human movement. Results demonstrate that the proposed robust network models identify mobility pattern changes in maritime conditions.

Keywords: Mobility parameters, Population-based analysis, Physical health assessment.

1. Introduction

Human mobility is fundamental to the physical activity required for maintaining physical health. A substantial number of studies have recognized the importance of human mobility in health [1-3]. Moreover, the impact of mobility on a number of medical and physical properties has been established in several studies [ref 4-6]. For example, variability associated with muscle fatigue, joint problems, or neurological problems has been correlated to mobility characteristics, and mobility has been used as an efficient indicator of such conditions in other studies [7-8]. Capturing irregular mobility characteristics by performing a mobility analysis is commonly used to identify mobility impairment. Falling risk, for instance, has been widely monitored by the variability of mobility patterns in the elderly, and declining

mobility intensity has been determined by balance disorders during mobility [9-10]. These studies have typically used multiple wearable sensors. Recent research has tried to utilize mobility data from wearable sensors to make informative decisions on inclusively addressing the multidimensional characteristics of mobility [11-12]. However, the importance of methodology in mobility analysis has not been significantly considered, and there is a lack of data analytics methods that systematically analyze mobility characteristics and interpret the results from clinical perspectives [17].

This problem motivated our preliminary study [24], which employed robust network modeling methodology to analyze human mobility patterns. The proposed model in the preliminary study focused on population-based analysis instead of individual

granularity to infer useful decisions by considering individual patterns of the population characteristics.

Robust network models consider the natural variability of mobility. Variability is a crucial aspect of human movement that should be considered in mobility analysis [13]. However, the variability of mobility, including internal and external conditions, is difficult to assess by deterministic approaches such as Manhattan and Euclidean distance methods. Classification of mobility patterns into finite numbers of categories could be appropriate and useful for a more comprehensive analysis of mobility variations.

Robust models also provide robust decision criteria when determining clinically problematic mobility statuses. The decision criteria would be flexibly achieved if individual patterns could be compared to similar population characteristics. In our preliminary work [24], correlation analysis was selected to obtain population-based criteria. Correlation analysis, as one of several population-based analytics, takes into account the variation of mobility patterns for analyzing individuals' mobility patterns, based on their characteristics as related to a given population. Correlation networks measure the statistical relationships among items. Using correlation analysis, embedded associations among subject mobility patterns can be observed. Although correlation analysis cannot establish a causal relationship between mobility patterns, it can compare each mobility pattern with the others. When the association among different mobility signatures is interpreted, it is important to consider characteristics of identified groups with various descriptive and clinical information.

This paper introduces and describes the methodology to build robust network models for analysis, including three different ways of determining weights among nodes. First, pattern-based networks are used when multiple, distinctive mobility conditions are present. The Pearson correlation coefficient is used to define weights among elements in the correlation network. Second, the magnitude-based option is primarily utilized when only a single mobility condition is available when monitoring mobility patterns. The difference of magnitude is used to determine weights on the edges of the network. Lastly, the hybrid option is where both magnitude and correlation are sequentially applied to examine distinctive differences between clusters in the network. The last option is suggested when mobility data are obtained where mobility conditions are not clearly defined or reported.

The following chapters are organized as follows: Section II provides descriptive information of the three modeling methods including construction of the networks. Section III presents the experimental results of applying the proposed modeling methods. Simulated mobility data are used to demonstrate the conceptual feasibility of the proposed models and results from the validation study using collected mobility data. The last section concludes with contributions and limitations.

2. Robust Network Modeling

Three different weight determination methods are available to construct robust networks. Appropriate selection of the network modeling method is based on the nature of the mobility conditions and parameters when collecting mobility data.

2.1. Pattern-Based Mobility Model

Nodes in the network represent individual subjects, and the connecting edges, i.e., correlation coefficients, among nodes represent the significance of associations in mobility. Correlation networks are implemented using the genome data in bioinformatics research [8]. After determining specific thresholds, parts of the nodes are shown in clusters in the network. The highly connected nodes of the network have significant association or similarity in terms of mobility parameters used for network construction.

This pattern-based network model is constructed using the patterns of the mobility parameter values obtained from the individuals. The correlation coefficient calculated for all pairs of individuals ranges on a scale from negative one to positive one. A coefficient of negative one means total opposite directional correlation, and a coefficient of positive one means total positive correlation. In practice, a coefficient greater than 0.75 or less than -0.75 is considered a significant linear correlation. The significance of a correlation coefficient between any two individual pairs is estimated by the statistical significance parameter (p). A p value of less than 0.05 is a significant correlation. Additionally, the pattern-based model enables us to flexibly apply different sampling granularity such as minutes, hours, and days. Higher granularity obtained by integrating mobility data over more extended time periods improves the generalization of results, whereas utilizing precise time periods can provide better sensitivity to describe different mobility patterns.

Pattern-based mobility network modeling can be applied to mobility data from different conditions. The different mobility conditions include physical mobility conditions such as hard, soft, and unstable mobility platforms and different mobility contexts such as before and after injury, day and night, and during and after work. Pattern-based models can be used in a variety of mobility conditions to analyze the changes and characteristics of mobility by visually illustrating outcomes. Notably, it is strongly suggested that pattern-based mobility models be applied if the mobility data are collected from different mobility conditions. The robust network will be more efficient when it is built using a pattern-based mobility model when the mobility data are obtained from different environments.

2.2. Magnitude-Based Mobility Model

Nodes in the magnitude-based mobility networks represent individual subjects, and the nodes are connected by edges among any pair of two individuals using weighted magnitude difference (WMD). Table 1 illustrates simulated sample data based on the magnitude of a mobility parameter during four consecutive days of mobility monitoring. Edges are connected among nodes whose weighted magnitude differences are significant between any pair of two individuals. The significance of weighted magnitude difference can be flexibly defined based on the purpose of mobility analysis. Equation (1) is used to estimate WMD between two subjects, A and B, as follows:

$$\Delta WMD_{A-B} = |M_A - M_B| / 0.5 (M_A + M_B) \times 100 \quad (1)$$

For example, the first subject took 300 and 3000 steps in two consecutive days, respectively, and the second subject took 3000 and 300 steps during the same days. The pattern-based model considers a weight for this two- subject pairing as a high negative correlation pair. However, the number (i.e.,

magnitude) of steps taken by these two subjects is also significant to explain the association of the pair. The two subjects are similar in mobility except that they have different mobility properties on these two days. The distinctive pattern of the magnitude difference is efficient to describe the similarity between the two, while avoiding elimination of the magnitude discrepancies.

The magnitude-based mobility model is recommended when the mobility data are collected under similar mobility environments. Since the magnitude-based model is not able to consider differences from different observations, a mobility experiment or monitoring is required to be performed under the equivalent condition. Then, WMD among any pair of individuals is calculated and represented as the edge in robust networks.

With the magnitude-based model, for example, robust correlational networks for concurrent weeks to observe mobility change can be analyzed. The method also can be extended to assist in preventive analysis of physical health through the correlational networks. Adjustment of the level of aggregation of the networks produces different cluster formations and weights of networks.

Table 1. Sample Mobility Data Representing 4-Consecutive Days of Mobility Level (left) and an Edge Weight Table (right) Based on Weighted Magnitude Difference.

	Sub1	Sub2	...	Sub 30	Edge No.	Subject	Subject	Magnitude Difference
Day 1	42.3	84.0	1	Subj 1	Subj 2	0.17
Day 2	80.1	61.6	2	Subj 1	Subj 3	0.08
Day 3	28.1	89.4
Day 4	46.3	47.5	434	Subj 28	Subj 29	0.23
Mean	49.2	70.6	435	Subj 29	Subj 30	0.15

2.3. Hybrid Mobility Model

The hybrid mobility model sequentially applies both pattern- and magnitude-based mobility models. Nodes in the hybrid network also represent individuals, and the connecting edges among nodes represent the significance of associations in mobility using both correlation coefficients and WMD. Both the pattern- and magnitude-based mobility models require conditions of mobility data when constructing the correlational networks. Although the conditions of mobility are crucial, available or existing mobility data are not always collected under well-controlled mobility conditions. To address this common limitation in collecting mobility data, both magnitude- and pattern-based networks models are applied to construct correlation networks.

In hybrid-based mobility, due to the insufficiency of complete information of mobility conditions, both the correlational coefficient and WMD are utilized to build the correlational network. The correlation networks are first built using the correlation coefficient between pairs of any of two individuals to connect the edges. When clusters are available, WMD between the subjects is estimated, and the subjects in that specific cluster are again clustered based on WMD [13-14]. The sequence between two models can be applied in another way by applying WMD followed by the correlation coefficient. Conceptually, the hybrid model has similarity to the overlying in communication networks [18]. Fig. 1 illustrates the hybrid mobility model construction with comparisons of before and after the clustering process.

We believe that the hybrid model can be applied when properties of the mobility samples collected are

not well known. By considering both the patterns and the magnitude, the resultant correlational network has the most important edges, and the model can include all the vital mobility characteristics [16]. The pattern or the weighted magnitude difference between the subjects in the two sets of clusters should be

significant enough to improve the model by overlaying. Otherwise, this may result in minimal information gain from the correlational network. Table 2 summarizes important characteristics of the three models.

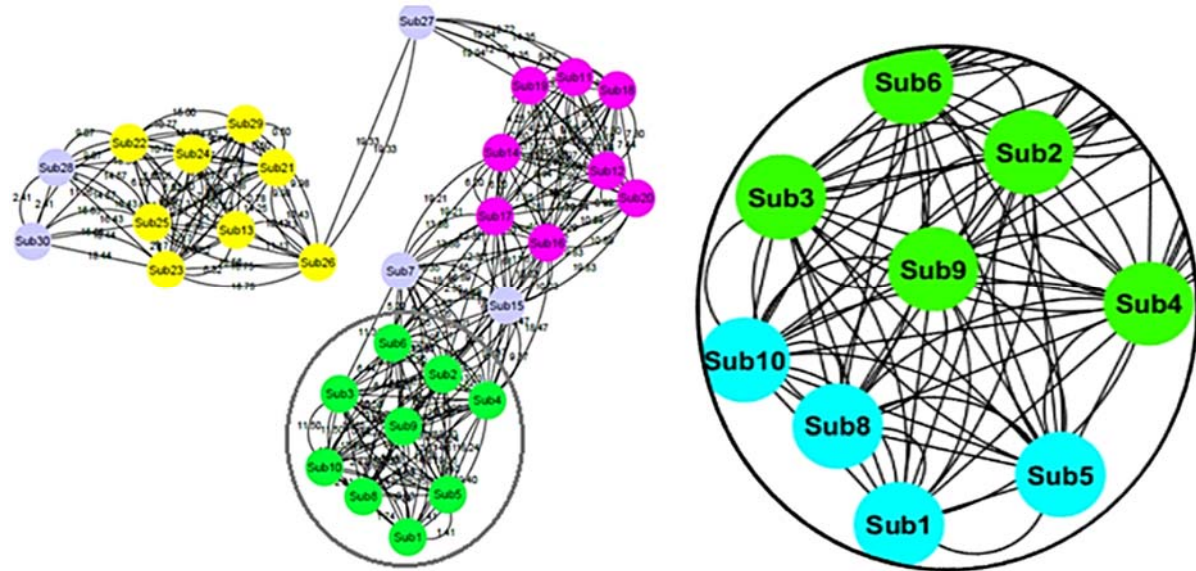


Fig. 1. Hybrid network by pattern-based clustering (left) and by magnitude-based clustering (right).

Table 2. Summary of Three Robust Network Modeling Methods.

	Pattern-based Mobility Model	Magnitude-based Mobility Model	Hybrid-based Mobility Model
Edge weight definition	Correlation coefficient between nodes	Magnitude difference between nodes	Combinatorial meaning
Mobility conditions	Need to control each experimental condition	Same experimental condition is fine	Need to control experimental condition
Treatment in Experiment	Heterogeneous experimental conditions	Homogeneous experimental condition	Heterogeneous experimental conditions
Sample size effect	Larger sample size is better to get robust correlation coefficient	Will not affect the robustness of network	Partial effect within clusters
Advantages	Robust population-oriented analysis	Comprehensive correlation analysis	Enables conducting an in-depth mobility mining
Disadvantages	Difficult to control heterogeneous experimental settings	Mobility characteristics can be excessively aggregated	Need to have heterogeneous experimental conditions

3. Experimental Study

In this section, two network models are constructed by using simulated and collected mobility data. The simulated mobility data are used to examine feasibility of the robust network model, and collected mobility data are applied to validate the model in stable and unstable mobility settings.

3.1. Feasibility Using Simulated Mobility Data

The advantages of using the correlation networks for constructing and analyzing human mobility networks are described in this section. Wearable sensor-based continuous mobility monitoring provides researchers and clinicians a better understanding of free-living mobility characteristics. Wearable

accelerometers are wireless devices that capture unidimensional or multidimensional accelerometer data. A large amount of emerging research has been introduced to improve the efficiency and longevity of human mobility data processing.

To examine feasibility of the robust network models, simulated mobility data based on a realistic scenario are used. The process to construct the robust network additionally helps to improve reproductively of the robust network models by demonstrating how the correlation network can be used to analyze mobility data in a specific case study. In the simulated scenario, we consider a mobility monitoring of thirty nurses in a hospital setting, and robust correlation networks are constructed using the magnitude-based model.

The primary goal of this experiment is to examine associations by the magnitude of a mobility parameter among different subjects. The second goal is to illustrate how the cluster formation changes during different sampling periods. The first samples of different subjects are generated using the normal distribution with a mean value of 500 and 15.86 percent of a coefficient of variance according to the 68–95–99.7 rule [19].

To produce different mobility patterns across time, different mobility level reduction rates are applied to the simulated data. The first ten nurses exhibit a decrease in mobility by ten percent for every sampling period, the next ten nurses by twenty percent, and the last nurses by thirty percent. Simulated mobility data are shown in Table 3.

Table 3. Simulated Mobility Data Representing Mobility Levels during an 8-hour shift of Thirty Nurses.

	Sub1	Sub2	...	Sub30
Work start	553.78	384.85
2nd hours	498.40	269.40
4th hours	448.56	188.58
6th hours	403.71	132.01
Work end	363.34	92.40

Since we assume that simulated mobility data are collected in the same mobility environment including time and spatial conditions, the magnitude-based mobility model is appropriate to construct correlational networks. WMD among the thirty nurses is calculated for periodic time intervals (see Table 3). By applying a threshold of WMD of 20 percent, the networks are constructed as shown in Fig. 2, Fig. 3, Fig. 4 and Fig. 5. The first ten subjects are represented as green, the next ten as pink, and the last ten as red.

The robust network shown in Fig. 2 shows that all the nurses show similar mobility at the initial time period. After constructing the next robust network at the second-time period in Fig. 3, a subset of nurses (i.e., nurse-13, nurse-28 and nurse-30) belongs to a distinctive cluster in the network.

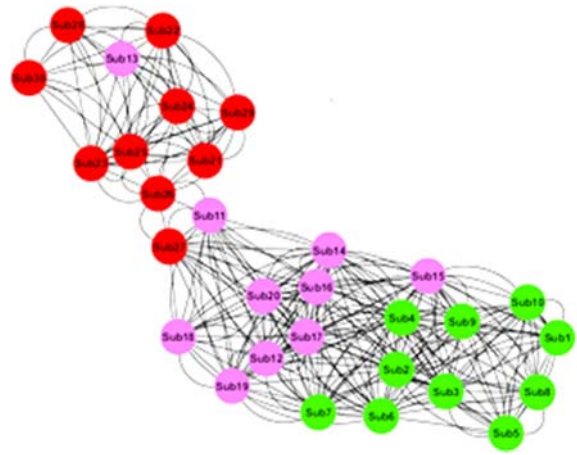


Fig. 2. Mobility network (work start).

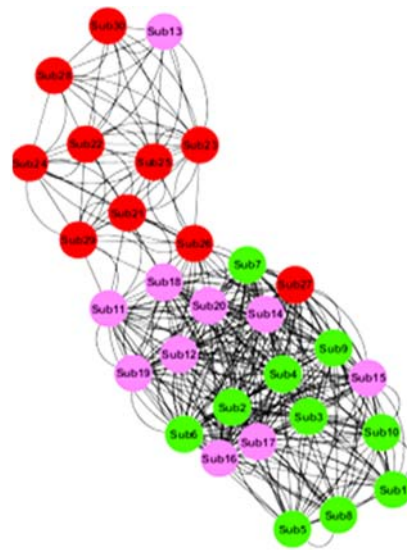


Fig. 3. Mobility network (2-hour shift).

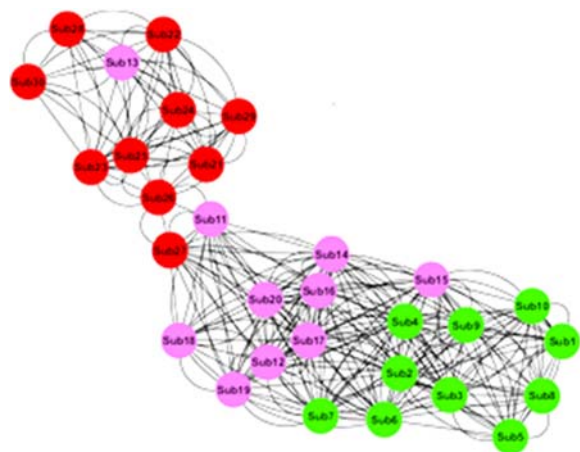


Fig. 4. Mobility network (6-hour shift).

By observing labels and node colors of the nurses in clusters in Fig. 4, the different mobility decline rates of the three groups of nurses are more clearly separated into two clusters as time progresses.

The robust network at the last periodic time interval in Fig. 5 efficiently describes the intended mobility differences by providing three distinctive clusters in the robust network. Each cluster is, finally, analyzed by given detailed mobility data to infer the underlying causes of the separation in the networks. For example, in Fig. 5, a cluster containing nurse-1 through nurse-10, shown in green, shows the higher mobility. The remaining two clusters display a lower mobility. The cluster with red color nodes shows the least mobility. Some subjects like nurse-7, nurse-15, nurse-27, nurse-28 and nurse-30 display an erratic mobility, because the nurse group contains a reasonable range of outliers outside of the normal distribution used to simulate mobility data.

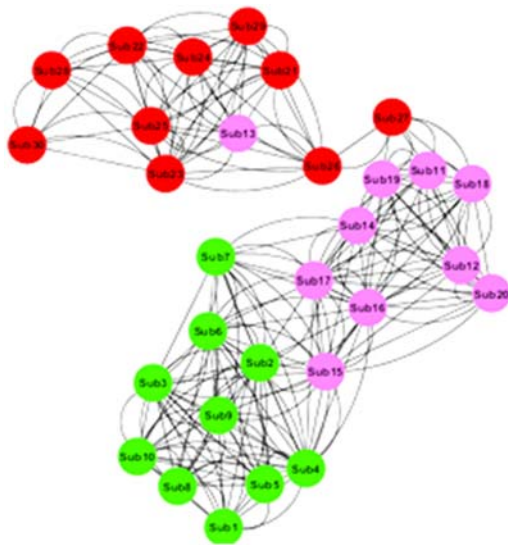


Fig. 5. Mobility network (work end).

In summary, mobility trend changes over time are efficiently described by using simulated mobility data. The robust networks along with time progression reveal that three different rates of mobility decrease as distinctive mobility characteristics of the group, although initial mobility levels of all thirty nurses were similar. Additionally, a few nodes showed an interesting transit among clusters that represent the natural variability of mobility patterns. Finally, two useful thresholds were identified to classify all nurses into active, moderate, and inactive mobility groups based on the population of nurses as a whole. These findings strongly support the proposed robust network analysis as an efficient population-based mobility analysis method.

3.2. Validation using Collected Mobility Data

The robust network models are applied to collected mobility data using wearable accelerometers in both stable and unstable mobility settings. Since the mobility data were collected in two different mobility

conditions, the pattern-based mobility model was selected in this experimental study.

Data Collection. In total, 14 healthy college students between the ages of 22 and 26 years participated in the validation study. Table 4 shows the characteristics of the subjects. In the first session of the experiment, subjects performed functional balance tests including the Timed-up-and-Go test (TUG), Romberg Tandem test (RTT), and Functional Reach Test (FRT) to evaluate the balance function of each participant. The detailed information of the functional balance test is shown in Table 5. The second session for mobility data collection was performed on one of two training ships at Mokpo National Maritime University in South Korea. During the second session, acceleration data during mobility were collected using two accelerometers. These accelerometers were placed right above the lateral malleoli using elastic straps. All 14 participants walked in a stable condition when the ship was in the harbor, and walked in an unstable condition during a sea voyage. To collect acceleration data, participants wore three small and lightweight 3-axis accelerometers, called Shimmer3 [20]. Collected data were processed to extract appropriate mobility parameters from the raw acceleration.

Table 4. Descriptive Data of Participants for Stable and Unstable Mobility Experiments.

Characteristics	Descriptive data (Mean \pm SD)
<i>N</i>	14
Female / male	2/12
Age (yrs)	23.2 \pm 1.6
BMI (kg/m ²)	24.9 \pm 1.8
Height (cm)	173.7 \pm 6.7
Weight (kg)	73.6 \pm 8.8

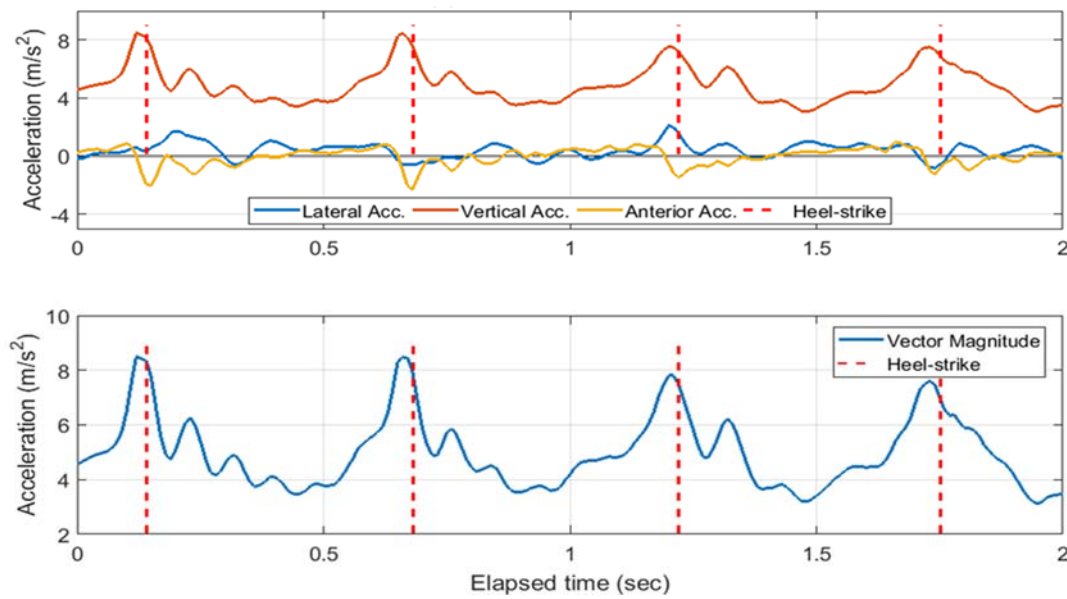
Mobility Parameter Extraction. To extract appropriate mobility parameters, the continuous acceleration data were first fragmented into acceleration data of individual steps. This process is commonly called step recognition, and peaks of acceleration from heel-strike actions are typically detected to recognize steps. The recognized steps, for example, are illustrated in Fig. 6 with red vertical dotted lines around peaks of vertical acceleration.

Once the raw acceleration was fragmented, the Mean of Vector Magnitude (MVM) and Symmetry of Vector Magnitude (SVM) were extracted as two key mobility parameters for constructing robust correlational networks. The vector magnitude of acceleration is estimated using Equation (2) below:

$$VM = \sqrt{(ACCx^2 + ACCy^2 + CCAz^2)} \quad (2)$$

Table 5. Summary of Three Functional Balance Tests.

Functional Balance Test	Description	Expected Outcome
Timed-Up-and-Go Test (TUG)	Test for assessing functional mobility that requires both static and dynamic balance control [21]	Higher functioning tends to achieve a shorter time period
Romberg Tandem Test (RTT)	Test to examine neurological balance functioning [22]	Higher functioning tends to maintain a longer time period
Functional Reach Test (FRT)	Test to assess of functional balance by measuring reach forward beyond arm's length [23]	Distance of arm position between standing and leaning forward

**Fig. 6.** Collected 3-D acceleration data (up) and step recognition results (down).

Step recognition and mobility parameter extraction algorithms were developed in the custom MATLAB 9.1 (Mathworks, Natick, MA) environment.

Correlation Network-based Analysis. Since the mobility data were collected in different mobility conditions (i.e., stable and unstable mobility platforms), pattern-based correlation networks have been applied to examine associations of mobility patterns between stable and unstable mobility environments.

Nodes in the sea mobility networks represent individual subjects and edges connect associated nodes based on correlation coefficients of four observations of mobility data. The significance of correlation coefficients between any two individual pairs was carefully examined by the statistical significance parameter (p). A value of statistical significance less than 0.05 was considered a significant correlation. Coefficient thresholds greater than 0.75 or less than -0.75 were considered significant linear correlation. Fig. 7 illustrates pattern-based correlation networks using MVM. MVM is an

efficient mobility parameter to identify distinctive mobility characteristics between stable and unstable conditions. After constructing the robust network using MVM in Fig. 7, a subset of participants (i.e., H-4, H-5, H-8, and H-13) fall into an inappropriate cluster (i.e., stable mobility although unstable mobility data were given). The nodes of four participants are illustrated by red dotted circles. The balance functional test records of the participants show that the average of TUG and FRT results of the four subjects was 24.4 % and 18.3 %, respectively, below the average of all 14 participants.

Fig. 8 illustrates pattern-based correlation networks using SVM. SVM also efficiently represents the different mobility conditions of stable and unstable conditions. After constructing the robust network using SVM in Fig. 8, the same subset of participants (i.e., Node ID: H-4, H-5, H-8, and H-13) belongs to an inappropriate cluster. Based on the two robust networks, MVM better describes notable mobility differences compared to SMV in terms of mobility parameter efficiency.

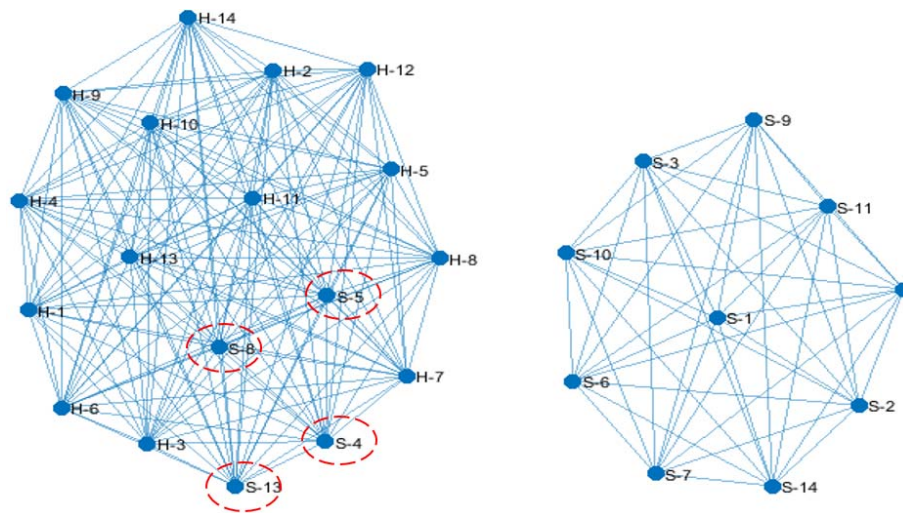


Fig. 7. Pattern-based correlation networks clusters of a stable mobility (left) and an unstable mobility (right) by using MVM.

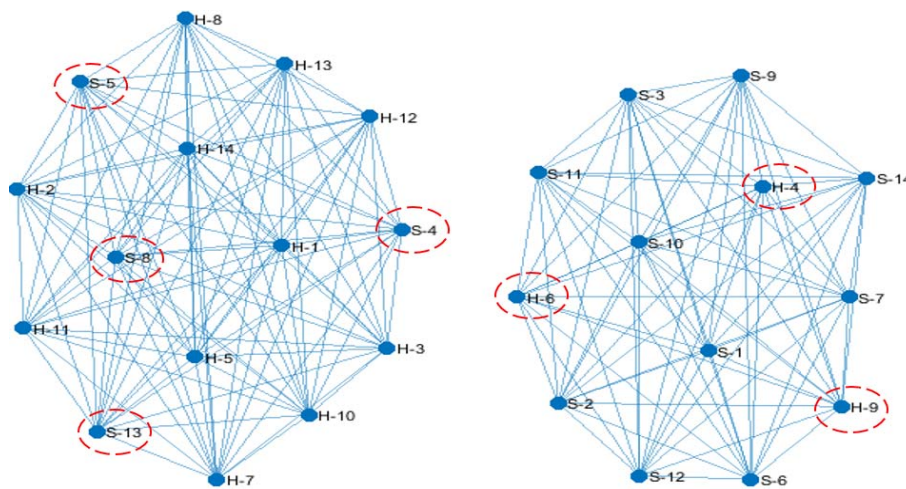


Fig. 8. Pattern-based correlation networks clusters of a stable mobility (left) and an unstable mobility (right) by using SVM.

4. Conclusions

There has been a lack of mobility data analysis methodologies while a large amount of human mobility data is available through wearable sensors. In this work, robust network modeling from our preliminary study has been validated in a real-world scenario such as stable and unstable mobility conditions. The robust models that are based on population analysis utilize mobility data and extract distinctive mobility characteristics for robust mobility characteristic descriptions. The use of correlation networks in relation to population-based analysis efficiently considers the natural variability of human movement. Results demonstrate that the proposed robust network models enable the identification of mobility pattern changes in a real-world scenario. Furthermore, distinctive clusters efficiently recognize distinctive mobility characteristics associated with physical health levels by assisting in the interpretation of results from a clinical perspective.

References

- [1]. D. E. Warburton, C. W. Nicol, S. S. Bredin, Health benefits of physical activity: The evidence, *CMAJ: Canadian Medical Association Journal, Journal De l'Association Medicale Canadienne*, Vol. 174, No. 6, 2006, pp. 801-809.
- [2]. W. W. Spirduso, K. L. Francis, P. G. MacRae, *Physical dimensions of aging*, 1995.
- [3]. M. E. Nelson, W. J. Rejeski, S. N. Blair, P. W. Duncan, J. O. Judge, A. C. King, Physical activity and public health in older adults: Recommendation from the American college of sports medicine and the american heart association, *Circulation*, Vol. 116, No. 9, 2007, pp. 1094-1105.
- [4]. Nicol C. W., D. E. Warburton, Bredin S. S., Health benefits of physical activity, *Journal Association Medicale Canadienne*, Vol. 174, No. 6, 2006, pp. 801-809.
- [5]. Pahor M., Guralnik J. M., Ambrosius W. T., Blair S., Bonds D. E., Church T. S., Groessl E. J., Effect of structured physical activity on prevention of major mobility disability in older adults: The LIFE study

- randomized clinical trial, *Jama*, Vol. 311, No. 23, 2014, pp. 2387-2396.
- [6]. L. Piwek, D. A. Ellis, S. Andrews, A. Joinson, The rise of consumer health wearables: Promises and barriers, *PLoS Medicine*, Vol. 13, No. 2, 2014, e1001953.
- [7]. L. I. Iezzoni, E. P. McCarthy, R. B. Davis, H. Siebens, Mobility difficulties are not only a problem of old age, *Journal of General Internal Medicine*, Vol. 16, No. 4, 2001, pp. 235-243.
- [8]. I. H. Youn, D. Khazanchi, J. H. Youn, K. C. Siu, Multidimensional Mobility Metric for Continuous Gait Monitoring using a Single Accelerometer, in *Proceedings of the Int. Conference Health Informatics and Medical Systems (HIMS'16)*, 2016, pp. 3-8.
- [9]. N. Cortes, J. Onate, S. Morrison, Differential effects of fatigue on movement variability, *Gait & Posture*, Vol. 39, No. 3, 2014, pp. 888-893.
- [10]. N. Stergiou, L. M. Decker, Human movement variability, nonlinear dynamics, and pathology: is there a connection ?, *Human Movement Science*, Vol. 30, No. 5, 2011, pp. 869-888.
- [11]. R. Gravina, P. Alinia, H. Ghasemzadeh, G. Fortino, Multi-sensor fusion in body sensor networks: State-of-the-art and research challenges, *Information Fusion*, Vol. 35, 2017, pp. 68-80.
- [12]. C. Habib, A. Makhoul, R. Darazi, C. Salim, Self-adaptive data collection and fusion for health monitoring based on body sensor networks, *IEEE Transactions on Industrial Informatics*, Vol. 12, Issue 6, 2016, pp. 2342-2352.
- [13]. N. Giladi, J. Hausdorff, Y. Balash, Episodic and continuous gait disturbances in Parkinson's disease 22, *Scientific Basis for the Treatment of Parkinson's Disease*, 2013, pp. 417.
- [14]. K. B. Currall, R. Hallworth, H. Ali, A new approach for sequence analysis: Illustrating an expanded bioinformatics view through exploring properties of the prestin protein, in *Bioinformatics: Concepts, Methodologies, Tools, and Applications*, IGI Global, 2013, pp. 1536-1556.
- [15]. K. Dempsey, H. Ali, Evaluation of essential genes in correlation networks using measures of centrality, in *Proceedings of the IEEE International Conference on Bioinformatics and Biomedicine Workshops (BIBMW)*, 2011, pp. 509-515.
- [16]. K. Dempsey, S. Bonasera, D. Bastola, H. Ali, A novel correlation networks approach for the identification of gene targets, in *Proceedings of the 44th Hawaii International Conference on System Sciences (HICSS)*, 2011, pp. 1-8.
- [17]. Y. Wang, Z. Wang, L. Zhang, Internet traffic engineering without full mesh overlaying, in *Proceedings of the 20th Annual Joint Conference of the IEEE Computer and Communications Societies INFOCOM 2001*, 2001, pp. 565-571.
- [18]. J. Fekete, D. Wang, N. Dang, A. Aris, C. Plaisant, Interactive poster: Overlaying graph links on treemaps, in *Proceedings of the IEEE Symposium on Information Visualization Conference Compendium (InfoVis' 03)*, 2003, pp. 82-83.
- [19]. B. Jiang, B. Ravindran, H. Cho, Probability-based prediction and sleep scheduling for energy-efficient target tracking in sensor networks, *IEEE Transactions on Mobile Computing*, Vol. 12, Issue 4, 2013, pp. 735-747.
- [20]. A. Burns, B. R. Greene, M. J. McGrath, T. J. O'Shea, B. Kuris, S. M. Ayer, SHIMMER™ – A wireless sensor platform for noninvasive biomedical research, *IEEE Sensors Journal*, Vol. 10, Issue 9, 2010, pp. 1527-1534.
- [21]. D. Podsiadlo, S. Richardson, The timed "Up & go": A test of basic functional mobility for frail elderly persons, *Journal of the American Geriatrics Society*, Vol. 39, No. 2, 1991, pp. 142-148.
- [22]. I. Diamantopoulos, E. Clifford, J. Birchall, Short-term learning effects of practice during the performance of the tandem Romberg test, *Clinical Otolaryngology*, Vol. 28, No. 4, 2003, pp. 308-313.
- [23]. E. Jonsson, M. Henriksson, H. Hirschfeld, Does the functional reach test reflect stability limits in elderly people?, *Journal of Rehabilitation Medicine*, Vol. 35, No. 1, 2003, pp. 26-30.
- [24]. I. Youn, A. Patolla, H. H. Ali, Robust Network Models for using Mobility Parameters for Health Assessment, in *Proceedings of the 11th International Conference on Sensor Technologies and Applications (SENSORCOMM' 2017)*, 10-14 September 2017, Rome, Italy, pp. 8-13.



A Novel Routing Fault Tolerant Reliable Protocol for Wireless Sensor Networks

¹Islam MOURSY, ²Mohamed ELDERINI and ³Magdy AHMED

^{1,2} Computer and Systems Engineering Department, Faculty of Engineering, Alexandria University
Alexandria, 11432, Egypt

³ Vice Dean for Graduate Studies and Research, Faculty of Engineering Alexandria University
Alexandria, 11432, Egypt

¹ Tel.: +20 10 0170 4152

E-mail: islam.moursy@alexu.edu.eg, elderini@alexu.edu.eg, magdy@alexu.edu.eg

Received: 10 November 2017 /Accepted: 10 December 2017 /Published: 29 December 2017

Abstract: Wireless sensor networks operate in very challenging environments that make them prone to different types of faults. Hence, there is a high need for a reliable protocol that offers an acceptable functionality in the presence of faults. In this paper, we propose the Fault Tolerant Reliable Protocol (FTRP), a novel routing protocol designed to be used in wireless sensor networks. FTRP offers fault tolerance reliability for packet exchange, as well as adaptation for dynamic network changes. The key concept in this protocol is the use of node logical clustering. The protocol delegates the routing ownership to the cluster heads, where the fault tolerance functionality is implemented. FTRP utilizes cluster head nodes along with cluster head groups as intermediate storage for transient packets. In addition, FTRP utilizes broadcast in its routing messages communication. This technique substantially reduces the message overhead as compared to classical flooding mechanisms. FTRP manipulates Time to Live (TTL) values for the various routing messages in addition to utilizing jitters in messages transmission. FTRP performance has been evaluated through extensive simulations. Aggregate Throughput, Packet Delivery Ratio and End-to-End delay have been used as performance metrics. The results obtained showed that FTRP ensures high Throughput, high Packet Delivery Ratio, and acceptable End-to-End delay in the presence of changing networking conditions. FTRP performs well in dense and sparse networks while nodes are mobile. Stationary simulations represented the worst-case behavior. This is attributed to synchronized nodes, where nodes send similar messages at the same time.

Keywords: Fault tolerance, Proactive routing, Wireless sensor networks, NS-3.

1. Introduction

Wireless Sensors Networks (WSNs) continue to present a lot of interest in both the research domain as well as the industry [1]. WSNs are highly adaptive to various domains, including - but not limited to - energy control systems, environmental monitoring, security, surveillance, health applications, area monitoring and Internet of Things [2].

Typical WSNs are networks composed of a large number of sensor nodes. Each node is equipped with sensors to detect various attributes of the surrounding environment. WSNs are built to operate for prolonged time and even in a hostile environment, which increases the need for fault tolerant reliable communication protocols [3].

There are many research papers on routing protocols. However, only few are adopted by the

industry. The Institute of Electrical and Electronics Engineers (IEEE) had adapted the topic and introduced Low-Rate Wireless Personal Area Network (Lr-WPAN) [4] as a standard Media Access Control (MAC) layer for WSNs, which opens a great opportunity for WSNs. This paper introduces a new fault tolerant reliable routing protocol for WSNs, which is efficient under mobility conditions.

Mahmoud, *et al.* [5] introduced a novel three-dimensional reference model for research in WSN reliability. The model categorizes WSN protocols into one of two techniques, which are retransmission or redundancy. Reliability is ensured within those techniques either by using a hop-by-hop or an end-to-end method to recover the lost data while maintaining either packet or event level reliability. Chouikhi, *et al.* [6] classify fault tolerance techniques according to the time at which the fault tolerance is triggered (before or after the fault occurrence). According to this, these techniques are classified as preventive or curative. Hence, the proposed protocol is classified as a proactive protocol that is retransmission based, connection oriented (end-to-end), with packet level reliability and utilizing a curative technique to achieve fault tolerance.

Fault Tolerant Reliable Protocol (FTRP) operates as a table driven proactive protocol [7]. FTRP regularly exchanges topology information with selected nodes of the network. Initially, nodes are in learning mode and broadcast a status of not being in a sensor domain in preparation to join one. If no answer is received, the nodes stay in that state until an answer is received. If an answer is received, the node evaluates the answer depending on its source and its included attributes. A cluster then begins to form according to the proposed protocol.

After cluster formation, Cluster Member (CM) nodes send data messages to their designated cluster head (CH). The CH, in turn, decides how many copies of the message to be retained until an acknowledgment (ACK) is received from the destination. The CH stores that message in the cluster head group (CHG) according to the protocol-defined parameters. The proposed protocol utilizes the following main techniques.

1.1. Retransmission-based Reliability

Retransmission is the traditional way of ensuring reliability [5]. This is achieved by allowing the sender node to wait for an ACK for its previously sent packets. In case, no ACK is received, the packet is considered lost and retransmission takes place to ensure reliability. FTRP implementation relieves the responsibility of packet storage and retransmission to higher entity nodes (CHs, CHGs or Sinks), as will be elaborated in Section III.

1.2. End-to-End Reliability

End-to-End reliability is a connection-oriented scheme for achieving reliability in which only the two communicating end nodes (source and destination) are responsible for ensuring reliability. FTRP implementation expands the end-to-end reliability by relieving the source node from this task, and transferring it to the CH. The CH determines, according to the replicas parameters, which CHGs to be used as storage. Whenever the destination node receives the packets, it broadcasts a message only processed by CHs or CHGs to release their locally stored corresponding replicas.

1.3. Packet Level Reliability

Packet level reliability ensures that all the packets carrying sensed data from all the related nodes are reliably transported to their destinations.

The rest of the paper is organized as follows. In Section 2, the most relevant related works are presented. In Section 3, the relevant FTRP protocol operations are detailed. The performance analysis of the FTRP protocol is presented in Section 4. Finally, Section 5 concludes the paper and lists ongoing and future work.

2. Related Work

In this section, we review literature work addressing the same elements as our protocol, namely retransmission based, connection oriented (end-to-end) and packet level reliability.

Reactive routing protocols such as Ad hoc On-demand Distance Vector (AODV) protocol [8] have the ability to discover the route when required. AODV uses the flooding mechanism to broadcast the route request to determine for new route during failure and can be very expensive to perform. AODV does not distinguish failure. It relies on the link layer feedback and the distance traverse by the packet to determine whether to broadcast for new route or drop the packet. As WSNs are prone to different failures with different durations caused by neighboring nodes, external radio devices, moving object and operating environments, nodes can suffer from transient, intermittent and permanent failure. Combinations of these failures may occur and may produce a complex unpredictable behavior that cannot be addressed with a single protocol. For example, transient failures may trigger the link layer to notify failure to the AODV and result in route discovery. When the next-hop neighbor experiencing the transient failure recovers, it will respond to the request while other nodes propagate the route request to all its local nodes. This will create a ripple effect that may congest the network. It is necessary to provide a reliable mechanism for the

nodes to change their routing strategy according to the current network topology in order to re-establish the network connection. This leads to a motivation to investigate the potential of a new fault tolerant routing protocol.

Protocols such as Sensor Protocols for Information via Negotiation, (SPIN) [9] were developed to allow querying the WSN for data without being able to address particular nodes and to implement energy savings at the same time. SPIN follows an interest advertisement-request strategy in which information is described by meta-data which initially is exchanged between the nodes. Nodes, which acquired new data, advertise it via its meta-data classification. Neighboring nodes, which have an interest in that kind of data, reply with a request, on which the advertising node transmits the data to the requesting node. After receiving the new data, the requesting node advertises it to its neighbors. SPIN achieves a high-energy efficiency compared to flooding, as only requested information is transported in the network [10]. However, there is no standard meta-data format, as this is supposed to be application specific. In addition, the delivery of data is not guaranteed by SPIN's advertisement mechanism, as the nodes interested in a specific class of data might be distant from the node acquiring this data. If intermediate nodes are not interested in the given class of data, the interested node will never receive it.

To address the issues of scalability and energy preservation in a different way, the notion of hierarchy was introduced in several WSN routing protocols with the goal of avoiding an overload of sink nodes by too many received messages, as well as reducing the amount of overall message transmissions. To achieve this, nodes are grouped into clusters, which feature a node designated as cluster head. Information is relayed to this cluster head, which aggregates data to bundle the information and reduce the number of messages, which are sent to the sink nodes. With this strategy, communication is forced into a multi-hop manner, relaying information over neighboring nodes, which in turn preserves energy as the energy cost of radio communication increases with the distance. Low Energy Adaptive Clustering Hierarchy (LEACH) [11] is one of the first routing protocols applying this strategy.

Iyer, *et al.* [12] proposed the Sensor Transmission Control Protocol (STCP), an end-to-end reliability protocol with a congestion control mechanism that is sink-centric. STCP dynamically controls the application data flow by utilizing a controlled variable reliability mechanism where the application type controls the throughput. Reliability is maintained by using ACK or Negative Acknowledgement (NACK) as end-to-end retransmission mechanisms. Packets are cached locally in each node until an ACK is received from Sink. Whenever Sink receives information about congested paths, the Sink directs the downstream-congested nodes to select alternative paths. Reliability in STCP is achieved through connection-oriented explicit ACKs, which involves only the end nodes.

STCP is considered scalable for a large number of nodes with high hop counts from a source node to the Sink. STCP nodes are prone to huge end-to-end delay time [5], which results in high latency and cache overflow.

Marchi, *et al.* [13] proposed a Distributed Transport for Sensor Networks (DTSN). DTSN is non-sink centric, end-to-end and an energy oriented packet reliability protocol. DTSN is based on two mechanisms, full and differential reliability mechanisms. Full reliability is achieved via retransmission based explicit ACKs, while differential reliability is performed independently. In the full reliability mechanism, the source node keeps transmitting the packets until the number of transmitted packets equals the size of the acknowledgement window. An explicit acknowledgement request is issued from the source node to the destination to confirm message delivery. If the sequence of the packets is in order, an ACK is sent. These packets are then removed from the buffer of the source node. If a NACK is received then retransmission of the missing sequence of packets is performed. The key contribution of DTSN is the integration of mechanisms involved in achieving reliability, such as partial buffering at the source and intermediate nodes and the utilization of erasure coding. However, DTSN does not provide details on how the reliability level is maintained when network conditions change.

3. FTRP Operations

3.1. Protocol Overview

FTRP [14] operations utilize a simple messaging system to communicate different protocol statuses to the participating nodes. This messaging system is used to transition the node from one state to another in order to form a logical grouping of nodes referenced later as a cluster. FTRP tries to overcome the issues in STCP [12] by utilizing a distributed cache rather than preserving the cache at the sender node. This approach allows the cluster head to control the amount of cache allocated and where to store the data packet. FTRP introduces a retry count for locally cached entries. Whenever a packet entry reaches its max retry count, (the default is six retries), it is flushed out of the cache to overcome cache overflow. In fact, FTRP is well suited for a changing environment, where its messages update the network paths and handle nodes failure well.

FTRP communicates using a unified packet format for all data related to the protocol. This provides an easy way to combine different messages in a single packet transmission. These packets are encapsulated into User Datagram Protocol (UDP) [15] datagrams. On the other hand, FTRP messages contain a sequence number, which is incremented for each message. In such case, the recipient of a control message is able to

identify which information is more recent and to ignore those older unprocessed messages.

3.2. Definitions of Main Nodes Status

1) **Sink:** The Sink is the central node of the network, having information about all nodes. Usually, it is connected to a wired network and it has access to the wireless sensor domain.

2) **Cluster Head (CH):** The Cluster Head can be regarded as a Sink, but for a subset of nodes. It is responsible for relaying all information from and to the nodes controlled under its domain.

3) **Cluster Head Group (CHG):** CHGs are normal nodes selected by the CH as per the protocol parameters to act as local cluster storage for messages in transient.

4) **Cluster Member (CM):** CMs are normal nodes composing the cluster and are managed by the respective CH.

5) **Cluster Bridge Head (CBH):** If the CH is far away from the Sink, the CBH is the node within another cluster that links the cluster with the nearest CH.

6) **Learning:** Initially, a node is not in a cluster or it does not know route to a Sink.

7) **Swarm:** A node has identified another node that is not in its domain and it has knowledge of other nodes (nonsink).

8) **Discovered:** A discovered node is a node that is discovered from either a Sink or another cluster.

The life cycle begins with a node in a Learning state. A few nodes who have knowledge of their respective existence can form a swarm. Few swarm nodes can then transition to a discovered state upon sensing a nearby Sink. The Sink nominates a discovered node to be a CH. The CH can request nearby nodes for association as CMs. Few CMs can then be nominated as CHGs, as per the predefined configuration parameters of the protocol.

Fig. 1 depicts the state transition for nodes in FTRP.

3.3. FTRP Messaging System

FTRP inherits the general packet structure of the Optimized Link State Routing Protocol (OLSR) [16] where a packet header is appended to multiple FTRP messages and has a sequence number. The choice of OLSR packet format was made to benefit from piggybacking multiple types of messages in the same packet. A single FTRP packet can contain multiple routing messages. Messages share a common structure as well.

3.3.1. Hello Message (HELLO)

A nonsink node lifecycle begins in a Learning state, where it periodically broadcasts a hello message

exposing its status and other parameters. Hello messages have their Time to Live (TTL) [17] value set to one, in order not to flood the whole network. A Hello message is populated with the sending node known attributes, and its known existing members, if any. Hello messages are broadcasted as keep alive periodically. The behavior of each node is different upon receiving a Hello message, according to the receiving node status.

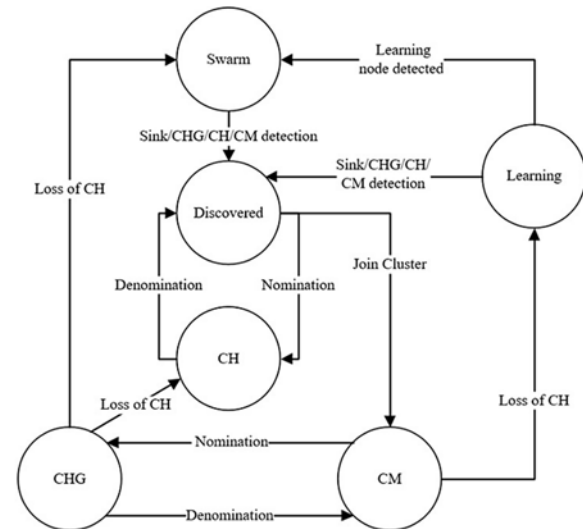


Fig. 1. FTRP State Transition Diagram.

A Sink node receiving a Hello message checks if the incoming node has not yet joined a domain, and if it is not a member of any other cluster. In that case, the Sink sends an association request. If the node had already been identified in a domain yet had not joined any cluster, the Sink will not take any action. This mechanism is adopted in order to control the allocation of CHs and to allow the network clustering formation to converge by favoring the node to join a cluster than to promote it to a new CH. The Sink will ignore any Hellos from other Sinks and will update the information received from any other CH.

3.3.2. Association Message (ASC)

ASCs are used to instruct nodes to join a cluster or domain. Only the Sink and the CHs are allowed to send association to other nodes. ASC messages have two classes.

1) **Regular association:** A regular association messages have their TTL value set to one, so that association does not flood the network.

2) **Broadcasted Association (ASCb):** A broadcasted association messages have their TTL value set to 255 in order for a CH to be nominated when it has no direct link to the Sink. It uses its nearest CBH to reach the Sink through the distress Save-Our-Ship (SOS) mechanism.

A node populates the ASC message with its members. Having that, members of a Sink are the CHs known to that Sink and members of a CH are those nodes under the CH control as fault tolerance domain.

3.3.3. Control Message (CTL)

CTLs are used as decision-making mechanism and out of band, status updates of different protocol aspects. It has the following subclasses

1) **Reject CH promotion:** Reject CH promotion is issued in the case when a Sink at some point in time decided to promote a CM to CH however, this CM was earlier acquired by another CH. In that case, rejecting the CH promotion is favored so that the CH ID pool is not depleted too fast. In return, the CM issues a Reject CH Promotion control message to notify the Sink to release the allocated CH ID.

2) **Members check:** A swarm node that was nominated to be CM or CH knows about the existence of other swarm nodes whom with which a swarm was formed. This swarm must be checked against a high entity node (Sink in case the node is CH or CH in case the node is CM). The receiving node (Sink or CH) checks the incoming member list for local existence in its data structures, and then replies to the sender node with a "Release swarm members" message for those members the higher entity does not know about.

3) **Release swarm members:** When this message is received, the node drops the sending node from its local base as swarm, and sends them swarm release notify control message.

4) **Swarm release notify:** This message is processed by swarm to drop the sender from its local base.

5) **Swarm SOS:** Whenever the swarm is about to drop its last member, it issues swarm SOS to the sender of the release notify so that the sender is treated as bridgehead and relays the SOS to the Sink. The Sink will then send an ASCb, with its TTL value set to 255, to this swarm node to be nominated as new CH.

6) **Fault Tolerant message release (FT_Release):** Whenever a node successfully receives its data packet, it sends this message in broadcast mode, i.e., its TTL value set to 255, to notify CHs and CHGs to release the local copies of the messages considered for fault tolerance.

3.4. Message Emission and Jitter

To avoid synchronization of messages, jitter is introduced to allow protocol messages to be emitted such that they avoid synchronization. Emission of protocol messages from neighboring nodes may, for various reasons (mainly timer interactions with packet processing), become synchronized such that several neighbor nodes attempt to transmit messages simultaneously. This may or may not lead to collisions and hence message loss of several subsequent

messages. To avoid synchronizations of messages, the following strategy is utilized. A node adds an amount of jitter to the interval at which messages are generated. The jitter is a random value for each message generated. Thus, for a node utilizing jitter:

$$FMI = OMI - \text{jitter}, \quad (1)$$

where *FMI* is the final message interval, *OMI* is the original message interval and jitter is a uniform random value selected from the interval [0, original message interval/4]. Jitter is also used when a message is to be forwarded by a node. The message is kept in the node during a short time period equals the jitter interval.

This scheme increases the opportunity to piggyback other messages in the same routing packet and contributes to the reduction of the overall number of packet transmissions.

3.5. Wrap-around

FTRP utilizes sequence number in packets and messages to be able to discard messages that are repeated or are received out of order. The limited number of bits (16 bit) for representing sequence numbers can cause repeated values to be present which is called a wrap-around (i.e. sequence number is incremented from the maximum possible value to zero). To be able to distinguish which sequence number is more recent. This recovery technique was inherited from OLSR [16] by defining the following:

$$seq = (seq + 1) \bmod (MaxValue + 1), \quad (2)$$

where *seq* is the Sequence Number and *MAXVALUE* is the maximum value that can be held in the number of bits defined. Thus, even in the presence of wrap-around, it is possible to determine which message contains the most recent information.

3.6. Routing Function and Fault Tolerance

The default forwarding scheme for a node is to direct the outgoing packets to its master (CH in case of a node, and a Sink in case of a CH). The scheme below also applies in case the CH or Sink is initiating a packet send. Upon the reception of a forward request, the routing function checks local parameters for replica count and then stores the message in the CHGs accordingly. Then, finally, the packet is forwarded normally.

CHs and CHGs are using a timed queue to store the packets. The receiving node, upon successful reception of a packet, generates an FT_Release message having the packet unique identification. Each receiving CHG, CH or Sink accepts this message and removes the requested message (if it exists) from its local queue. Upon the expiry of the queue timer, the local fault tolerance queue is checked for packets that

had not exceeded their retry time, and those packets are resent. Packets having expired retry time are removed from the queue and are considered undeliverable due to unreachable destination.

4. Simulation and Performance Evaluation

4.1. Assumptions

The simulation model is based on the following assumptions:

- The Sink has infinite power source, while nodes have not.
- Each node can behave as both a client and a router.
- Each node has a single interface running the FTRP protocol on that interface.
- The nodes have the same capabilities, i.e., same coverage area and same antenna.
- The nodes are randomly placed.
- The nodes follow a 2d-walk mobility pattern in mobility scenarios and follow a constant position model for stationary simulations.
- The nodes can either receive or transmit at a time.
- There is no turn around time between transmitting and receiving. Nodes can switch between transmit and receive instantly.
- Mobility is uncorrelated among the nodes and links fail independently.

4.2. Performance Metrics

The following performance metrics are used to analyze the behavior of FTRP.

1) Aggregate Throughput: This is the sum of the throughputs in the uplink and the downlink.

2) Packet Delivery Ratio (PDR): This is the number of successfully delivered packets divided by the total number of transmitted packets

3) End-to-End Delay (E-2-E): This is the sum of time taken for packets transmitted from sources to destinations divided by the total number of received packets.

4.3. Simulation Environment

The FTRP routing model is built using NS-3 network Simulator [18] on top of IEEE 802.11 MAC model of NS-3. Due to simulator limitations, model parameters have been tuned to match the 802.15.4 MAC layer.

The Random 2d-walk model [19] was adopted for driving mobile clients. In the Random 2d-walk mobility model, each instance moves with a speed and direction chosen randomly until either a fixed distance has been walked or until a fixed amount of time has passed. If a node hits one of the boundaries (specified by a rectangle) of the model, it rebounds on the

boundary with a reflexive angle and speed. This model is often identified as a Brownian motion model. The speed is varied from no mobility using a constant position model, 1 m/sec to 2 m/sec. Table 1 depicts the parameters set for the simulation model that is common for all our simulations.

Table 1. Parameters for Simulation Model.

Simulation Parameter	Value
Simulator	NS-3 (version 3.25)
Operating system	Linux (Ubuntu 14.04)
Simulation time	50 secs
Simulation Area	100 m × 100 m
Number of nodes	20 for sparse, 40 for dense
Node transmission range	50 meters
Movement model (for mobility tests)	Random Walk 2d Mobility Model
Stationary model (for no mobility tests)	Constant Position Mobility Model
Nodes Position allocator	Random Disc Position Allocator
Speed of mobile nodes	1 m/sec and 2 m/sec
Traffic type	CBR
Data payload	512 bytes
Packet rates	20 p/sec to 80 p/sec
MAC Layer	802.11 DCF with RTS/CTS
Radio Frequency	2.4 GHz
Radio Channel rate	2 Mbps
Propagation loss model	Friis Propagation Loss Model
Propagation Delay Model	Constant speed propagation delay model

4.4. Results and Analysis

FTRP is simulated using various networking scenarios with the help of the NS-3 simulator. The scenarios and results along with detailed analysis are presented in the following sections.

4.4.1. Scenario I

In this scenario, we analyze the performance of FTRP in terms of throughput, PDR and E-2-E delay in a sparse network comprising of 20 nodes. The simulation is performed by varying the number of data packets sent per second, while maintaining a constant number of flows and system load. Number of packets per flow ranged from 20 packets/sec to 80 packets/sec. The simulation was repeated using no mobility model, 1 m/sec and 2 m/sec walking models. Other parameters considered for simulations are the same as shown in Table 1.

Fig. 2 depicts PDR against increasing traffic load in a sparse network. It is observed that increasing the data rate beyond 280 kb/s causes PDR to begin to drop, although not significant.

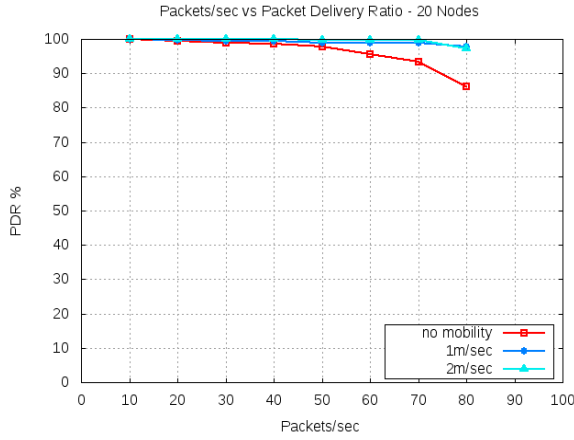


Fig. 2. PDR in a sparse network.

As per our simulation parameters, a data rate of 240 kb/s corresponds to 60 packets/sec and a data rate of 280 kb/s corresponds to 70 packets/sec. Mobile nodes achieve a good PDR with regard to the maximum data rate supported by Lr-WPAN [4] standard, which are 250 kb/s (approximately 63 packets/sec). While nodes are stationary, the obtained PDR results fall to above 94 % at the target data rate of 60 packets/sec, which is acceptable.

Fig. 3 depicts Aggregate throughput against increasing traffic load in a sparse network.

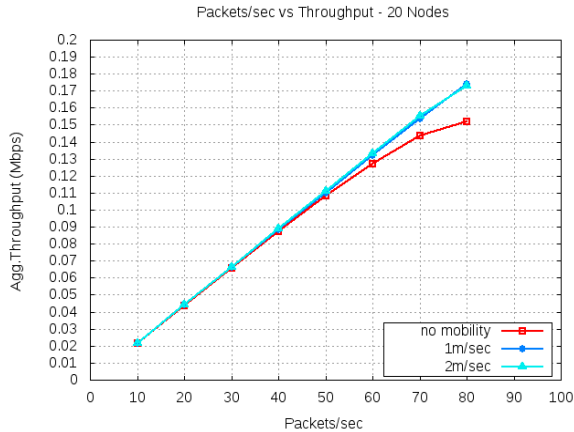


Fig. 3. Aggregate Throughput in a sparse network.

It is observed that the throughput increases as the data rate increases. Both low and high mobility scenarios achieve good throughput as data rate increases even for data rates above the targeted 250 kb/s. The stationary nodes performance is lower than that of mobile ones, which can be attributed to the nodes synchronized states.

Fig. 4 depicts E-2-E delay against increasing traffic load in a sparse network. It is observed that, as the data rate increases, the E-2-E delay increases significantly in a stationary scenario. The E-2-E delay increases within acceptable range for mobile scenarios.

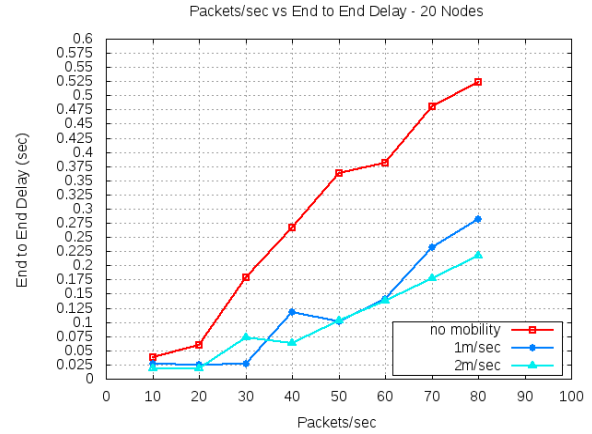


Fig. 4. End to End Delay in a sparse network.

The increase in E-2-E delay is expected due to the introduction of fault tolerance mechanism, which uses store and forward. In the stationary scenario, the increase is significant and can be justified by the nature of FTRP being too communicative. In the stationary scenario, the collision rate of packets can increase, while mobility helps to decrease collision. This can be attributed to the variations of node states. This variation reduces messages exchanged, reduces collisions and maintains good E-2-E delay.

4.4.2. Scenario II

In this scenario, we analyze the performance of FTRP in terms of throughput, PDR and E-2-E delay in a dense network composed of 40 nodes. The simulation is performed by varying the number of data packets sent per second, while maintaining a constant number of flows and system load. The number of packets varied per flow ranged from 20 packets/sec to 80 packets/sec. The simulation was repeated using no mobility model, 1 m/sec and 2 m/sec walking models. Other parameters considered for simulations are the same as depicted in Table 1. Scenario II results emphasize the results of scenario I. It is found that in a dense network with no mobility, PDR drops, Aggregate Throughput tends to saturate early and E-2-E delay increases significantly. In mobility scenarios, PDR is within acceptable ranges at 70 packet/sec rate, the Aggregate Throughput increases and E-2-E delay is within acceptable ranges.

Fig. 5 depicts PDR against increasing traffic load in a dense network.

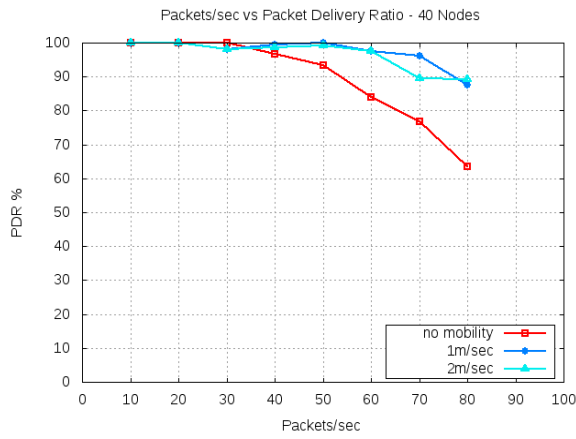


Fig. 5. PDR in a dense network.

It is observed that, while nodes are mobile, the PDR is almost the same. However, for data rates higher than 260 kb/s (65 packets/sec) higher mobility nodes PDR tends to saturate while for less mobile nodes PDR tends to decrease. Stationary nodes are the worst performer, result which can be attributed to synchronized nodes states.

Fig. 6 depicts Aggregate Throughput against increasing traffic load in a dense network. It is observed that, while nodes are mobile, the throughput is almost the same. However, for data rates higher than 250 kb/s, higher mobility nodes' throughput tends to increase while for less mobile nodes throughput tends to saturate. Stationary nodes are the worst performer, which can be attributed to synchronized nodes states.

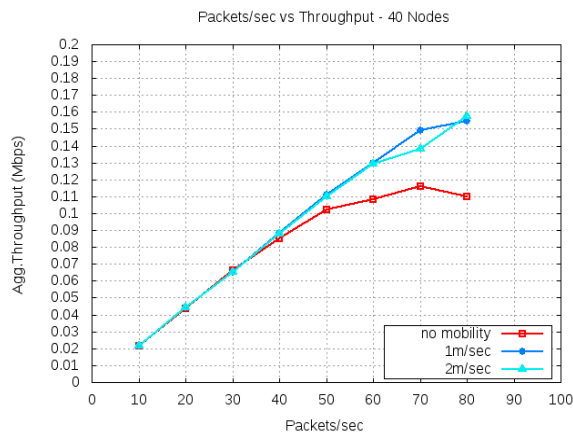


Fig. 6. Aggregate Throughput in a dense network.

Fig. 7 depicts E-2-E delay against increasing traffic load in a dense network. It is observed that, while nodes are mobile, E-2-E is almost the same and for data rates higher than 250 kb/s all mobile nodes' E-2-E tends to increase. Stationary nodes are the worst performer, which is directly linked to the fault tolerance function, in which, for every sent packet, an ACK for reception is needed to consider a packet is delivered. This increases the time when a packet is considered successfully delivered.

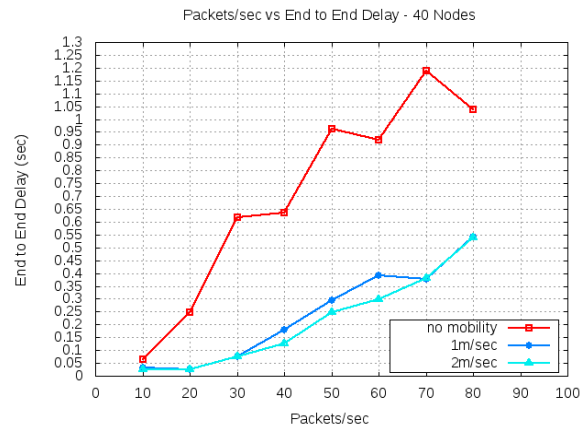


Fig. 7. End to End Delay in dense network.

The ACK packet as well might get lost due to network collisions and synchronized nodes states, which in turn will cause the source node to resend the packet and wait for another ACK. This significantly affects the E-2-E delay for FTRP.

5. Conclusions

This paper introduced a novel reliable fault tolerant routing protocol, FTRP, for wireless sensors networks. FTRP creates a communication path between source and destination nodes and forwards packets on that path.

FTRP performance has been evaluated through extensive simulations using NS-3. Aggregate throughput, Packet Delivery Ratio and End-to-End delay have been used as performance metrics. In terms of Packet Delivery Ratio and Aggregate throughput, FTRP is an excellent performer in all mobility scenarios, whether the network is sparse or dense. In stationary scenarios, FTRP performed well in sparse networks; however, in dense networks, FTRP's performance had degraded, still remaining in an acceptable range. In terms of End-to-end delay, FTRP is considered a good performer in all mobility scenarios where the network is sparse. In the sparse stationary scenario, FTRP is still considered a good performer. However, in dense stationary scenarios, FTRP's performance is considered as worst-case behavior, which can be attributed to synchronized nodes states that occur when nodes send similar messages at the same time.

There are times when properly receiving a network message carrying crucial information is more important than other costs, such as, but not limited to, energy or delay. That makes FTRP suitable for a wide range of WSNs application domains, such as military applications by monitoring soldiers' biological data and supplies while on the battle field as well as battle damage assessment. FTRP can also be used in health applications by tracking and monitoring doctors and patients inside a hospital and elderly assistance, in addition to a wide range of geo-fencing, environmental monitoring, resource monitoring,

production lines monitoring, agriculture and animals tracking.

FTRP should be avoided in dense stationary deployments such as, but not limited to, scenarios where a high application response is critical and life endangering, such as biohazards detection or within intensive care units.

As future work, it is planned to improve the performance of FTRP in stationary scenarios. FTRP performance was evaluated through simulations. It is planned to extend the FTRP implementation in a WSN operating system to compare the complexity of a real system against the simulation results. The effect of varying the number of attempts to retransmit a non-delivered packet (max retry count) should be investigated. Furthermore, the energy efficiency has to be evaluated for various FTRP operations.

References

- [1]. A. Ajith Kumar S., K. Vsthus, L. M. Kristense, An Industrial Perspective on Wireless Sensor Networks - A Survey of Requirements, Protocols and Challenges, *IEEE Communications Surveys & Tutorials*, Vol. 16, No. 3, 2014, pp. 1391-1412.
- [2]. C. Alcaraz, P. Najera, J. Lopez, R. Roman, Wireless Sensor Networks and the Internet of Things Do We Need a Complete Integration, in *Proceedings of the 1st International Workshop on the Security of the Internet of Things*, 2010, pp. 32-37.
- [3]. S. Misra, I. Woungang, S. C. Misra, Guide to Wireless Sensor Networks, *Springer*, London, 2009.
- [4]. IEEE Standard for Low-Rate Wireless Networks, 2016. [Online]. Available: <http://standards.ieee.org/getieee802/download/802.15.4-2015.pdf>. [Accessed 7 7 2017].
- [5]. M. A. Mahmood, W. K. Seah, I. Welch, Reliability in Wireless Sensor Networks: A Survey and Challenges, *The International Journal of Computer and Telecommunications Networking*, Vol. 79, 2015, pp. 166-187.
- [6]. S. Chouikhi, I. El Korbi, Y. Ghamri-Doudanec, L. Azouz Saidane, A Survey on Fault Tolerance in Small And Large Scale Wireless Sensor Networks, *The International Journal for the Computer and Telecommunications Industry*, Vol. 69, 2015, pp. 22-37.
- [7]. Basu Dev Shivahare, Charu Wahi, Shalini Shivhar, Comparison of Proactive and Reactive Routing Protocols in Mobile Adhoc Network Using Routing Protocol Property, *International Journal of Emerging Technology and Advanced Engineering*, Vol. 2, No. 3, 2012, pp. 356-359.
- [8]. C. E. Perkins, E. M. Royer, Ad-hoc On-Demand Distance Vector Routing, in *Proceedings of the WMCSA*, 1999.
- [9]. J. Kulik, W. Rabiner, H. Balakrishnan, Adaptive Protocols for Information Dissemination in Wireless Sensor Networks, in *Proceedings of the 5th Annual ACM/IEEE International Conference on Mobile Computing and Networking*, Seattle, Washington, USA, pp. 174-185, 1999.
- [10]. K. Akkaya, M. Younis, A Survey On Routing Protocols For Wireless Sensor Networks, *Ad Hoc Networks*, Vol. 3, No. 3, 2005, pp. 325-349.
- [11]. M. J. Handy, M. Haase, D. Timmermann, Low Energy Adaptive Clustering Hierarchy With Deterministic Cluster-Head Selection, in *Proceedings of the 4th International Workshop on Mobile and Wireless Communications Network*, Stockholm, Sweden, 2002, pp. 368-372.
- [12]. Y. Iyer, S. Gandham, S. Venkatesan, STCP: A Generic Transport Layer Protocol for Wireless Sensor Networks, in *Computer Communications and Networks*, San Diego, CA, USA, pp. 35-42, 2005.
- [13]. B. Marchi, A. Grilo, M. Nunes, DTSN: Distributed Transport for Sensor Networks, in *Proceedings of the 12th IEEE Symposium on Computers and Communications*, Las Vegas, NV, USA, 2007, pp. 165-172.
- [14]. I. Moursy, M. El-Derini, M. Ahmed, FTRP: A Fault Tolerant Reliable Protocol for Wireless Sensor Networks, in *Proceedings of the 11th International Conference on Sensor Technologies and Applications (SENSORCOMM' 17)*, 10-14 September 2017, Rome, Italy, pp. 24-30.
- [15]. RFC 768 - User Datagram Protocol - IETF, [Online], Available: <https://www.ietf.org/rfc/rfc768.txt> [Accessed 11 5 2017].
- [16]. RFC 3626 - Optimized Link State Routing Protocol, IETF. [Online]. Available: <https://www.ietf.org/rfc/rfc3626.txt> [Accessed 11 5 2017].
- [17]. RFC 791 - Internet Protocol, IETF, [Online], Available: <https://tools.ietf.org/html/rfc791> [Accessed 07 07 2017].
- [18]. T. Henderson, "NS-3 Overview," [Online], Available: <http://www.nsnam.org/docs/ns-3-overview.pdf> [Accessed 11 5 2017].
- [19]. NS-3 Manual, [Online], Available: <https://www.nsnam.org/docs/manual/ns-3-manual.pdf> [Accessed 11 5 2017].



A Modular Wireless Sensor Platform with a Sensor Identification Scheme

**Yi-Jie Hsieh, Chih-Chyau Yang, Yi-Jun Liu, Wei-Lin Lai, Chien-Ming Wu,
and Chun-Ming Huang**

National Chip Implementation Center
National Applied Research Laboratories,
No. 26, Prosperity Rd. 1, Hsinchu City, Taiwan
Tel.: (+886)3-5773693

E-mail: yjhsieh@cic.narl.org.tw, ccyang@cic.narl.org.tw, yjliu@cic.narl.org.tw,
willai@cic.narl.org.tw, wucm@cic.narl.org.tw, cmhuang@cic.narl.org.tw

Received: 10 November 2017 /Accepted: 10 December 2017 /Published: 29 December 2017

Abstract: In this paper, a modular wireless sensor platform with a sensor identification scheme is presented. Our presented modular wireless sensor platform consists of sensor modules, and each sensor module is a part of the sensor system and in charge of one job in the system, such as computation, communication, output or sensing. Users can stack multiple modules together to build a unique sensor system. Since users are able to easily replace one module with others, our platform is highly extendable and reusable. A low-cost sensor identification scheme is proposed in this paper to detect which sensor is mounted on the platform automatically. This scheme utilizes a unique I²C address to identify the sensor type. A low-cost Electrically-Erasable Programmable Read-Only Memory (EEPROM) only needs to be setup in the non-I²C sensing modules. Furthermore, a firmware initialization process is also adopted to achieve the sensor identification mechanism. To demonstrate the proposed platform, we show an ambient temperature detection application and a carbon dioxide detection application in the paper. The results show that the proposed platform is suitable for academic researches and industrial prototype verification.

Keywords: Flexible sensing platform, Sensor system.

1. Introduction

The Internet of Things (IoT) development has progressed rapidly in the past few years. This concept was widely used not only for the industry and research purposes, but also in commercial products in our daily life [1-5]. The idea of IoT is to group “things” together with internet, allow “things” to communicate or interact with each other, and even, to gather their information and utilize it. Numerous IoT devices have used wireless sensors to recognize environments due to the continuously increasing

availability of wireless sensors. Besides, wireless sensors are also widely used in many research fields, such as sensor networks and sensor fusion.

There are several ways to build a sensor platform. The first one is to manually compose different sensor units according to requirements. In [6], Spanbauer, *et al.* proposed a sensor cube called MICA. Each MICA node contains multiple sensors inside. Different kinds of MICA nodes can be applied in various applications. To build up these kinds of sensor platforms, users must have enough hardware knowledge and resources. Besides, these self-made

sensors are designed for specific purposes, so they have limited extendibility and reusability. The second way is to use existing sensor platforms. However, most ordinary sensor platforms are designed for sensing only one feature, so multiple sensors have to be used for multi-sensing applications. This will increase cost, lose accuracy, and cause synchronization problems. There are also products that divide a sensor node into wireless module and sensor boards, such as MicaZ [7]. For different purposes, users can stack different sensor boards on the wireless module, so the reusability is further increased. However, the architecture usually allows only one sensor board connecting with the wireless module. Although some sensor boards have multiple sensor modules, the flexibility is still confined.

To support various researches and product developments, a broad range of wireless sensors is required. In this paper, we present a flexible wireless sensor platform which enables users to arbitrarily combine different modules with few constraints, so that they can create a unique sensor system according to their requirements. For the purposes of extensibility and reusability, we divide the sensor system into six units: output, sensing, communication, processing, power, and debug unit. Each unit is in charge of one specific function in the system. To build a sensor platform, users can select required sensor modules and stack them one by one, just like building bricks. This feature makes the proposed platform highly flexible and reusable.

Since our presented platform supports a variety of sensor types and sensor interfaces, how to make the sensor system easy to use has become an important task. Normally, every time we stack a different sensing module on the processing module, we have to download the corresponding firmware code to the Micro Control Unit (MCU) in order to drive this module. This work not only increases complexity for application developers, but also brings inconvenience to common users. A sensor identification scheme is therefore inevitable to identify which sensor is mounted on the platform automatically. In [8-9], R. Morello, *et al.* adopted the Transducer Electronic Data Sheet (TEDS) based on IEEE P1451 standard to store sensor information. This method allows microprocessors to access data through a standardized protocol and to realize the sensor self-identification. For the only purpose of the sensor identification, the hardware cost of this method is high since the TEDS memory needs to be setup in each sensing module. K. Mikhaylov, *et al.* [10-11] proposed a sensor identification mechanism by using the Intelligent Modular Periphery Interface (IMPI). The IMPI is implemented as a daisy chain interface based on the Serial Peripheral Interface (SPI) bus. However, the bus routing complexity is high while the number of interconnections becomes large. In this paper, a sensor identification scheme is proposed to identify the sensors on the platform automatically. This scheme utilizes a unique I²C address to identify the sensor type. A low-cost EEPROM only needs to

be setup in the non-I²C sensing module. Furthermore, a firmware initialization process is also adopted to enable the sensor identification mechanism.

The rest of this paper is organized as follows. In Section II, we present the idea of modular sensor platform. Then, the hardware implementation and the proposed sensor identification scheme are described in Section III. Next, we use two examples for demonstration in Section IV. Finally, the conclusions are given in Section V.

2. Flexible Sensor Platform

Our presented sensor system is divided into six units for the purposes of extensibility and reusability. Each unit is in charge of one function in the system:

1) Power unit which provides power to all other units is the key influence factor of the sensor life time and sensor size. A power unit can be, for example, Li-Po battery, button cell battery, or car charger.

2) Processing unit has to drive other units and execute firmware commands. A processing unit can be a MCU, a Field-Programmable Gate Array (FPGA), or just a controller.

3) Sensing unit is one of the main components in the sensor system to recognize surrounding environments, such as acceleration, color, image and so on.

4) Communication unit is used for communication. It can receive commands, transmit results, and relay messages. Here we focus on only wireless transmission, such as Bluetooth Smart (BLE), ZigBee, or Wi-Fi.

5) Output unit shows computational results and reminds users by screen, sound, or vibration.

6) Debug unit provides debug functions. When a sensor module is stacked on the debug unit, the designer can check signals of each pin and download images from PC.

Each unit has I/O pins to receive commands and transmit data. These pins can be standardized I/O pins such as Inter-Integrated Circuit (I²C), Serial Peripheral Interface Bus (SPI), Inter-IC Sound (I²S) and Universal Asynchronous Receiver/Transmitter (UART), or they may be General-Purpose Input/Output (GPIO) pins defined for the specific usage. For communication between different units, we define a universal bus that connects all units together and is implemented by connectors, as shown in Fig. 1. The universal bus contains three kinds of pins, standard I/O pins, GPIO pins, and power lines. All signals from the processing unit are physically connected to the universal bus, so the processing unit can control other units through the universal bus. As for the power lines, they deliver electric power from the power unit to others.

Under the definition of each unit, we further classify a unit into modules. Each unit can have multiple modules. Each module is one of the implementations of the unit. For example, the transceiver unit may have BLE module and Wi-Fi

module, the sensing unit may have compass module and thermometer module, and the power unit may have Li-Po battery module and button cell battery module. The reason we classify a sensor platform into units and modules is to increase flexibility. For each unit in a highly flexible platform, users should have more choices to replace one module with others. Fig. 1 shows the schematic view of a sensor module in the proposed platform. The green and black areas are PCB substrate and electronic components, respectively. Each module is implemented on an equal-size PCB substrate which has connectors on both front side and back side. Thanks to the universal connector, different modules can be combined concurrently, as illustrated in Fig. 2. Here, two connectors are used in order to increase the stability of the architecture. The area between two connectors on the PCB substrate is for placement of electronic components.

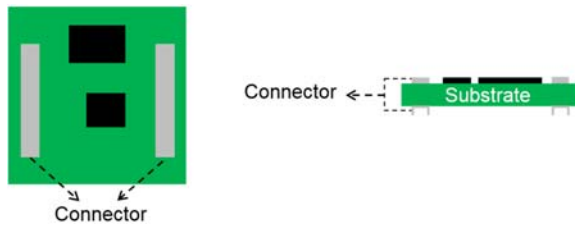


Fig. 1. The top schematic view and side schematic view of a sensor module.

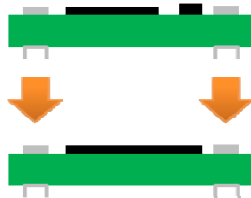


Fig. 2. Combination of two modules.

3. Implementation

In this section, we introduce the implementation of the presented sensor platform and the proposed auto sensor identification scheme.

3.1. Hardware Implementation

Our presented flexible wireless sensor platform primarily consists of

- 1) Power module;
- 2) Processing module;
- 3) Sensing module;
- 4) Communication module;
- 5) Output module;
- 6) Debug module.

The power module includes a Li-Po battery, a power management unit, a Near-Field-

Communication (NFC) control, a wireless charging unit and the coils. In the current implementation, the processing module includes not only an MCU unit but also a 9-axis motion sensor and a BLE unit. The sensing module, communication module, output module or debug module can be integrated in the platform through the I²C, SPI, UART, I²S, and analog interfaces. Fig. 3 shows the appearance of our power module, processing module, and sensing module. Each module size is 35 mm × 35 mm. The processing module is a 32-bit ARM Cortex-M3 processor, supporting I²S, I²C, SPI, UART, and analog interfaces. The BLE communicates with the MCU by SPI interface. There are four universal connectors on each module, two on the top side and the other two on the bottom side. As mentioned in the previous section, all peripheral signals and power lines are delivered through these connectors.

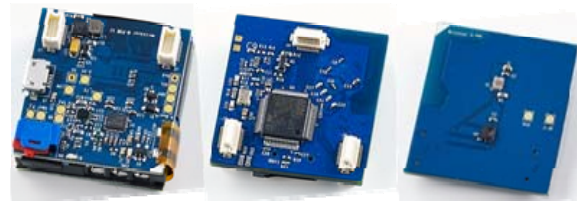


Fig. 3. The pictures of power module, and processing module and an temperature sensing module.

Another important feature of the proposed sensor platform is the mountable ability. For some applications, such as altitude detection, the sensor has to be tightly mounted on the object. For this purpose, we design packages for sensor boards. Fig. 4 shows packaged sensor bricks with different colors. Each sensor unit is given a unique color.



Fig. 4. Packages for attachable and wearable applications.

The mapping table of sensor units and their corresponding colors are described in Table 1. Besides the five colors mapping to five units, the purple ones are sensor mounts. Currently, there are mounts for bats, wrists, tripods, belts, flat surface, and magnetic surface.

Table 1. Package colors and sensor units.

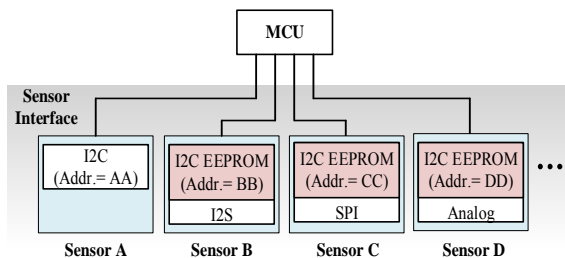
Color	Units	Color	Units
Blue	Analog sensing unit	Orange	Processing unit
Green	Digital sensing unit	Red	Power unit
Yellow	Communication unit	Purple	Sensor mount

3.2. Auto Sensor Identification Scheme

In this paper, an auto sensor identification scheme is proposed to detect which sensor is mounted on the platform automatically. The users can therefore launch the corresponding user's application according to the identified sensor type. This scheme utilizes the unique I²C address to identify the sensor type. A low-cost EEPROM only needs to be setup in the non-I²C sensing module. Moreover, a firmware initialization process is also adopted to enable the sensor identification mechanism.

Currently, the transmission interfaces of the sensor modules to MCU can be analog voltage output, I²C, I²S, UART and SPI, etc. Among these interfaces, the I²C device possesses a unique 7-bit address, which is used to appoint a certain I²C device to perform the operations of data write or read. Normally, the unique I²C device address is configured in advance, so that the address for each I²C sensor device can be different. This characteristic can thus be used to perform the sensor identification. For those non-I²C sensor devices, we can just add an I²C-interfaced EEPROM on the sensing module and use it to perform the sensor identification as the method used in I²C sensors.

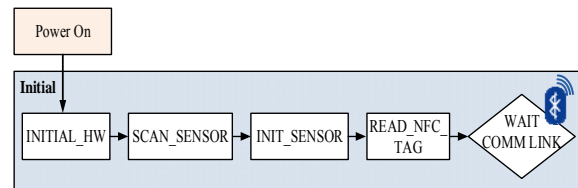
Fig. 5 shows the hardware architecture of our proposed sensor identification scheme. All the sensor signals are connected directly to the MCU. Each sensor with I²C interface owns its unique I²C address (Addr.), and for the rest of non-I²C sensing modules, we add an I²C EEPROM and configure it with a unique I²C address. Before the MCU starts to read sensor data, it scans the I²C address of the sensor first.

**Fig. 5.** The hardware architecture of the sensor identification scheme.

Since the I²C address of each sensor is set to be unique, it can be used to identify the sensor type. For example, if the result of I²C address scan is AA, the MCU identifies that the sensor is "Sensor A", and

then starts to read the sensor data with the I²C protocol; if the result of I²C address scan is BB, the MCU determines that the sensor is "Sensor B". Since the interface of Sensor B is I²S interface, the MCU starts to read the sensor data with the I²S protocol. The same flow can be applied to the other sensors. With this kind of hardware design, we can identify the sensor type automatically by using the unique I²C address.

To achieve the auto-sensor-identification function in our presented platform, the MCU needs to perform a firmware initial process, as shown in Fig. 6. First, we need to turn on the power of the flexible platform. The MCU then starts to perform the hardware initialization setting (INITIAL_HW) which initializes required peripheral controllers. After the hardware initialization completes, MCU starts to scan the number of sensors plugged-on and the sensor IDs (SCAN_SENSOR). The sensor IDs are defined based on the I²C address of the sensing module. When the scan process completes, MCU begins to initialize those sensors connected on it (INIT_SENSOR) and put the initial sensor data in the built-in table. In the following step, MCU reads the Media Access Control (MAC) address of the BLE device and writes it in the Near-field communication (NFC) Tag (READ_NFC_TAG). Then, the MCU enters the waiting status, and waits for the BLE connection and communication (WAIT COMM LINK).

**Fig. 6.** Firmware initialization process.

After the presented flexible platform finishes the firmware initialization process, it is ready to connect the smart phone App with the BLE. For now, there are two ways to establish BLE connection. Firstly, users can open the App in their smart phone and see all available proposed platforms around with different MAC addresses. Afterwards, users manually select the target device to establish the BLE connection. Secondly, users can use the NFC functions of both the smart phone and the platform to set up the connection. Once you move the NFC sensing area of the platform towards that of a smart phone, the smart phone detects the MAC address of the flexible platform through NFC tag thus knows which device to connect with. The BLE connection can thus be established automatically.

In the case of the BLE transmission between the smart phone and the platform, the smart phone acts as a master and the platform acts as a slave. After the BLE connection between the two devices is established, the smart phone starts to send

commands, while the platform starts to receive and decode the commands, then responds to the smart phone. Fig. 7 shows the handshaking flow for realizing auto-sensor-identification. The smart phone sends a command to be aware what sensors are plugged on the platform (Retrieve Sensor List), while the platform decodes the command and responds with the sensor IDs and quantity (Receive Sensor ID & No.). In this way, the smart phone can identify what sensors are present on the platform, and open the corresponding App page. The smart phone then sends a command to retrieve the measurement results of the sensors (Retrieve Sensor Data). The platform executes the command and transfers the sensor data to the smart phone (Receive Sensor Data). Consequently, the smart phone shows the received data on the App. Normally, the smart phone will send the Retrieve Sensor Data command continuously to get the latest sensor data.

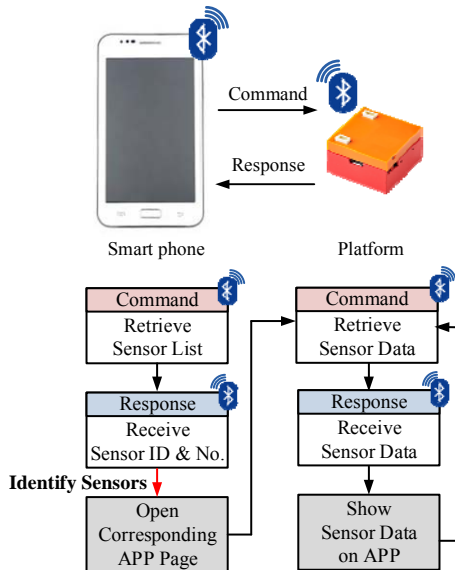


Fig. 7. Communication flow path between smart phone and platform.

4. Applications and Results

For demonstration of the proposed platform, an ambient temperature detection application and a CO₂ concentration sensor system are given as examples in this section. Users can develop more applications by combining different modules together. In the first example application, we use an I²C semiconductor-based temperature sensing module, a processing module, and a power module, as shown in Fig. 8.

The main difficulty of this application is the sensor calibration. Since each temperature sensor in the sensing module has slightly inaccuracy, we have to individually calibrate each sensor module. Fig. 9 shows the instrument of temperature forcing chamber [12] used to perform the sensor calibration. The temperature sensor system is first setup in this

temperature chamber. The corresponding sensor temperature can be recorded according to each target temperature set in the temperature chamber. In this way, we can therefore obtain the mapping table between temperature values of sensing module and the chamber.



Fig. 8. A temperature sensor system and its smart phone App.

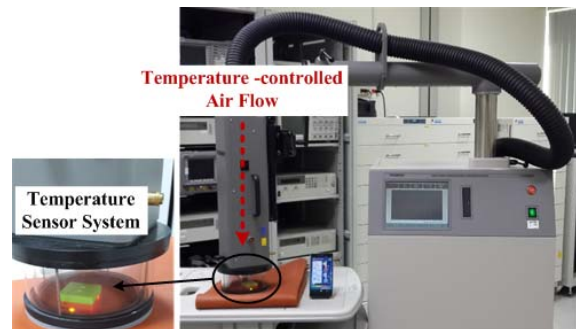


Fig. 9. Experimental environment of a temperature sensor system.

The relationship between the temperature in the sensing unit and the temperature in the chamber reading is shown in Fig. 10. The vertical axis indicates the target temperature set in the chamber, while the horizontal axis represents the corresponding temperature obtained from the sensing module in our platform. The temperature of each temperature sensor system can be modeled as a function of the temperature obtained in the chamber. The transfer function can be expressed by the following equation:

$$y = -0.0011x^2 + 1.1915x - 5.6884, \quad (1)$$

where y indicates the chamber readings (°C), and x represents the sensor readings (°C). The App can thus use the equation to quickly obtain a calibrated and accurate temperature. Fig. 11 shows the temperature errors before and after the calibration in different target temperature values. Before the calibration,

large errors mostly fall on the low and high ends of the temperature, i.e., 0 °C and 80 °C, and the error can be up to 6 °C. After the calibration, the temperature error is balanced in different target temperature values and the temperature error can be thus lower than 1.5 °C.

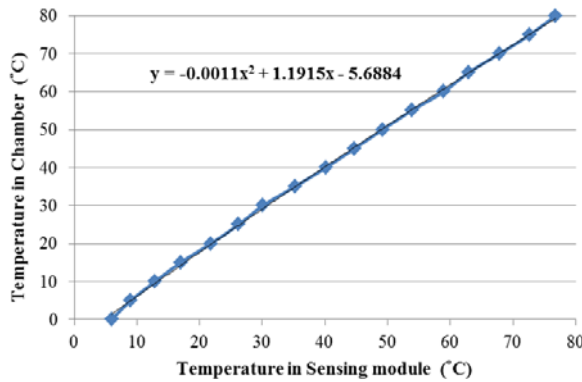


Fig. 10. Relationship between sensor readings and chamber readings with transfer equation.

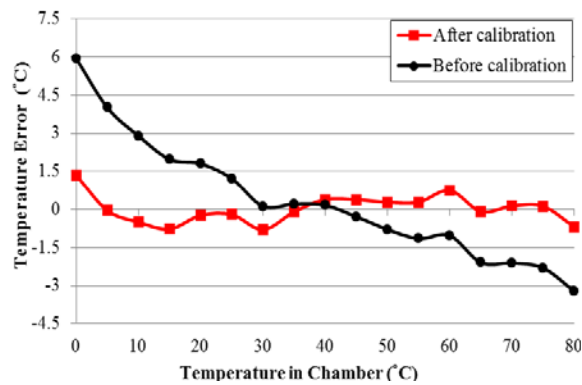


Fig. 11. Temperature errors in different target temperature values.

Most of the commercial sensors, like the temperature sensor just mentioned, have built-in readout circuits. In addition, they provide users with digital interfaces to easily configure the sensor or to retrieve the sensor data with an MCU. Furthermore, some even have automatic calibration mechanism that guarantees different sensor chips have similar output values. However, there are many analog interface sensors in the market, whose sensor signals are primitive and vary little in the form of current. We have adopted some sensors of this kind. To successfully retrieve the sensor value, we append a readout circuit that amplifies the output signal and transform it into the form of voltage for MCU's ADC controller to read. Besides, since the signals are primitive and not calibrated, the output will vary from chip to chip. We have to map the output voltage to a meaningful value for different chips.

We take the carbon dioxide (CO₂) sensor module for example to demonstrate how we calibrate this

kind of sensors. To obtain the corresponding relationship between the sensor output voltage and its actual meaning, we build a simple experiment environment as shown in Fig. 12. We use sealed plastic chamber and CO₂ gas cylinder to create a test environment, where the concentration of CO₂ is controllable. We place both the CO₂ sensor system and a commercial CO₂ monitor [13] in this airtight plastic chamber. In addition, we attach the CO₂ gas cylinder to the plastic chamber with a plastic soft tube. To increase the concentration of the CO₂ in the chamber, we turn on the air valve on the cylinder to allow CO₂ gas flow into the chamber. From the voltage output of the CO₂ sensor and the reading of the CO₂ monitor, we can therefore get the relationship between the CO₂ sensor readings and the CO₂ concentration.

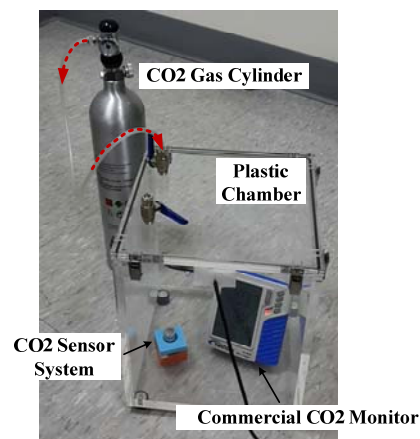


Fig. 12. Experiment environment of a CO₂ sensor system.

Each sensor needs to be calibrated individually due to the differences in their electrical characteristics. In Fig. 13, the vertical axis indicates the reading of the commercial CO₂ monitor, and the horizontal axis shows the corresponding voltage output of our CO₂ sensor module, green round nodes, red square nodes and blue triangle nodes are readings from three different sensors.

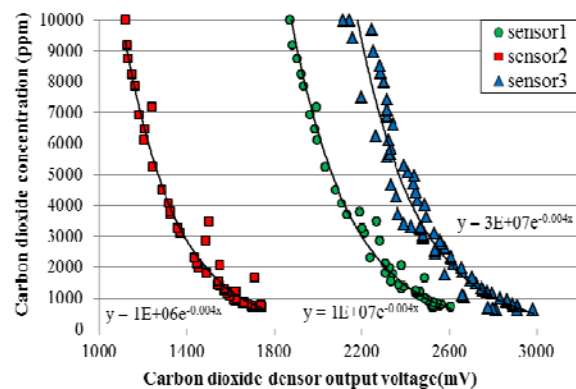


Fig. 13. Relationship between sensor readings and commercial CO₂ monitor.

It can be observed that the trends of three different sensors are similar, but there is a significant voltage bias. Each trend can be approximated with an equation, for example, the transfer equation of sensor1 is as follow:

$$y = 10^7 \cdot e^{-0.004x}, \quad (2)$$

where y represents the CO₂ concentration (ppm) in the chamber, and x represents the voltage output (V) of the sensor. User can therefore derive the CO₂ concentration from the voltage output with this equation easily.

To avoid the tedious work that individually measures each sensor and finds out the transfer function for each one, we build a simple calibration methodology which makes use of the characteristic of the CO₂ sensor, as shown in Fig. 13. Obviously, different initial voltages lead to different transfer equations, where the initial voltage is the sensor output voltage under 1000 ppm CO₂ concentration. We try to collect data from as many sensors as possible, and find that we can classify those sensors into different categories based on their initial output voltage. Each category has one specific transfer function which can be built in the smart phone App. Once you know the initial voltage of a certain CO₂ sensor, you know which equation it fits. The App page is as Fig. 14 shows. For now, the atmospheric CO₂ concentration is about 410 ppm. It is recommended to turn on the CO₂ sensor system at a ventilated space, which is likely to have the CO₂ concentration under 1000 ppm, and click the switch icon on our App to read the current CO₂ output voltage to know which category this CO₂ sensor belongs to.



Fig. 14. A CO₂ sensor system and its smart phone App.

In this section, an ambient temperature detection application is adopted to show this sensor platform with a sensor identification scheme can work correctly. The calibration method for this temperature sensor system is also presented. After that, we take our CO₂ sensor system to demonstrate how to

calibrate an analog-type sensor. The firmware/hardware flexibility can also be observed from Fig. 8 and Fig. 14 that once the sensor brick is changed, the corresponding App page will pop-up automatically.

Until now, we have developed several kinds of sensor systems [14] and can rapidly integrate more kinds of sensors with this modular firmware/hardware framework. For each developed sensor system, the sensor calibration is performed and the corresponding transfer function according to the calibration result is embedded in the delivered Apps.

In the following, we compare 3 kinds of sensor systems in terms of their extensibilities, flexibility, identification methods, and cost. As shown in Table 2, our presented sensor platform owns better extensibility and flexibility benefited from the modular design. Besides, our platform also has lower cost feature while implementing a sensor identification scheme since a low-cost EEPROM only needs to be setup in the non-I²C sensing modules.

Table 2. Comparisons of 3 kinds of sensor systems.

	[8]	[10]	This Work
Extensibility	Fair	Fair	Good
Flexibility	Fair	Fair	Good
Identification Method	TEDS	IMPI	EEPROM
Cost	Low	Fair	Low

5. Conclusion and Future Work

In this paper, we present a novel architecture of modular sensor platform. The most significant features of the proposed architectures are high flexibility and reusability. By stacking different modules together, users can create their own sensor system. In addition, a low-cost sensor identification scheme is also proposed to detect which sensor is mounted on the platform automatically. A temperature sensor system and a CO₂ sensor system are demonstrated to show that our presented platform works correctly. The comparisons of 3 kinds of sensor systems are also given in this paper regarding cost, extensibility and flexibility. Currently, this platform has been licensed to an industrial company and has become a commercial product. Users' feedback shows that the platform is very useful especially for the purposes of academic researches and industrial prototype verification. In the future, we will focus on providing more modules per users' requirement.

References

- [1]. C. Savaglio, G. Fortino, Mengchu Zhou, Towards interoperable, cognitive and autonomic IoT systems:

- An agent-based approach, in *Proceedings of the IEEE Conference World Forum on Internet of Things (WF-IoT)*, Dec. 2016, pp. 58-63.
- [2]. N. Matthys, *et al.*, μ PnP-Mesh: The plug-and-play mesh network for the Internet of Things, in *Proceedings of the IEEE Conference 2nd World Forum on Internet of Things (WF-IoT)*, December 2015, pp. 311-315.
 - [3]. A. Al-Fuqaha, M. Guizani, M. Mohammadi, Internet of Things: A Survey on Enabling Technologies, Protocols, and Applications, in *IEEE Communications Surveys & Tutorials*, Vol. 17, No. 4, June 2015, pp. 2347-2376.
 - [4]. J.-A. Stankovic, Research Directions for the Internet of Things, in *IEEE Internet of Things Journal*, Vol. 1, No. 1, March 2014, pp. 3-9.
 - [5]. C. Perera, A. Zaslavsky, P. Christen, Context Aware Computing for The Internet of Things: A Survey, in *IEEE Communications Surveys & Tutorials*, Vol. 16, No. 1, May 2013, pp. 414-454.
 - [6]. A. Spanbauer, A. Wehab, B. Hemond, I. Hunter, L. Jones, Measurement, instrumentation, control and analysis (MICA): A modular system of wireless sensor, in *Proceedings of the IEEE International Conference on Body Sensor Networks*, 2013, pp. 1-5.
 - [7]. Y.-M. Yusof, A.-M. Islam, S. Baharum, An experimental study of WSN transmission power optimisation using MICAz motes, in *Proceedings of the IEEE International Conference on Advances in Electrical Engineering (ICAEE)*, 2015, pp. 182-185.
 - [8]. R. Morello, Use of TEDS to Improve Performances of Smart Biomedical Sensors and Instrumentation, *Sensors Journal IEEE*, Vol. 15, Issue 5, 2015, pp. 2497-2504.
 - [9]. A. Fatecha, J. Guevara, E. Vargas, Reconfigurable architecture for smart sensor node based on IEEE 1451 standard, *IEEE Sensors*, 2013, pp. 1-4.
 - [10]. K. Mikhaylov, M. Huttunen, Modular wireless sensor and Actuator Network Nodes with Plug-and-Play module connection, *IEEE Sensors*, Nov. 2014, pp. 470-473.
 - [11]. K. Mikhaylov, A. Paatelma, Enabling modular plug&play wireless sensor and actuator network nodes: Software architecture, *IEEE Sensors*, 2015, pp. 1-4.
 - [12]. The temperature forcing system: Thermonics T-2500SE datasheet (https://www.atecorp.com/ATECorp/media/pdfs/data-sheets/Thermonics-T-2500SE_Datasheet.pdf)
 - [13]. The CO₂ monitor: Twintex TE-702D.
 - [14]. Y.-J. Hsieh, C.-C. Yang, Y.-J. Liu, W.-L. Lai, C.-M. Wu, C.-M. Huang, A Flexible Wireless Sensor Platform with an Auto Sensor Identification Scheme, in *Proceedings of the 11th International Conference on Sensor Technologies and Applications (SENSORCOMM' 2017)*, 10-14 September 2017, Rome, Italy, pp. 46-50.



Published by International Frequency Sensor Association (IFSA) Publishing, S. L., 2017 (<http://www.sensorsportal.com>).



International Frequency Sensor Association (IFSA) Publishing

ADVANCES IN SENSORS:
REVIEWS **1**

Modern Sensors, Transducers and Sensor Networks

Sergey Y. Yurish, Editor



Formats: printable pdf (Acrobat) and print (hardcover), 422 pages
ISBN: 978-84-615-9613-3,
e-ISBN: 978-84-615-9012-4

Modern Sensors, Transducers and Sensor Networks is the first book from the Advances in Sensors: Reviews book Series contains dozen collected sensor related state-of-the-art reviews written by 31 internationally recognized experts from academia and industry.

Built upon the series Advances in Sensors: Reviews - a premier sensor review source, the *Modern Sensors, Transducers and Sensor Networks* presents an overview of highlights in the field. Coverage includes current developments in sensing nanomaterials, technologies, MEMS sensor design, synthesis, modeling and applications of sensors, transducers and wireless sensor networks, signal detection and advanced signal processing, as well as new sensing principles and methods of measurements.

Modern Sensors, Transducers and Sensor Networks is intended for anyone who wants to cover a comprehensive range of topics in the field of sensors paradigms and developments. It provides guidance for technology solution developers from academia, research institutions, and industry, providing them with a broader perspective of sensor science and industry.

http://sensorsportal.com/HTML/BOOKSTORE/Advance_in_Sensors.htm

Repeater Protocol to Extend Signal Coverage

¹Eloísa Alexandre Nielsen Matthiesen, ²Omar Carvalho Branquinho,
³Guilherme Lopes da Silva and ⁴Paulo Cardieri

^{1,2}PUC Campinas, Rodovia Dom Pedro I, Km 136, s/n - Parque das Universidades,
Campinas – SP postal address, 13087-571, Brazil

^{3,4}UNICAMP, Cidade Universitária Zeferino Vaz - Barão Geraldo, Campinas - SP, 13083-970, Brazil
^{1,2}Tel.: 3343-7000, ^{3,4}Tel.: 3521-7000

E-mail: eloisa.anm1@puc-campinas.edu.br, branquinho@puc-campinas.edu.br,
gitalos@gmail.com, cardieri@decom.fee.unicamp.br

Received: 10 November 2017 /Accepted: 10 December 2017 /Published: 29 December 2017

Abstract: This paper describes the tests carried out with a Wireless Sensor Network in order to examine the radio coverage in the large space of a university food court. Due to the challenging environment, the development of a multi-hop protocol was necessary. The protocol deems a sensor node as a repeater to extend the signal reach. We used the Radiuino open-source platform to develop the protocol with the flexibility to design an address strategy in the packet. The preliminary results indicate that the protocol developed is feasible, stable and robust.

Keywords: WSN, Multi-hop topology, Routing protocol.

1. Introduction

Wireless Sensor Networks (WSNs) play an important role in Internet of Things (IoT) applications, having low-power sensors and easy installation. Indoor WSNs will be essential in smart homes, monitoring appliances and systems, such as closing the windows automatically based on the weather forecast [1].

Usually, a WSN consists of sensing nodes that report their results to a base station node. The base station node can process the data and monitor the network [2].

Two major types of topology are seen in WSN, one-hop and multi-hop, when the base node and the sensor node are geographically arranged in a way they can communicate directly the one-hop topology is used. On the multi-hop topology, the sensor nodes communicate with each other until the packet reaches the destination [3].

If a WSN needs to cover a wide area and the sensing nodes can not communicate directly with the base station node, a change in the topology of the nodes can be a solution, as seen in [4].

In this project, the sensing nodes were placed inside the food court of the Pontifícia Universidade Católica of Campinas in Brazil, and the base station node was placed in a laboratory. The distance between the base station node and the repeater node was 200 meters. Although is a small distance, it is in non-line-of-sight (NLOS), making the direct communication impossible.

To extend the range of the signal, a multi-hop protocol was created, using protocol stacks with five layers, akin to the Transmission Control Protocol/Internet Protocol (TCP/IP) concept.

The rest of the paper is structured as follows. In Section II, we discuss the state-of-the-art. In Section III, we present the payout of the WSN. Section IV shows preliminary results and we conclude in Section V with the outcome of the experiment.

2. State of the Art

WSNs can have a distributed or a centralized routing protocol. The majority of articles found in literature use a distributed routing protocol, such as [5-7], in which the protocol runs in a peer-to-peer mode, requiring all the nodes to possess processing power. Another used protocol is the Routing Protocol for Low Power and Lossy Networks (RPL), but it is also a distributed protocol [8], being different from the protocol shown in this project.

Although, by using the distributed protocol, the system does not depend on a centralized process unit. It also uses more energy, decreasing the equipment's lifetime. The base station node, in both cases, always needs to be connected to the Internet and to have processing power.

Another advantage of centralized routing is the simplicity of the network nodes. Only the base station node demands more complex processing capabilities. It also allows the development of the multi-hop protocol that would not be possible with a distributed routing management.

That simplicity makes it easier to meet the Quality of Service (QoS) parameters, like changing the routing path, changing radio attributes, such as power and channel. This ability is important for WSN operators, as seen in [9]. Without a centralized routing protocol, this operator can not attest to the QoS parameters.

Further, it is possible to change priorities, for example, the information importance of the nodes can change over time. Considering those aspects, the WSN of this paper has a centralized routing protocol.

3. Material and Methods

In this setup, we employed seven sensor nodes using the open *Radiuino* [10] platform, a library of Arduino that allows the user to work in five layers. This platform was chosen because it allows a change of network topology, differently from other platforms like *ZigBee* [11].

The logical view of the network is shown in Fig. 1. The base station node uses the first three layers (PHY, MAC and Net) while the sensors nodes use five layers (PHY, MAC, Net, Transp and App).

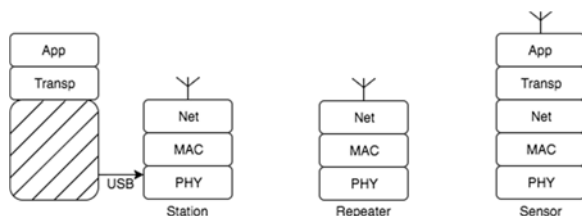


Fig. 1. Logical view of the WSN layers.

The communication modules used in the set up were BE990 and BE900, both homologated by the

Brazilian National Telecommunications Agency (ANATEL). These modules carry an ATmega328 processor and a CC1101 RF transceiver with a bandwidth filter, operating in the Industrial, Scientific and Medical (ISM) frequency of 915 MHz. The BE990 module also has a CC1190 that integrates a power amplifier (PA) with a low-noise amplifier (LNA) for improved wireless performance [12].

The communication module BE900 can reach up to 100 meters indoors and 500 meters outdoors. The communication module BE990 can reach up to 1000 meters indoors and 8000 meters outdoors. Those distances are considering it is in line-of-sight (LOS), which we did not have in this project.

One sensor node was programmed to work only as a repeater, receiving data from the base station node and forwarding the packet to the other five sensor nodes. For a better performance, the base station node, the repeater node and the Sensor 5 node used the BE990 (16 dBm) module, while sensors nodes from 1 to 4 used BE900 (10 dBm). The positions of the sensor nodes in the food court can be shown in Fig. 2.

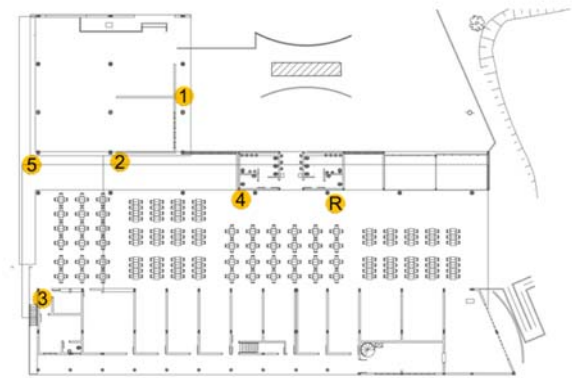


Fig. 2. Position of the sensors.

In the layout of the system, the base station node is B, the repeater node R and the sensors are S1, S2, ..., Sn. Fig. 3 shows this layout.

Radiuino packet has 52 bytes. The first 4 layers have 4 bytes each, forming a 16 bytes header. The rest of the packet belongs to the Application layer. The remaining 36 bytes are split into two halves, 18 bytes to measure proprieties and 18 bytes to control processes.

The WSNs have a centralized protocol where the base station node is responsible for the routing protocol. The routing protocol approach is hierarchical. The route is chosen trough the ID of the nodes.

The protocol algorithm uses the bytes from 8 to 11 (bytes of the Net layer header). In byte 8 is placed the address (ID) of the next node that is to receive the packet; in byte 9 goes the address of the final node in downlink; in byte 10 goes the ID of the sender in the hop and in byte 11 goes the address of the final node in uplink.

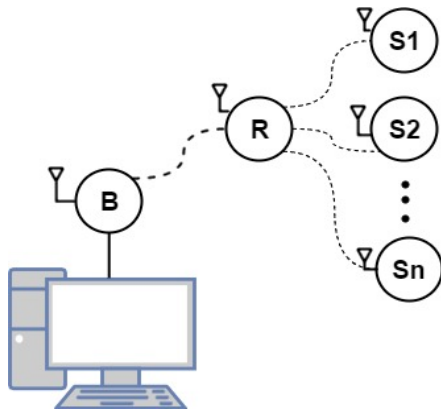


Fig. 3. Layout of the system.

An example of the protocol where the base station node's ID is 0, the repeater node's ID is 20 and the sensor node's ID is 1 is shown in Fig. 4. The protocol was designed to work only with the message in the packet, so the node sensor reacts, changing the addresses for the next hop. The advantage of this strategy is that it allows the sensor nodes to be scalable.

The repeater node, which is predefined, works with bytes 8 and 10, it inputs the data of byte 8 in byte 10 (its address) and inputs the data of byte 9 in byte 8 (the sensor address). The sensor node swaps byte 8, for the data, in byte 10, and swaps byte 9, for the data, in byte 11. After that, it inputs its own address (ID = 1) in bytes 10 and 11.

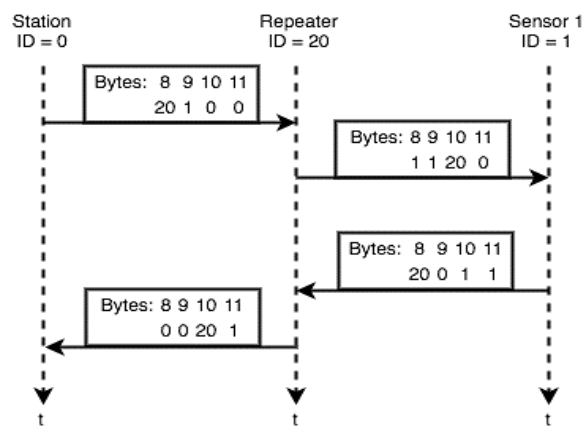


Fig. 4. Sequence diagram of the packet.

4. Preliminary Results

The first test lasted for six hours, from 1 pm to 7 pm, while the received signal strength indicator (RSSI) of down and uplink were measured. Fig. 5 shows the RSSI of Sensor 1 node as a function of time. The sensor's position was crucial in this case, between the repeater node and the Sensor 1 node there was a lot of obstacles and passers-by. Therefore, this sensor had the lowest RSSI and lost about 13 % of its packets.

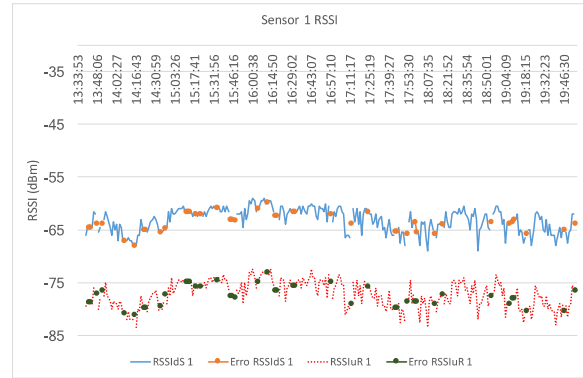


Fig. 5. Chart of RSSI of Sensor 1.

The solid line is the downlink RSSI, that is, the RSSI that the sensor is measuring. The dotted line is the uplink RSSI, that is, the RSSI measured by the repeater node. The solid points showing in both lines are the errors, when the packet was lost in transmission.

The Sensor 2 node was in a better position, only lost about 5 % of the packets. Its RSSI, shown in Fig. 6, was the second best from all the sensor nodes. It also helped that didn't had many passers-by.

The position of the Sensor 3 node also influences the RSSI stability. It was near the employee's entrance, making Sensor 3 node less susceptible to the food court flux, losing less than 3 % of it packets (Fig. 7).

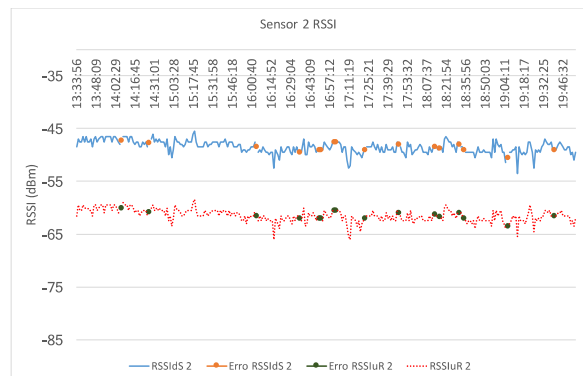


Fig. 6. Chart of RSSI of Sensor 2.

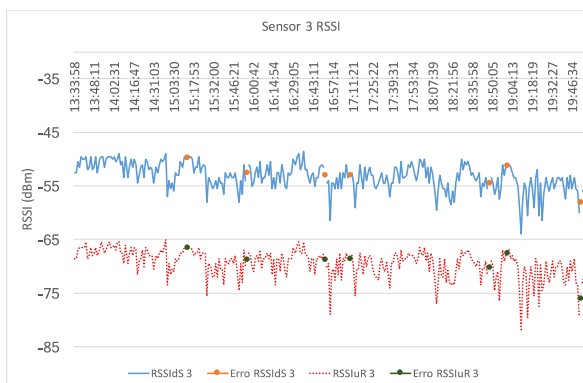


Fig. 7. Chart of RSSI of Sensor 3.

Sensor 4 node was the closest to the repeater. Still wasn't in line of sight because it had two pillars between them.

The disturbance in RSSI, Fig. 8, it's due the toilets behind the sensor nodes and the people passing through, it had the smallest packet loss, less than 2 %.

The discrepancy shown is the result of different communication modules in the repeater node and in the Sensor 1 to 4 nodes.

The Sensor 5 node used the BE990 module, the same as the repeater, that's why it's downlink RSSI and uplink RSSI, shown in Fig. 9, are overlapping.

Its position reflects the variation of the chart, it was between both entrances to the food court.

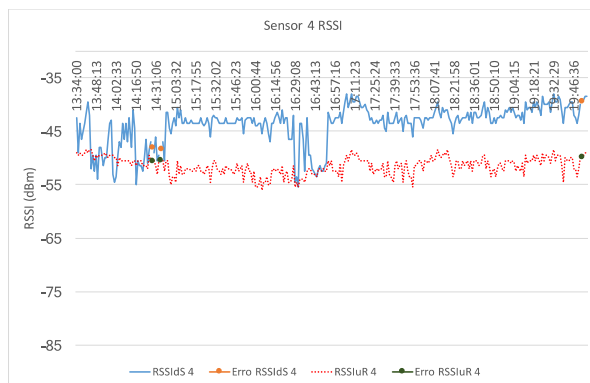


Fig. 8. Chart of RSSI of Sensor 4.

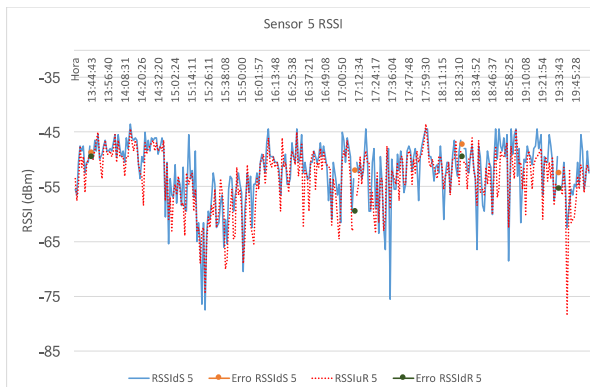


Fig. 9. Chart of RSSI of Sensor 5.

5. Conclusion

The purpose of this project was to cover university's food court. A pretest was made trying the direct communication between Sensor 3 node and the base station node, which was impossible due numerous obstacles between them.

After the development of the protocol and the placement of the repeater node, the communication was possible.

Sensor 1 to 4 nodes follows a Gaussian distribution, while Sensor 5 node follows a Rayleigh distribution. This data is important to manage the WSN and take decisions about it.

The RSSI improvement that is shown in Sensor 3, 4 and 5 nodes can be attributed to the different location and to different communication modules.

For future projects, the repeater will have two communication modules in it, therefore, having two antennas. That will allow a bigger expansion of the WSN.

It will also use the Raspberry Pi 3 with a Zabbix server working as a Proxy Manager, sending all the data to the Internet.

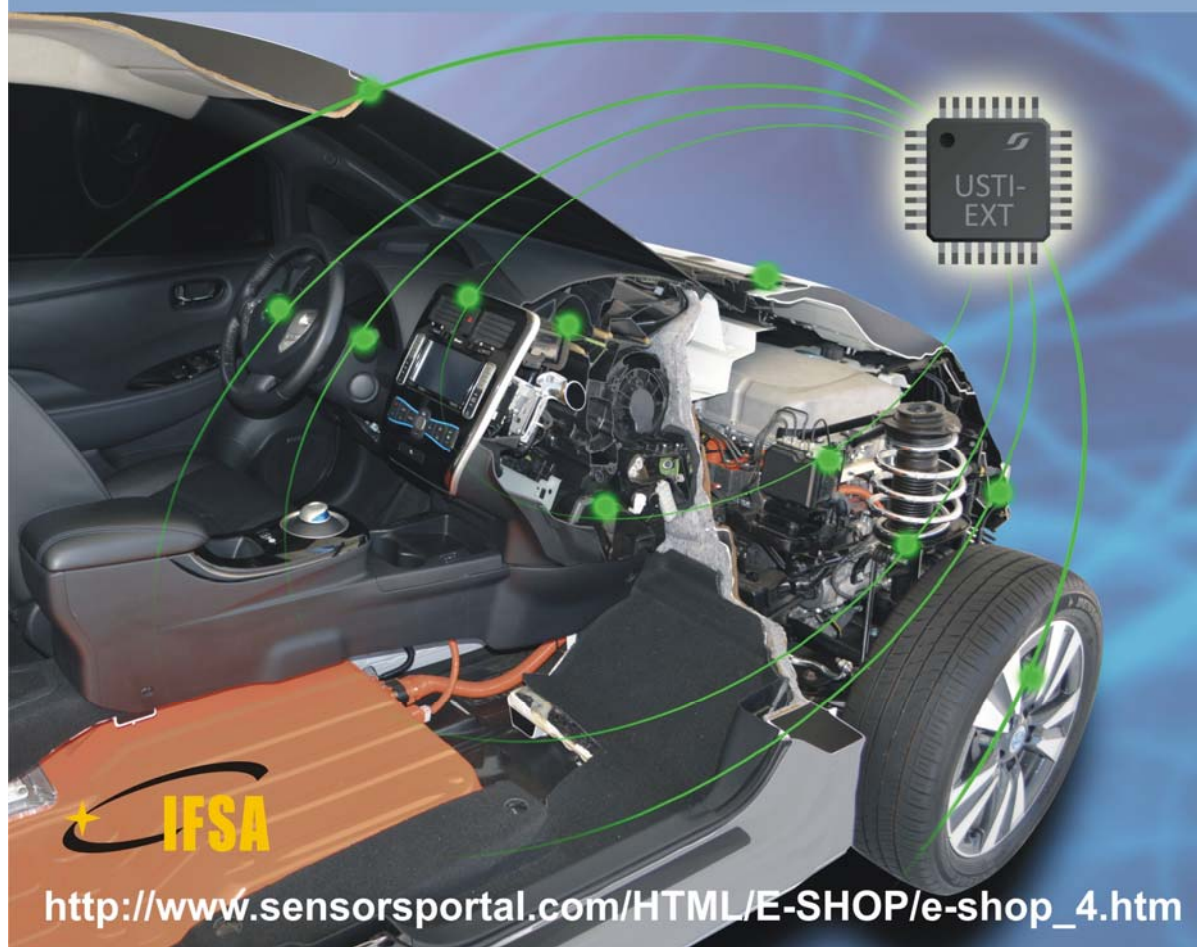
Using Zabbix, the statistics will be easier, being compiled while the tests are running, estimating the average of the signal and its standard deviation.

References

- [1]. A. Al-Fuqaha, M. Guizani, M. Mohammadi, M. Aledhari, M. Ayyash, Internet of Things: A Survey on Enabling Technologies, Protocols, and Applications, *IEEE Communications Surveys & Tutorials*, Vol. 17, No. 4, 2015, pp. 2347–2376.
- [2]. L. Atzori, A. Iera, G. Morabito, The Internet of Things: A survey, *Computer Networks*, Vol. 54, No. 15, 2010, pp. 2787–2805.
- [3]. W. Dargie, C. Poellabauer, Fundamentals of Wireless Sensor Networks: Theory and Practice, *John Wiley & Sons, Chichester, West Sussex, UK*, 2010.
- [4]. E. Matthiesen, O. Branquinho, G. Silva, P. Cardieri, Multi-Hop Protocol to Extend Signal Coverage, in *Proceedings of the 11th International Conference on Sensor Technologies and Applications (SENSORCOMM' 2017)*, 10-14 September 2017, Rome, Italy, pp. 37–39.
- [5]. K. Cheng, K. Lui, Y. Wu, V. Tam, A Distributed Multihop Time Synchronization Protocol for Wireless Sensor Networks using Pairwise Broadcast Synchronization, *IEEE Transactions on Wireless Communications*, Vol. 8, No. 4, 2009, pp. 1764–1772.
- [6]. E. Alnawafa, IMHT: Improved MHT-LEACH Protocol for Wireless Sensor Networks, in *Proceedings of the 8th International Conference on Information and Communication Systems (ICICS)*, 2017, pp. 246–251.
- [7]. H. Shafieirad, R. S. Adve, Opportunistic Routing in Large-Scale Energy Harvesting Sensor Networks, in *Proceedings of the IEEE Globecom Workshops (GC Wkshps)*, 2016.
- [8]. M. O. Farooq, C. J. Sreenan, K. N. Brown, T. Kunz, RPL-based routing protocols for multi-sink wireless sensor networks, in *Proceedings of the IEEE 11th Int. Conf. Wirel. Mob. Comput. Netw. Commun. WiMob*, 2015, pp. 452–459.
- [9]. G. Gaillard, D. Barthel, F. Theoleyre, F. Valois, Service Level Agreements for Wireless Sensor Networks: A WSN operator's point of view, in *Proceedings of the IEEE Network Operations and Management Symposium (NOMS)*, 2014, pp. 1–8.
- [10]. Radiuino, Teoria do Radiuino, 2016. [Online]. Available: <http://radiuino.cc/projetos/>. [Accessed: 25-May-2017].
- [11]. A. Elahi, A. Gschwendner, ZigBee wireless sensor and control network, *Prentice Hall*, 2010.
- [12]. Texas Instruments, 850 – 950 MHz RF Front End, 2009.

Universal Sensors and Transducers Interface (USTI-EXT) Series of IC for Automotive Applications

- Precision measurements of frequency-time parameters of sensor outputs
- rpm measurements
- Cx, Rx and Resistive Bridges measurements
- Extended temperature range from -55°C to $+150^{\circ}\text{C}$
- I²C, SPI and RS232



A Fine-Grained Visible Light Communication Position Detection System

^{1, 2, 3} M. Vieira, ^{1, 2} M. A. Vieira, ^{1, 2} P. Louro, ^{1, 2} A. Fantoni and ^{1, 4} P. Vieira

¹ ADETC/ISEL/IPL, R. Conselheiro Emídio Navarro, 1959-007 Lisboa, Portugal

² CTS-UNINOVA Quinta da Torre, Monte da Caparica, 2829-516, Caparica, Portugal

³ DEE-FCT-UNL Quinta da Torre, Monte da Caparica, 2829-516, Caparica, Portugal

⁴ Instituto das Telecomunicações, Instituto Superior Técnico, 1049-001, Lisboa, Portugal

¹ Tel.: +351218317000, fax: +351218317114

E-mail: mv@isel.ipl.pt

Received: 10 November 2017 /Accepted: 10 December 2017 /Published: 29 December 2017

Abstract: An indoor positioning system where trichromatic white Light Emitting Diodes (LEDs) are used both for illumination proposes and as transmitters and an optical processor, based on a-SiC:H technology, as mobile receiver is presented. On-Off Keying (OOK) modulation scheme is used, and it provides a good trade-off between system performance and implementation complexity. The relationship between the transmitted data and the received digital output levels is decoded. LED bulbs work as transmitters, sending information together with different identifiers, IDs, related to their physical locations. A triangular topology for the unit cell is analysed, and a 2D localization design, demonstrated by a prototype implementation, is presented. Fine-grained indoor localization is tested. The received signal is used in coded multiplexing techniques for supporting communications and navigation concomitantly on the same channel. The location and motion information is found by mapping the position and estimating the location areas.

Keywords: a-SiC: H technology, Optical sensor, Transmitter, Receiver, Demultiplexer, WDM, Indoor positioning.

1. Introduction

Research on indoor localization and navigation has long been a popular topic. Localization is one of the essential modules of many mobile wireless applications. Although Global Positioning System (GPS) works extremely well for an open-air localization, it does not perform effectively in indoor environments, due to the inability of GPS signals to penetrate through in-building materials. Therefore, precise indoor localization is still a critical missing component and has been gaining growing interest from a wide range of applications, e.g., location detection of assets in a warehouse, patient tracking

inside the hospital, and emergency personnel positioning in a disaster area. Although many methods are available, such as WiFi-based [1-2] and visual indoor topological localization [3-4], they require dense coverage of WiFi access points or expensive sensors like high-performance cameras to guarantee the localization accuracy. In the sequence, we propose to use modulated visible light (carried out by white low cost Red, Green, and Blue, RGB, LEDs) to provide globally consistent signal-patterns to perform indoor localization.

We present a 2D localization design, demonstrated by a prototype implementation. The main issue is to divide the space into spatial beams originating from

the different light sources, and identify each beam with a unique time sequence of light signals. The receiver, equipped with a light sensor, determines its spatial beam by detecting the light signals, followed by optimization schemes to refine its location within the beam. Fine-grained indoor localization can enable a multitude of applications. In supermarkets and shopping malls, exact location of products can greatly improve the customer's shopping experience and enable customer analytics [5-6].

Visible Light Communication (VLC) is a data transmission technology [7-9] and [10], based on the use of visible light. Due to the combination of illumination and communication, a lot of research has been performed for VLC applications [11-12] and [13]. With this technology, it is possible to achieve simultaneous illumination and data transfer by means of LEDs. This functionality has given rise to VLC, where LED luminaires are used for high-speed data transfer [14-15]. Moreover, both interior lighting of a room and data transfer will be achieved without the need of an additional communication system. Aside from integrability with the illumination system, VLC has many advantages compared with other radio based technologies: radio frequency (RF) interference free, RF interference immune, safe for human health, and more secure [16]. Luminaires equipped with multi colored LEDs can provide further possibilities for signal modulation and detection in VLC systems [17].

The use of Red-Green-Blue (RGB) LEDs is a promising solution to high-speed VLC systems as they offer the possibility of the Wavelength Division Multiplexing (WDM), which can greatly increase the transmission data rate. In the recent past, we have developed a WDM device that enhances the transmission capacity of optical communications in the visible range. The device was based on tandem a-SiC:H/a-Si:H pin/pin light controlled filter with two optical gates that select the different channel wavelengths. When different visible signals are encoded in the same optical transmission path [18-19] the device multiplexes the different optical channels, and performs different filtering processes: amplification, switching, and wavelength conversion. Finally, it decodes the encoded signals recovering the transmitted information.

This paper provides detailed characteristics of various components in a VLC system such as transmitter and receiver, multiplexing techniques, system design and visible light sensing and applications, such as indoor localization and motion recognition. A 2D localization design, demonstrated by a prototype implementation will be analyzed. Fine-grained indoor localization is tested. The proposed system, composed data transmission and indoor positioning, involves wireless communication, smart sensor and optical sources network, which constitutes a transdisciplinary approach framed in cyber-physical systems.

This paper is organized as follows. In Section I, an introduction is presented. In Section II, the system configuration and its characterization is explained.

In Section III, indoor positioning is analyzed while, in Section IV, some navigation system examples are shown. Finally, Section V summarizes the conclusions.

2. System Configuration and Characterization

2.1. Transmitter

The positioning system's topology is a self-positioning system in which the measuring unit is mobile. This unit receives the signals of several transmitters in known locations, and has the capability to compute their location based on the measured signals. LED bulbs work as transmitters, sending information together with different IDs related to their physical locations. Each LED lamp transmits data during the time slot it occupies, i.e., the individual LED lamp transmits its own data depending on the area it locates. An optical receiver inside the mobile terminal extracts the location information to perform positioning and, concomitantly, the transmitted data from each transmitter.

The beam area of light radiation of an LED, in the array, has the form of a circle. The estimate distance from the ceiling is used to generate a circle around each transmitter (see Fig. 1) on which the device must be located in order to receive the transmitted information (generated location and coded data). To receive the information from several transmitters, the device must be positioned where the circles from each transmitter overlap, producing at the receiver a MUX signal that, after demultiplexing, acts twofold as a positioning system and also a data transmitter. The receiver detects one or more signals from light beams of different LEDs. If the signal it receives is only from one LED, the coordinates of the LED are assigned the device's reference point. If the device receives multiple signals, i.e., if it is in the overlapping region of two or more LEDs, it finds the centroid of the received coordinates and stores it as the reference point. Thus, the overlap region is used as an advantage to increase the accuracy in position estimation because more overlapping region means more reference points.

The proposed system considers a set of LED bulbs on the ceiling and a mobile terminal. The ceiling plan for the LED array layout of a unit cell is shown in Fig. 1(a) (LED array = RGBV color spots). A triangular topology was considered for the unit cell (Fig. 1(a)). The proposed arrangement employs four modulated LEDs (RGBV), three of them (RGB-LED) are located at the vertices of an equilateral triangle and a fourth one (V) is located at its centroid. The geometric scenario used for calculation uses a calibration grid (triangular), smaller, to improve its practicality. Here, a beam radius of 2 cm was assumed for each LED. The chips of the white LEDs can be switched *on* and *off* individually in a desired bit sequence and are 3 cm away from the receiver. For each RGB-LED, only one chip (R, G, B) is modulated in order to broadcast the

specific information (payload data). The extra violet LED sends the network cell's. We name point 1 where all the four locations overlap. Points 2, 3 and 4 refer to the locations with three overlaps, points 5, 6 and 7 with two overlaps, and finally 8, 9 and 10 where no overlap occurs. The grid size was chosen in order to have the triangle inscribed inside the generated circle estimated around the violet transmitter.

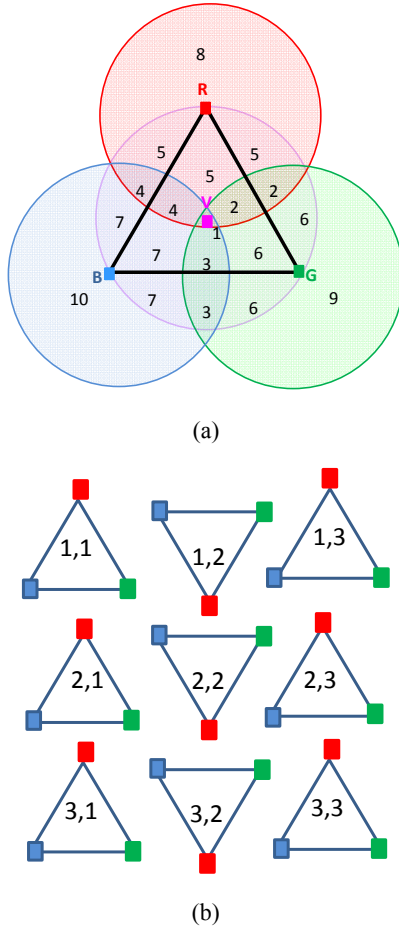


Fig. 1. The next closest grid positions in lighting design.
(a) unit navigation cell, (b) network cell's.

The calculation of the areas underneath each optical pattern was computed assuming the geometry of Fig. 1(a), where the coordinates of each emitter are: $V(0,0)$, $R(0, r)$, $G(\frac{\sqrt{3}r}{2}, \frac{r}{2})$ and $B(\frac{-\sqrt{3}r}{2}, \frac{r}{2})$.

This was evaluated integrating the shadowed area of each region, assuming a circular irradiation flux for each emitter of radius r [20].

The obtained values are displayed in Table 1. These values allow the evaluation of the accuracy on the determination on the spatial resolution of the positioning system.

The triangular topology allows the use of clusters cells and can be applied on large surfaces (Fig. 1(b)). A large-dimension indoor environment, like a supermarket or a library can be considered by dividing the room into unit navigation cells with an appropriate side length. In Fig. 1(b), the unit cell was repeated in

the horizontal and vertical directions in order to have an $m \times n$ matrix of unit cells that fill all the space and gives the geographical position assigned to each unit cell. The violet signal carries the ID of the unit cell. Cell's IDs are encoded as rows and columns [rrrr; cccc] using a binary representation for decimal number. For instance, number 11 is coded as "1011" ($2^3+0+2^1+2^0$). In case of the presented cell in Fig 1(a) being part of the cluster (Fig. 1(b)) the ID from the cell located at row 1: column 1, will be [0001 0001], whereas in case of row 2 column 3, an ID_BIT [0010 0011] will be send by the violet LED. With perfect information, this method will give an exact, unique answer, i.e., the cell location in the cluster and for each unit navigation cell, the single region at the intersection of the circles.

Table 1. Areas underneath each optical pattern.

Zone	Area
2 3 4	$\frac{2\pi - 3\sqrt{3}}{6}r^2$
5 6 7	$\frac{\sqrt{3}}{2}r^2$
8 9 10	$\frac{2\pi + 3\sqrt{3}}{6}r^2$

As stated, the employment of trichromatic RGB LEDs as transmitters offers the possibility of wavelength division multiplexing (WDM) which can greatly increase the transmission data rate. The optical characteristics of the commercial white LEDs are summarized in Table 2. We have adjusted the drive currents around 2 mA, in order to have beam radius, for the generation location, of 2 cm.

Table 2. White LEDs' optical characteristics at 25 °C.

	Red (R)	Green (G)	Blue (B)
Dominant wavelength (nm)	619 - 624	520 - 540	460 - 480
Luminous intensity (mcd)	355 - 900	560 - 1400	180 - 505
Spectral bandwidth @ 20 mA	24	38	28

Light produced by the LEDs is assumed to propagate as a Gaussian Beam. Under this assumption, in agreement with the LED's datasheet used for the laboratory experimental measurement, the electric field intensity propagates in free space in its unique fundamental model.

Light intensity (I) at distance z emitted by a LED with wavelength λ and divergence θ , can be calculated recurring to the following expression [21]:

$$I = I_0 \left(\frac{\omega_0}{\omega} \right)^2 \exp \left(-2 \left(\frac{r}{\omega} \right)^2 \right), \quad (1)$$

where I_0 is the emitted light intensity, r is the distance from the central axis, ω_0 is the beam waist and ω is the spot size parameter at a distance z :

$$\omega_0 = \frac{2\lambda}{\pi\theta}, \quad (2)$$

$$\omega = \omega_0 \sqrt{1 + \left(\frac{z}{z_R} \right)^2} \quad (3)$$

calculated as a function of the Rayleigh distance z_R :

$$z_R = \frac{\pi\omega_0^2}{\lambda} \quad (4)$$

The maximum value of light intensity, at the center of the light beam (corresponding to $r=0$) can be expressed as:

$$I_{\max} = I_0 \left(\frac{\omega_0}{\omega} \right)^2 \quad (5)$$

Applying this model, we calculate the light intensity projected on the target screen based on the LED characteristics: wavelength, intensity and divergence angle (60°).

In Fig. 2, the simulation of the projected light intensities is shown for the unit triangular cell. The coordinates of the LEDs, in centimeters, were set as: V (0, 0), R (0, 2), B (-1.72, -1), G (1.72, -1).

To transmit the data, an On-Off Keying (OOK) code was used.

In Fig. 3, an example of the digital signals (RGBV codeword) used to drive the LEDs is displayed. In this example, the ID_BIT [0101 0011] was sent by the violet LED and corresponds to the unit cell (5,3). The red, the green and the blue LED send the payload data.

2.2. Receiver

The optoelectronic sensor is a 1×1 cm double pin heterostructure produced by PECVD (Plasma Enhanced Chemical Vapor Deposition) sandwiched between two transparent conductive contacts (TCO). The device configuration is shown in Fig. 4. In the heterostructure, p-i(a-SiC:H)-n/p-i(a-Si:H)-n [17], the intrinsic layer of the front p-i-n photodiode is built of a-SiC:H while the back intrinsic layer is based on a-Si:H. As a result, both front and back diodes act as optical filters confining, respectively, the optical carriers resultant from the blue and red wavelength photons apart, while the optical carriers generated by the green wavelength photons are absorbed across both.

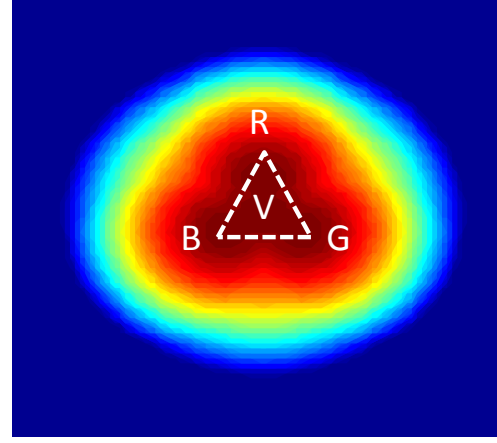


Fig. 2. Simulated light intensity in a triangular unit cell.

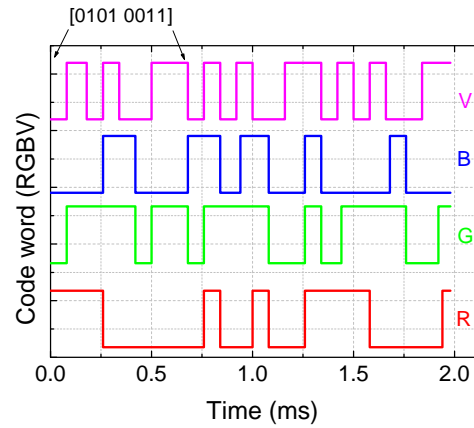


Fig. 3. Representation of the original encoded message [R G B V] ascribed to the cell (5,3).

The device operates within the visible range using for data transmission modulated low power light supplied by a violet (V), and three trichromatic LEDs. The RGB-LED are used together for illumination proposes and individually, one only chip, to transmit the channel location and data information. So, a polychromatic mixture of red, green, blue and violet; $\lambda_{R,G,B,V}$; pulsed communication channels (input channels, transmitted data) are combined together, each one with a specific bit sequence and absorbed accordingly to their wavelengths (see arrow magnitudes in Fig. 4). The combined optical signal (multiplexed signal; received data) is analyzed by reading out the generated photocurrent under negative applied voltage (-8 V), with and without 390 nm background lighting, applied either from front or back sides [18].

In Fig. 5, the measured signal due to the overlap of the four independent input channels (MUX signal) is displayed without applied optical bias (dark) and under front and back irradiation. On the top the driving signal applied to each R, G, B and V LED is presented, the bit sequence was chosen in order that when one channel is *on* the others are always *off*.

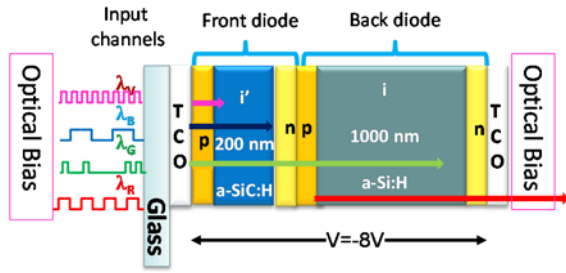


Fig. 4. Double pin configuration and device operation.

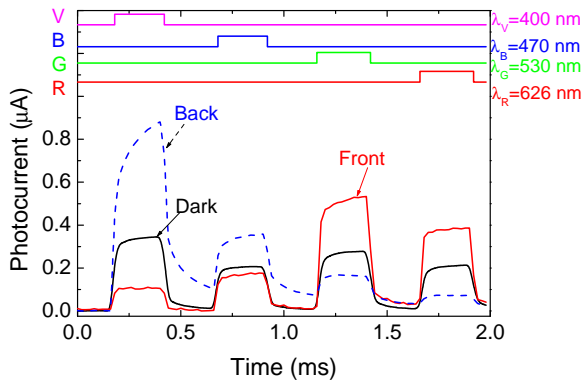


Fig. 5. Transient photocurrent without (Dark) and under front (Front) and back (Back) 390 nm irradiation.

Data analysis shows that the photocurrent depends, under irradiation, on the irradiated side and on the incoming wavelength, the irradiation side acting as the optical selector for the input channels. Under front irradiation, the long wavelength channels are enhanced and the short wavelength channels quenched while the opposite occurs under back irradiation. Note that, under back lighting, as the wavelength increases the signal strongly decreases while the opposite occurs under front irradiation. This nonlinearity is the main idea for decoding the MUX signal at the receiver.

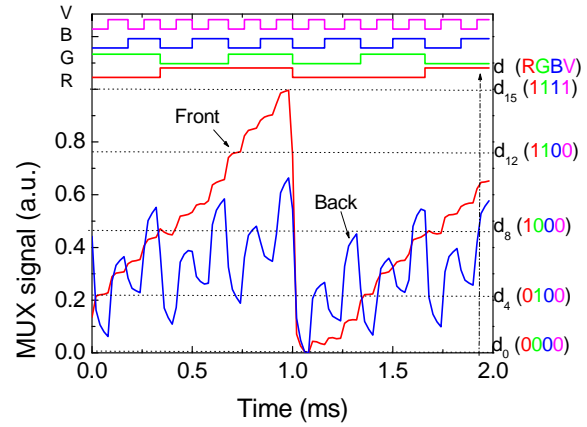
3. MUX/DEMUX Device

For the unit cell, and with the receiver at position generation 1 (see Fig. 1), the photocurrent generated by all the input channels was measured under front and back lighting.

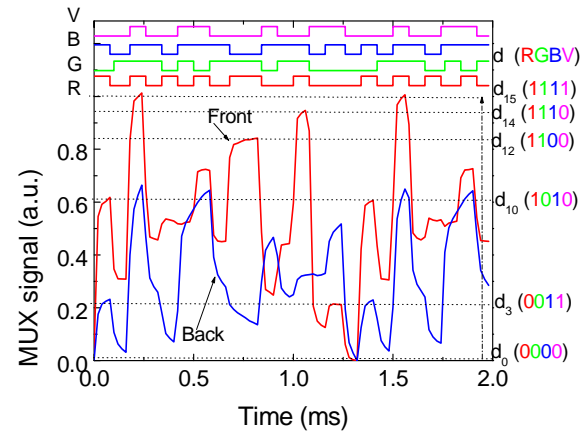
The bit sequence of each channel was adjusted in order to have all the *on/off* possible states in an ordered sequence. The photocurrent was normalized to its maximum value. In Fig. 6a this “standard” MUX signal is displayed, under front and back irradiation. In Fig. 6(b) a random sequence is shown under the same conditions. In the top of the figures, the digital decoded information is shown.

The MUX signal under front irradiation is quite different from the one under back lighting. Results from the “standard” sequence (Fig. 6(a)) show that for each possible 2^4 *on/off* states, it corresponds a well-defined level. Under front irradiation, sixteen separate

levels are detected (d_0 - d_{15}) and correspond to all possible combinations of the *on/off* states, concerning the input channels. Under back irradiation, the MUX signal trend is very close to the one of the violet input channel and allows the readout of the cell's ID-BIT. In Fig. 6(b), some *on/off* states are missing, but, as expected, the behavior is the same: front irradiation enhances the red/green channels while under back irradiation the violet channel is readout.



(a)



(b)

Fig. 6. MUX signal under front and back irradiation. On the top the transient optical signal from each RGBV are decoded.

The functional principle to decode the transmitted information is based on the adjustable penetration depths of the photons into the front and back diodes (see Fig. 4), which is linked to their absorption coefficient in the intrinsic front and back collection areas. Front irradiation is strongly absorbed at the beginning of the front diode and, due to the self-bias effect, increases the electric field at the back diode, where the red incoming photons are absorbed, resulting in an increased collection. Under back irradiation, the electric field decreases, mainly at the i-n back interface, quenching the red signals and enhancing the blue /violet ones (see Fig. 5).

The algorithms to decode the coded information are relatively straight-forward since the background acts as selector that chooses one of the 2^n sublevels, being n the number of transmitted channels, and associates to each level an unique n -bit binary code [22]. The combination of the four channels under irradiation, denotes the presence of all the possible sixteen (2^4) on/off states, clearly observed in Fig. 6(a). Here, each level is ordered by the correspondent gains in a 4 bit binary code $[X_R, X_G, X_B, X_V]$, with $X=1$ if the channel is *on* and $X=0$ if it is *off*. In Fig. 6, in the right side, it is presented the selection index for the 16-element look-up (d_0 - d_{15}) table, each one in its 4-bit binary code (RGBV) [18]. Therefore, by assigning each output level to an n digit binary code weighted by the optical gain of each channel, the signal can be decoded. A maximum transmission rate capability of 30 kbps was achieved in a four channel transmission using this device. In the top of the figure, the digital decoded information is shown.

4. Indoor Positioning

In Fig. 7, the MUX signals with the receiver at the nearest positions 2 and 6, under front lighting, are presented. In Fig. 7 (a), the “standard” bit sequence (Fig. 6 (a)) was analyzed, while in Fig. 7(b), the random one (Fig. 6 (b)) was imposed.

Along a n channel WDM message transmission, 2^n on/off states are possible during an interval of time T (see Fig. 6 and Fig. 7). The position of the device during the receiving process will be given by the highest detected level, i. e., the level where all the n received channels are simultaneously *on* [23]. So, the four (RGBV, Fig. 6), the three (RGV, Fig. 7) or two (GV, Fig. 7) received messages will be given by the decoding of the n received channels while the device position will be confirmed by looking at the highest level (dot-dash line).

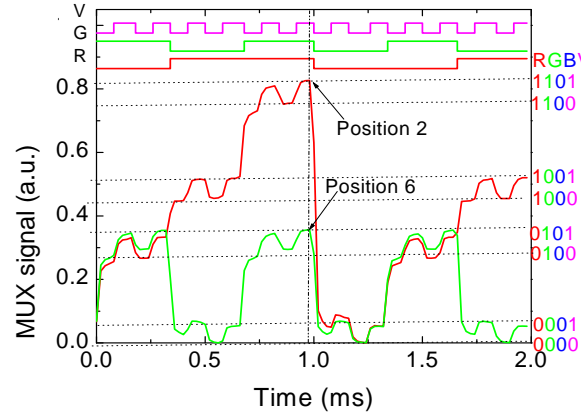
The position ID for the analyzed examples will appear as [1111] (point generation 1, ([1111] in Fig. 6) or [1101] (point generation 2, in Fig. 7), and [0101], (point generation 6, in Fig. 7). In Fig. 7(b), the eight first bits of the violet packet will give the 8-bit address of the unit cell, [0010 0110], that is located at line 2, column 6 from the network.

5. Navigation Data Bits

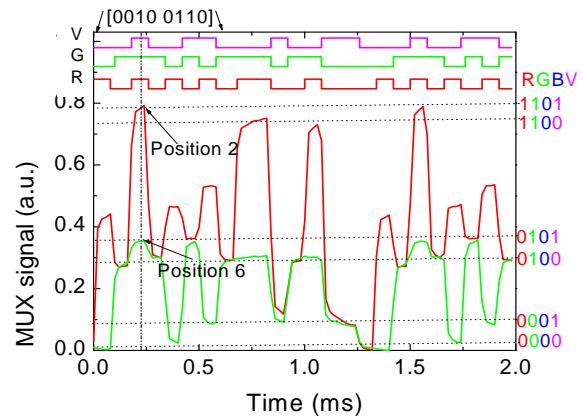
A challenge in LED-based navigation system is the way to improve the data transmission rate while maintaining the capability for accurate navigation.

The input of the aided navigation system is the MUX signal, and the output is the system state estimated at each time step. For each transition between an initial location and a final one, two code words are generated, the initial (i) and the final (f). If the receiver stays under the same region, they should be the same, if it moves away they are different

[24-25]. The suitability of the navigation data bit transition was tested. The navigation solution is to move the sensor unit along a known pattern path. One can performed signal acquisition on the different generated locations, for instance: beginning in point 5 and ending in point 3 (see Fig. 1), in four consecutive instants (t_1, t_2, t_3 and t_4) [26].



(a)



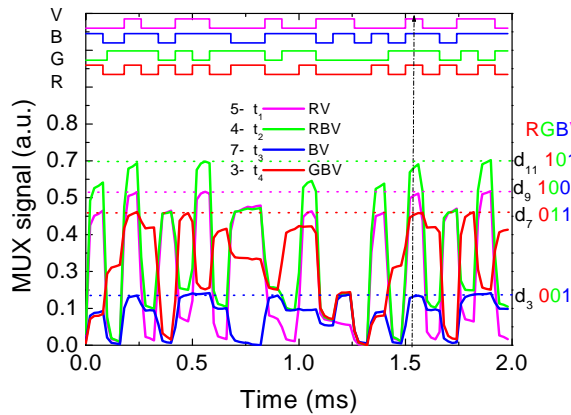
(b)

Fig. 7. MUX signals under 390 nm front and back irradiation. On the top the transmitted channels were decoded. (a) Standard bit sequence. (b) Random bit sequence.

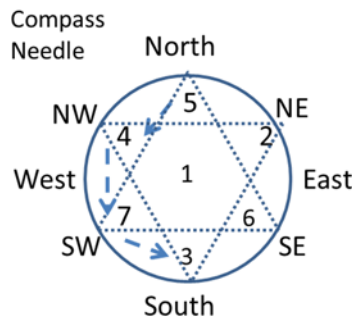
In a segment where the initial position of the receiver is point generation 5, then it moves to point 4, after that goes to point 7 and finally arrives to point 3, the acquired MUX signal at the instants t_1, t_2, t_3 , and t_4 is displayed in Fig. 8. The decoded channels are depicted on top. On the right hand, the highest levels (horizontal dotted lines), in each time interval, and the correspondent code words are pointed out.

As the receiver moves between generated point regions, the received information changes. In turn, red, green or blue channels are added or removed, but the violet is always present giving the location of the cell inside the cluster. In the considered example, the 8-bit positioning ID decoded from the violet channel was [0010 0110], which corresponds to line 2, column 6 of

the network. Hence, the retrieved information when the receiver was under point generation 4 (t_2) was: 8-bit positioning ID from the cell in the network [violet channel, 0010 0110], 4-bit positioning ID from the point generation cell: [RGBV, 1011], red channel payload packet: [1010 1010 1100 0100...]. When it moves to generation point 7 (t_3) the cell 4-bit positioning ID changes to [0011] the red information is lost and the blue payload data is maintained as: [1011 0111 0011 1010...]. Nevertheless, the 8-bit violet ID stays the same [0010 0110] since it correspond to the same unit cell (line 2, column 6) in the network.



(a)



(b)

Fig. 8. Triangular topology.

(a) MUX/DEMUX signals under different generation regions (5, 4, 7, 3). (b) Compass needle.

6. Conclusion

This paper presents a coupled data transmission and indoor positioning by using transmitting trichromatic white LEDs and an a-SiC:H/a-Si:H pin/pin SiC optical MUX/DEMUX mobile receiver. For data transmission, an On-Off Keying code was used. A triangular topology was considered for the unit cell. The proposed arrangement employs four modulated LEDs. Three of them are located at the vertices of an equilateral triangle to transmit the payload data and a fourth one is located at its centroid

to send the positioning BIT ID from the unit cell in the network. Fine-grained indoor localization was tested. A 2D localization design, demonstrated by a prototype implementation was developed.

A detailed analysis of the component's characteristics within the VLC system, such as transmitter and receiver, multiplexing techniques, system design, visible light sensing, and indoor localization and navigation recognition were discussed. The results showed that, by using a pinpin double photodiode based on a a-SiC:H heterostucture as mobile receiver and RBG-LED as transmitters, it is possible not only to determine the position of a mobile target inside the unit cell but also in the network and concomitantly to infer the travel direction along the time. For future work, by using multiple emitters and receivers, the transmission data rate through parallelized spatial multiplexing can be improved.

Acknowledgements

This work was sponsored by FCT – Fundação para a Ciência e a Tecnologia, within the Research Unit CTS – Center of Technology and systems, reference UID/EEA/00066/2013 and by the IPL project VLC_MIMO, 2016, and IPL/2017/SMART_VeDa/ISEL.

References

- [1]. Y. X. Sun, M. Liu, Q. H. Meng, Wifi signal strength-based robot indoor localization, in *Proceedings of the IEEE International Conference on Information and Automation (ICIA)*, 2014, pp. 250-256.
- [2]. P. Bahl, V. N. Padmanabhan, Radar: an in-building RF-based user location and tracking system, in *Proceedings of the 19th Annual Joint Conference of the IEEE Computer and Communications Societies (INFOCOM)*, Vol. 2, 2000, pp. 775-784.
- [3]. M. Liu, R. Siegwart, Dp-fact: Towards topological mapping and scene recognition with color for omnidirectional camera, in *Proceedings of the IEEE International Conference on Robotics and Automation (ICRA)*, May 2012, pp. 3503-3508.
- [4]. M. Liu, K. Qiu, S. Li, F. Che, L. Wu, C. P. Yue, Towards indoor localization using visible light communication for consumer electronic devices, in *Proceedings of the IEEE/RSJ International Conference on Intelligent Robots and Systems (IROS)*, Chicago, the USA, 2014, pp. 143-148.
- [5]. A. Jovicic, J. Li, T. Richardson, Visible light communication: opportunities, challenges and the path to market, *IEEE Communications Magazine*, Vol. 51, No. 12, 2013, pp. 26-32.
- [6]. S. T. Komine, M. Nakagawa, Fundamental analysis for visible-light communication system using LED lights, *IEEE Transactions on Consumer Electronics*, Vol. 50, No. 1, 2004, pp. 100-107.
- [7]. E. Ozgur E. Dinc, O. B. Akan, Communicate to illuminate: State-of-the-art and research challenges for visible light communications, *Physical Communication*, No.17, 2015, pp. 72-85.

- [8]. J. Armstrong, Y. Sekercioglu, A. Neild, Visible light positioning: a roadmap for international standardization, *IEEE Communications Magazine*, Vol. 51, No. 12, 2013, pp. 68-73.
- [9]. K. Panta, J. Armstrong, Indoor localisation using white LEDs, *Electron. Lett.*, Vol. 48, No. 4, 2012, pp. 228-230.
- [10]. T. Komiyama, K. Kobayashi, K. Watanabe, T. Ohkubo, Y. Kurihara, Study of visible light communication system using RGB LED lights, in *Proceedings of the IEEE SICE Annual Conference*, 2011, pp. 1926-1928.
- [11]. Y. Wang, Y. Wang, N. Chi, J. Yu, H. Shang, Demonstration of 575-Mb/s downlink and 225-Mb/s uplink bi-directional SCM-WDM visible light communication using RGB LED and phosphor-based LED, *Optics Express*, Vol. 21, No. 1, 2013, pp. 1203-1208.
- [12]. D. Tsonev, H. Chun, S. Rajbhandari, J. McKendry, S. Videv, E. Gu, M. Haji, S. Watson, A. Kelly, G. Faulkner, M. Dawson, H. Haas, D. O'Brien, A 3-Gb/s single-LED OFDM-based wireless VLC link using a Gallium Nitride μ LED, *IEEE Photon. Technol. Lett.*, Vol. 26, No. 7, 2014, pp. 637-640.
- [13]. D. O'Brien, H. L. Minh, L. Zeng, G. Faulkner, K. Lee, D. Jung, Y. Oh, E. T. Won, Indoor visible light communications: challenges and prospects, in *Proceedings SPIE 7091*, 2008, pp. 709106-1 – 709106-9.
- [14]. S. Schmid, G. Corbellini, S. Mangold, T. R. Gross, An LED-to-LED Visible Light Communication system with software-based synchronization, in *Proceedings of the IEEE Globecom Workshops*, 2012, pp. 1264-1268.
- [15]. Z. Zhou, M. Kavehrad, P. Deng, Indoor positioning algorithm using light-emitting diode visible light communications, *Journal of Optical Engineering*, Vol. 51, No. 8, 2012, pp. 085009-1 – 085009-6.
- [16]. S. T. Komine, M. Nakagawa, Fundamental analysis for visible-light communication system using led lights, *IEEE Transactions on Consumer Electronics*, Vol. 50, No. 1, 2004, pp. 100-107.
- [17]. E. Monteiro, S. Hranilovic, Constellation design for color-shift keying using interior point methods, in *Proceedings of the IEEE Globecom Workshops*, Dec. 2012, pp. 1224-1228.
- [18]. M. Vieira, P. Louro, M. Fernandes, M. A. Vieira, A. Fantoni, J. Costa, Three Transducers Embedded into One Single SiC Photodetector: LSP Direct Image Sensor, Optical Amplifier and Demux Device, *Advances in Photodiodes InTech*, Chap.19, 2011, pp. 403-425.
- [19]. M. A. Vieira, P. Louro, M. Vieira, A. Fantoni, A. Steiger -Garção, Light-activated amplification in Si-C tandem devices: A capacitive active filter model, *IEEE Sensor Journal*, Vol. 12, No. 6, 2012, pp. 1755-1762.
- [20]. P. Louro, M. Vieira, M. A. Vieira, J. Costa, Photodetection of modulated light of white RGB LEDs with a-SiC:H device, *Advanced Materials Proceedings*, 2017 (in press).
- [21]. E. A. Saleh Bahaa, M. C. Teich, Fundamentals of Photonics, *John Wiley & Sons*, Chapter 3 (Beam Optics), 1991, pp. 80-107.
- [22]. M. A. Vieira, M. Vieira, V. Silva, P. Louro, M. Barata, Optoelectronic logic functions using optical bias controlled SiC multilayer devices, *MRS Proceedings*, Vol. 1536, 2013, pp. 91-96.
- [23]. M. A. Vieira, M. Vieira, P. Louro, V. Silva, P. Vieira, Optical signal processing for indoor positioning using a-SiCH technology, *Opt. Eng.*, Vol. 55, No. 10, 2016, pp. 107105-1 – 107105-6.
- [24]. M. A. Vieira, M. Vieira, P. Louro, L. Mateus, P. Vieira, Indoor positioning system using a WDM device based on a-SiC:H technology, *Journal of Luminescence*, 2016.
- [25]. P. Louro, J. Costa, M. A. Vieira, M. Vieira, Optical Communication Applications based on white LEDs, *Journal of Luminescence*, Vol. 191, Part B, 2017, pp. 122-125.
- [26]. M. Vieira, M. A. Vieira, P. Louro, A. Fantoni, P. Vieira, Fine-grained Indoor Localization: Visible Light Communication, in *Proceedings of the 8th International Conference on Sensor Device Technologies and Applications, (SENSORDEVICES'17)*, Rome, Italy, September 10-14, 2017, pp. 41-46.



Vehicle-to-Vehicle and Infrastructure-to-Vehicle Communication in the Visible Range

^{1,2} M. A. Vieira, ^{1,2,3} M. Vieira, ^{1,3} P. Vieira and ^{1,2} P. Louro

¹ ADETC/ISEL/IPL, R. Conselheiro Emídio Navarro, 1959-007 Lisboa, Portugal

² CTS-UNINOVA Quinta da Torre, Monte da Caparica, 2829-516, Caparica, Portugal

³ DEE-FCT-UNL Quinta da Torre, Monte da Caparica, 2829-516, Caparica, Portugal

⁴ Instituto das Telecomunicações, Instituto Superior Técnico, 1049-001, Lisboa, Portugal

¹ Tel.: +351218317000, fax: +351218317114

E-mail: mv@isel.ipl.pt

Received: 10 November 2017 /Accepted: 10 December 2017 /Published: 29 December 2017

Abstract: This paper proposes the use of Visible Light Communication (VLC) for vehicle safety applications, creating a smart vehicle lighting system that combines the functions of illumination and signalling, communications, and positioning. The feasibility of VLC is demonstrated by employing trichromatic Red-Green-Blue (RGB) LEDs as transmitters, since they offer the possibility of Wavelength Division Multiplexing (WDM), which can greatly increase the transmission data rate, when using SiC double p-i-n receivers to encode/decode the information. Each chip, individually, is used to transmit the driving range distance and data information. An on-off code is used to transmit the data. Free space is the transmission medium. The receivers consist of two stacked amorphous a-H:SiC cells. Multiple Input Multiple Output (MIMO) architecture is used. For data transmission, Streetlights and headlights based on commercially available modulated white RGB-LEDs are used. For data receiving and decoding, three a-SiC:H double pin/pin optical processors symmetrically distributed at the vehicle tail are utilized. The process of accurately encoding and decoding positioning and the design of SiC navigation system are discussed and tested. A visible multilateration method estimates the drive distance range. Infrastructure-to-Vehicle (I2V) and Vehicle-to-Vehicle (V2V) Communication are simulated.

Keywords: a-SiC:H technology, LED, Visible Light Communication, Intelligent Transportation System, Optical sensor, WDM, Vehicular Communication.

1. Introduction

Modern vehicles are equipped with many electronic sensors which monitor a vehicle's speed, position, heading, and lateral and longitudinal acceleration. Although the technology exists to do so, vehicles rarely communicate this information wirelessly to other vehicles or roadside infrastructure. Researchers are anticipating the deployment of wireless vehicle communication, and have begun developing applications that use this new technology

to improve safety and reduce congestion. This system is known as connected vehicles.

Recently, the demand for the solution of road traffic problems such as accidents, congestion and the associated environmental pollution, has significantly increased. By enabling wireless communication among vehicles and between vehicles and infrastructure, the safety and the efficiency of road traffic can be substantially improved. Until recently, vehicles were unable to share their data in any meaningful way. Vehicle-to-vehicle (V2V)

communication was limited to brake lights, turn signals, and other low-tech methods. Infrastructure-to-vehicle (I2V) communication was likewise limited to dynamic message signs, highway advisory radio, traffic signals, and ramp meters.

Several modes of vehicular communications, such as infrastructure-to-vehicle (I2V), vehicle-to-vehicle (V2V) and vehicle-to-infrastructure (V2I) are becoming increasingly popular, boosted by navigation safety requirements [1].

Current solutions, such as intelligent traffic control systems, provide communication infrastructures along the road; vehicular communication and likewise, are research trends under the area of Intelligent Transportation Systems (ITS) [2-4].

Recently, LED-based optical wireless communication has been also proposed for car to car message delivery. This option turned out to be particularly effective in short range direct communications to explore Line-of-Sight (LoS) and overcome the issues related to the isotropic nature of radio waves. One additional benefit of LEDs is that they can switch to different light intensities at a very fast rate. This functionality has given rise to a novel communication technology (Visible Light Communication - VLC) where LED luminaires can be used for high speed data transfer [5-6].

In the recent past, we have developed a WDM device that enhances the transmission capacity of optical communications in the visible range. When different visible signals are encoded in the same optical transmission path [7-8] the device multiplexes the different optical channels, performs different filtering processes (amplification, switching, and wavelength conversion) and finally decodes the encoded signals recovering the transmitted information. This device is used as a receiver. Therefore, by utilizing VLC between vehicles, drivers are given a clearer knowledge of the preceding and nearby vehicles status.

In this paper, a traffic scenario is established. The transmitters and the receivers are characterized. To achieve vehicular communication (V2V) 4 bit string color messages in the visible range and their three parity bits for error control are used to transmit a codeword that is received and decoded by the SiC pinpin devices. Code and parity multiplex/demultiplex (MUX/DEMUX) signals are designed, transmitted and analyzed. The dependence of distance between the transmitter and receiver is presented. Driving range distance is discussed and tested using the VLC system. The proposed smart vehicle lighting system considers wireless communication, computer based algorithms and smart sensor and optical sources network, which builds a transdisciplinary approach framed in cyber-physical systems.

This paper is organized as follows. In Section 1, the introduction is present and in Section 2, the system design is explained. Section 3, reports the

encoder/decoder method and in Section 4, the driving distance is analyzed. In section 5, an example of I2V follow by V2V communication is presented. Finally, in Section 6, conclusions are drawn.

2. System Design

2.1. The Traffic Scenario

White RGB-LEDs using WDM can achieve higher data transfer rates and can also be used for lighting purposes [9]. For data transmission, we propose the use of two headlights based on commercially available modulated white RGB-LEDs. For data receiving and decoding, three a-SiC:H double pin/pin optical processors symmetrically distributed at the vehicle tail are used (see Fig. 1).

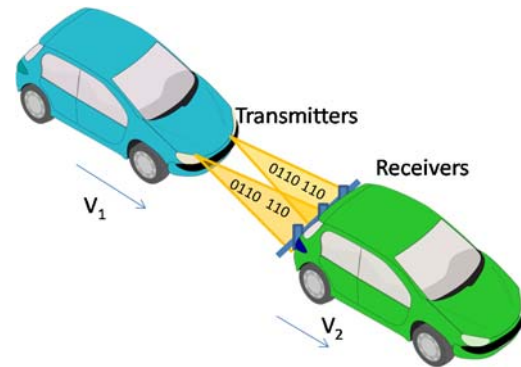


Fig. 1. Illustration of the V2V. Use Case: the follower vehicle sends the message that is received by the leader and can be retransmitted for the next car.

This VLC system enables the data transmission between vehicles, which is crucial to stack the information concerning the status of the vehicle (e.g., brake, speed, acceleration, engine failure, traffic congestion). To build a one-way VLC system that allows a feedback channel between the leader vehicle and the follower vehicle, the follower vehicle is assumed equipped with two headlamps transmitters. They send a codeword message [RGBV: P_R, P_G, P_B] composed of red, green, blue and violet 4-binary bits (four input data bits [R G B V]) and generate three additional parity bits [P_R, P_G, P_B] for easy decoding and error control [10]. The parity bits are SUM bits of the three-bit additions of violet pulsed signal, with two additional bits of RGB. The leader vehicle is assumed to be equipped with three a-SiC pinpin receivers to detect optical messages, as in Fig. 1. The spacing of the two transmitters is fixed while their distance to the receivers varies and depends on the speed (v_1, v_2). Both transmitters are oriented towards the receivers. In Fig. 2, the geometrical relation between the two vehicles (leader vehicle and follower vehicle) and the separating distances (A, B and C) are displayed. Here, the follower vehicle sends the

information using the modulated light from the headlamps forming a lighting coverage. The leader vehicle receives and decodes the message in three separated receivers at the tail and compares them. It was assumed that each LED chip sends light only perpendicular to the semiconductor's surface, and a few degrees to the side, which results in a light cone pattern (Fig. 2). Three situations are possible: A, the vehicles are at a safety distance and the three sensors receive the same message with the same intensity; B, the vehicles are in a warning distance, they are approaching and the left and the right sensor receive the same message but at the middle sensor the message arrives with double intensity; C the vehicles are too close, in the automatic braking distance, and the same message arrives to the left and to the right sensor and no message is read out by the middle one. Based on that, the driving range distance is calculated and a warning is sent to the driver or eventually activates the automatic braking system.

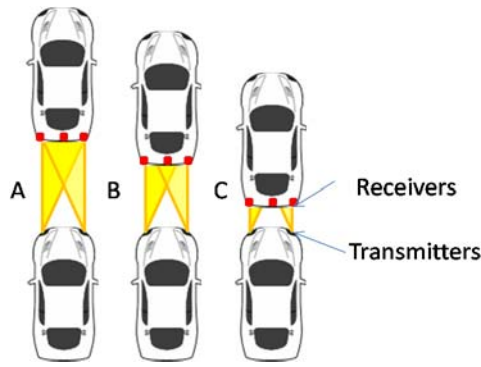


Fig. 2. Driving range distance showing the inter-vehicle distance decreasing as total photocurrent on the three receivers changes.

2.2. Transmitters

The usage of trichromatic RGB-LEDs as transmitters offers the possibility of WDM which can greatly increase the transmission data rate. For data transmission, we use commercially available violet and white RGB-LEDs whose spectra is displayed in Fig. 3.

The output spectra of the white LED contains three peaks assigned to the colors red, green and blue that mixed together provide the white perception to the eye. They are used for lighting purposes and when modulated, to transmit data. Each chip, in the trichromatic LED, can be switched *on* and *off* individually for a desired bit sequence [R G B]. An extra violet modulated LED [V] was added to increase data transmission and to generate parity bits [11] that allow error control [12].

In Table 1 the optical characteristics of the white LEDs at 25 °C are reported.

For data transmission, an on-off keying (OOK) code was used. In Fig. 4, an example of the digital signals (codeword) used to drive the LEDs is displayed.

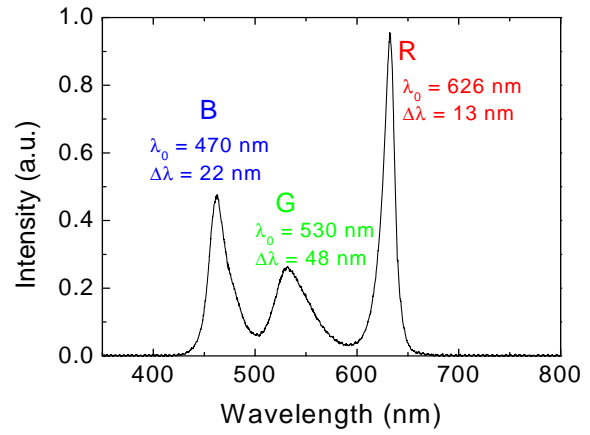


Fig. 3. Normalized emission spectra for the white RGB-LED.

Table 1. White LEDs characteristics at 25 °C.

	Red (R)	Green (G)	Blue (B)
Dominant wavelength (nm)	619	520	460
	624	540	480
Luminous intensity (mcd)	355	560	180
	900	1400	505
Spectral bandwidth @ 20 mA	24	38	28

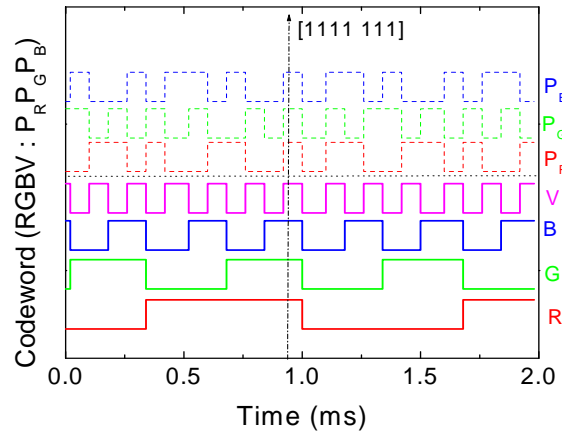


Fig. 4. Representation of the original encoded message [R G B V; P_R P_G P_B].

All the sixteen (2^4) *on/off* possible combinations of the 4 input channels (RGBV) are reported as well the corresponding parity bits. The arrow sets the seven bit [1111:111] codeword. Here, the Hamming (7,4) code [11] encodes the 4 bits (four input channels, RGBV) of data into 7 bits by adding 3 parity bits. The encoder takes four input data bits [R G B V] to which corresponds one of the possible 16 combinations and generates three additional parity bits, i.e., the parity bits are SUM bits of the three-bit additions of violet pulsed signal with two additional bits of RGB [12] and are given by:

$$P_R-(VRB) = V \oplus R \oplus B, \quad (1)$$

$$P_G-(VRG) = V \oplus R \oplus G, \quad (2)$$

$$P_B-(VGB) = V \oplus G \oplus B \quad (3)$$

Moreover, the seven-bit codeword at the output of the encoder will be in a format, with the data and the parity bits $[R \ G \ B \ V; P_R \ P_G \ P_B]$ separated.

2.3. Receiver

The optoelectronic sensor is a double pin heterostructure produced by Plasma Enhanced Chemical Vapor Deposition (PECVD) sandwiched between two transparent conductive contacts (TCO). The device configuration is shown in Fig. 5. In the stacked structure, p-i'(a-SiC:H)-n/p-i(a-Si:H)-n, the intrinsic layer of the front p-i-n photodiode is made of a-SiC:H while the back intrinsic layer is based on a-Si:H. The deposition conditions and optoelectronic characterization of the single layers and device as well as their optimization were described in [7] and [8]. Both front and back diodes act as optical filters confining, respectively, the optical carriers produced by the blue and red photons, while the optical carriers generated by the green photons are absorbed across both.

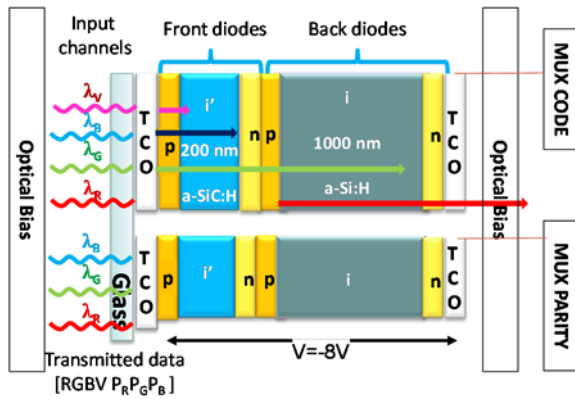


Fig. 5. Receiver configuration and operation.

A polychromatic mixture of red, green, blue and violet; $\lambda_{R,G,B,V}$; pulsed communication channels (input channels; transmitted data) are combined together, each one with a specific bit sequence and absorbed according to their wavelengths (see arrow magnitudes in Fig. 5). The combined optical signal (multiplexed signal; received data) is analyzed by reading out the generated photocurrent under negative applied voltage (-8 V), with and without 390 nm background lighting, applied either from front or back sides [13]. The RGB-LEDs are used together for illumination purposes and individually to transmit the channel location and data information.

2.4. Optical Filter

Four monochromatic input channels illuminated the device separately (transmitted data) or combined (MUX signal) with 12 kbps transmission rate. The generated photocurrent was measured. For the red and violet channels, the photocurrents without optical bias (no bias) and under front and back lighting are displayed in Fig. 6. Results show that front irradiation enhances the red signal and decreases the violet, while back irradiation has the opposite effect (see arrows in the figure).

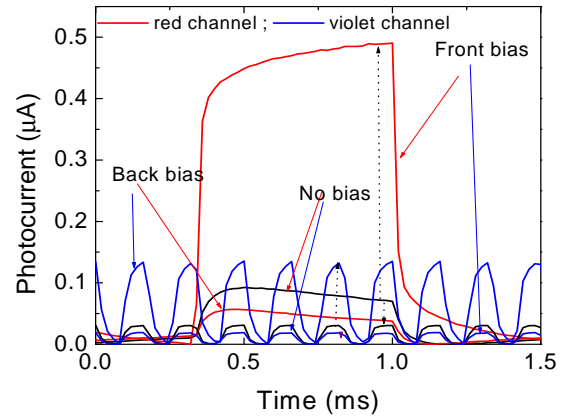


Fig. 6. Red and violet signals without (No bias) and under front (Front bias) and back (Back bias) irradiation.

The gathered data confirms that the optical gain, under irradiation, depends on the irradiated side and on the incoming wavelength acting as an active filter for the input channels [13]. Under front irradiation, the long wavelength channels are enhanced and the short wavelength channels quenched while the opposite occurs under back irradiation.

3. Encoder / Decoder

The algorithm to decode the information is relatively straightforward and the knowledge of the background acting as selector that chooses one or more of the 2^n sublevels (with n being the number of transmitted channels) and their n -bit binary code makes the communication reliable [14].

In Fig. 7, the received data, i.e., the MUX code signal, due to the combination of four (400 nm, 470 nm, 530 nm, 626 nm) input channels and the correspondent parity bits are displayed under front irradiation. The solid lines show the MUX signal that arises from the transmission of the four (R, G, B, V) wavelength channels. The dashed line marks the synchronized parity MUX signal transmitted with the data code. Due to the different optical gains, the colors red, green and blue were assigned respectively to the transmission of P_R , P_G and P_B .

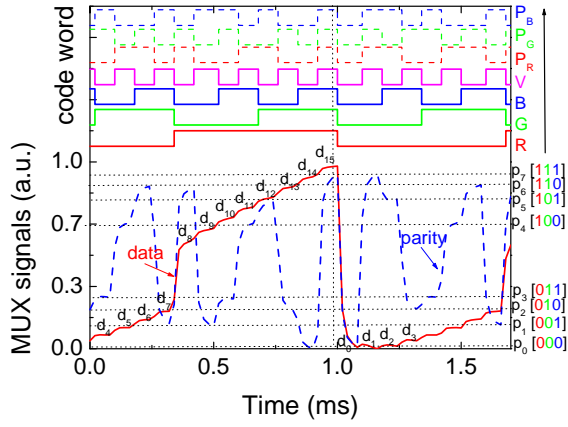


Fig. 7. Code and parity MUX/DEMUX signals under 390 nm front irradiation. On the top the transmitted channels [R G B V: P_R P_G P_B] are decoded.

The sixteen ordered levels (d_0 - d_{15}) of the data MUX signal are pointed out at the correspondent levels, and the ordered eight levels (p_0 - p_7) ascribed to the parity bits are displayed as horizontal dotted lines. On the right hand side of Fig. 7, the correspondence between the parity levels and the parity bits is shown. In the top, the decoded seven bit word [R, G, B, V, P_R, P_G, P_B] of the transmitted inputs is displayed. Results show that each of the 2^n possible *on/off* states corresponds to a well-defined level. In Fig. 7, all the *on/off* states are possible hence, 2^4 ordered levels are detected (d_0 - d_{15}) and correspond to all the possible combinations of the *on/off* states. Under front irradiation, each of those n channels is enhanced or quenched differently, resulting in an increase of red/green magnitude and a decrease on the blue/violet magnitude. In the sequence, by assigning each output level to a n digit binary code (weighted by the optical gain of the each channel), the signal can be decoded. A maximum transmission rate capability of 30 kbps was achieved in a four channel transmission.

The proximity of the magnitude of consecutive levels (Fig. 7) causes occasional errors in the decoded information that is corrected using the parity bits. For instance, levels d_1 , d_2 , and d_3 have similar magnitude and can be confused when reading a word message, however their parity levels, respectively, p_7 , p_5 and p_2 , are quite different. The parity of the word is checked after reading the word. The word is accepted if the parity of the bits read out is correct. If the parity of the bits is incorrect, an error is detected and should be corrected [12].

To automate the process of recovering the original transmitted data, an enhanced algorithm was developed. The transmitted information is decoded by comparing both the signal from the code and parity MUX levels under front irradiation, as shown in Fig. 7. The decoding algorithm is based on a proximity search [15]. The vector components are determined by the signal currents I_1 and I_2 , where I_1 (d levels) and I_2 (p levels) are the currents measured simultaneously, under front optical bias, for the 4-bit codeword (RGBV) and for the 3-bit parity [P_R, P_G

P_B]. The result is then compared with all vectors obtained from a calibration sequence (see Fig. 7) where each code level, $d(0-31)$, is assigned the correspondent parity level, $p(0-15)$. The color bits of the nearest calibration point are assigned to the time slot. A Euclidean metric is applied to measure the distances. We have tested the algorithm with different random sequences of the channels and we have recovered the original color bits, as shown in the top of Fig. 8.

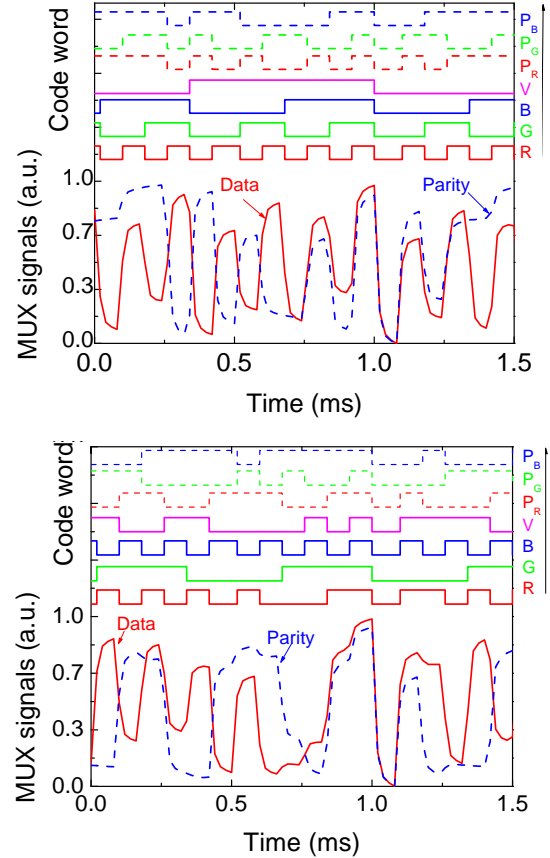


Fig. 8. Two different code and parity MUX/DEMUX signals under 390 nm front irradiation. On the top the transmitted channels are decoded.

4. Driving Distance

Lumens of light emitted by an LED depend on the current passing through the LED. For the luminous path loss (L_L), the conversion of the current flowing through the LED to lumens is given by [16].

$$L_L = \frac{1}{D^2} \times (\text{emitted power of the LED}), \quad (4)$$

where D is the distance between the LED and the receiver. The light generated by an LED is directly proportional to the forward current flowing through the device. In order to analyze the influence of white LED brightness (headlight-like) on the sensor response, the drive current applied to each chip was changed, keeping all the same level for equal white

perception. The intensity of the violet LED was kept constant at 30 mA. Each chip was modulated as shown on the top of Fig. 7. In Fig. 9(a), the MUX signal is displayed for different applied drive currents.

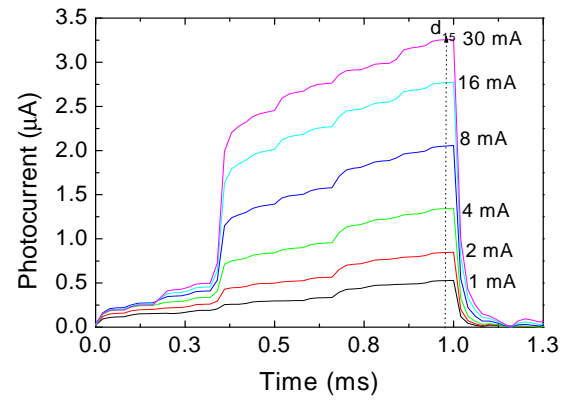
In Fig. 9(b), the [1111] code level magnitudes, d_{15} , (arrow in Fig. 9(a)) as a function of the drive current is displayed. The dotted curve shows the trend of the photocurrent with the relative distance from the receiver to the transmitter. Experimental results show that as the drive current increases, the intensity of the MUX signal also increases, but its shape remains the same. The sixteen levels, each one ascribed to an *on/off* possible state, are all detected allowing at the receiver the demultiplexing operation and the recovery of the transmitted information. Fig. 9(b), also shows that the code levels magnitude increases in a fast rate up to driving currents around 10 mA and then the photocurrent keeps increasing with the driving current but at a slow rate. Here, if we plot the photocurrent as a function of the one over the square of the driving current (dot plot) we can map the relative distances between the receiver and the transmitter. If the irradiance is calibrated for a known separation between the transmitter and the receiver, the irradiance at a given distance can be calculated using the inverse square law, hence, as the photocurrent increases the relative distance decreases exponentially. Three regions are detected: region A where the photocurrent decreases slowly with the distance; region B where its decrease is gradual; and region C, where a fast decrease occurs. These three regions can be directly correlated with the inter-vehicle driving distance from Fig. 2, after a calibration. So, by measuring the photocurrent at fixed code level it enables the prediction of the distance between vehicles and provides information to warn the driver about the safety distance (Fig. 2). This warning can be transmitted through one of the four available channels.

The VLC system compares the three received messages and infers the driving distance between the leader and the follower vehicles by reading the magnitude of the higher level (dash dot arrow in the figure) in the middle sensor. A warning message should be sent if the distance is lower than the safety distance.

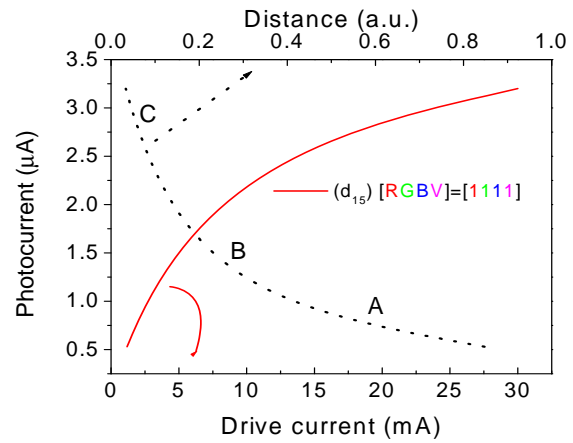
We have simulated the scenario B (Fig. 2). The drive current applied to the two LEDs (headlamps-like) was the same and adjusted in order to have the same lighting conditions of this region. Here, the right and the left sensor receive the same message and the one in the middle receives the overlap of both. We have applied to the RGB LED a current of the order of 4 mA and 30 mA to the violet one.

In Fig. 10, the received MUX signals on the right and left sensors or in the middle one are displayed.

The solid lines are ascribed to the MUX data word and the dotted lines to the correspondent parity MUX. The same 4:3 binary information (on the top of the figure) was sent simultaneously by both LEDs.



(a)



(b)

Fig. 9. (a) MUX signal under different drive currents applied to the chips of the trichromatic LED. (b) [1111] code level magnitude as a function of the drive current applied to the RGB chips.

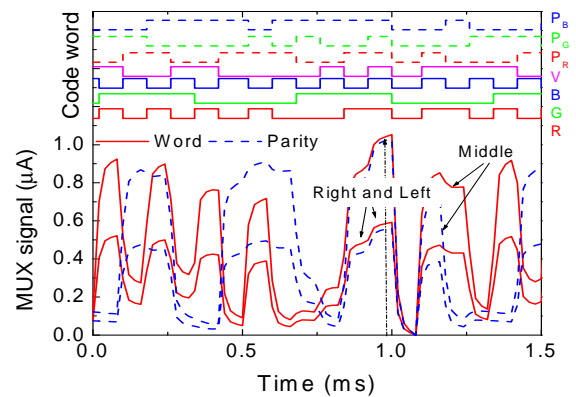


Fig. 10. MUX (solid line) and parity (dotted line) signals acquired by the right, the left and the middle receivers.

As expected, the shape of both code and parity MUX signals are the same but the intensity in the middle sensor ($\approx 1 \mu\text{A}$) is almost twice of the one received in the two others ($\approx 0.5 \mu\text{A}$).

Note that, when applying to each chip a forward current of the order of 4 mA, the magnitude of the data MUX signal is $\approx 1 \mu\text{A}$ (Fig. 9 (b)) to which

corresponds a relative distance around 0.4 that leads to region B.

5. I2V and V2V Hybrid Communication

The introduction of individual vehicle location data via connected vehicles allows the development of new types of mobility applications.

The VLC applications for vehicular communication fall into two categories: Infrastructure-to-Vehicle (I2V) and Vehicle-to-Vehicle (V2V). For the I2V applications they focus on utilizing the traffic related infrastructure, such as traffic light or street light to communicate useful information. There are two types of transmitters in V2I communications. In the first type, the street lights whose primary purpose is to provide illumination can be used for data communication with cars or pedestrians. The second type are traffic lights based on LEDs that can also communicate with cars, if modulated. Since their primary purpose is not illumination and because they are always ON (even when there is sunlight), they are suitable for applications such as vehicle safety, traffic information broadcast, etc. On the other hand, the illumination LEDs are available on streets even where there are no traffic lights, making them more suitable for Internet access and positioning.

An Infrastructure to Vehicle (I2V) follow by Vehicle to Vehicle (V2V) communication was simulated and its architecture displayed in Fig. 11. The street light sends a coded message (traffic message) that includes its ID (violet channel) and traffic information (RGB channels). Each lamp transmits data during the time slot it occupies, i.e., the individual LED lamp transmits its own data depending on the area it locates. This message is received and decoded by the follower vehicle and retransmitted to the leader.

In the I2V communication, the emitter was developed based on street lights, located on roadside, and the transmitted information received and decoded in the SiC pinpin device, located in the car roof. The street lights emit light signals within a capture range across one or more road lanes. When a probe vehicle enters the street light's capture range, the receivers in the probe vehicles respond to light signal and its unique ID and traffic message are assigned. They send a codeword message [RGBV: P_R , P_G , P_B] composed by red, green, blue and violet 4-binary bits (four input data bits [R G B V]) and generate three additional parity bits [P_R , P_G , P_B] for easy decoding and error control [10].

To build the V2V system that allows feedback channel between leader vehicle and follower vehicle, the follower vehicle sends the message that is received by the leader and can be retransmitted for the next car [17].

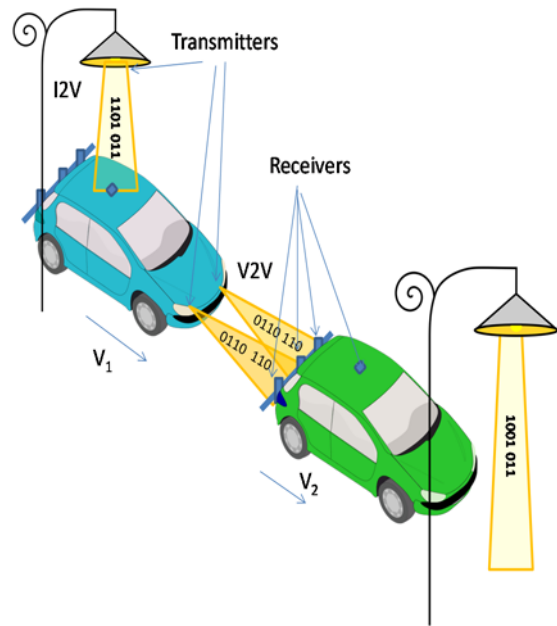


Fig. 11. Illustration of the proposed scenario: V2V and I2V hybrid systems.

In Fig. 12 the acquired MUX signals due to simulated an I2V communication follow by a V2V communication are presented.

In Fig. 12(a), the I2V MUX data (solid line) and parity (dash line) signals received by the roof sensor are displayed. In top the decoded signal is shown. In Fig. 12(b), the V2V MUX signals received on the right (R) and left (L) sensors or in the middle (M) one is displayed. The solid lines are ascribed to the MUX data word and the dash lines, to the correspondent parity MUX. The same 4:3 binary information (on the top of the figure) was sent simultaneously by both LEDs. Here, we have simulated the scenario B (see Fig. 2), the drive current applied to the two RGB-LEDs (headlamps-like) was the same and adjusted in order to have the same lighting conditions of this region. Experiments were conducted on straight and not on turning and zigzag paths.

Results (Fig. 12(a)) show that in the analyzed time slot, the street light send a code message that is received at the pinpin sensor located at the car roof (MUX signal, I2V data) and decoded (RGBV: $P_R P_G P_B$). This message is transmitted to the headlights and send to the leader vehicle (Fig. 12(b)). Here the right and the left sensor receive the same message and the one in the middle receives the overlap of both. We have applied to the RGB LED a current of the order of 4 mA and 30 mA to the violet one. As expected, the shape of both code and parity MUX signals are the same but the intensity in the middle sensor ($\approx 1 \mu A$) is almost twice of the one received in the two others ($\approx 0.5 \mu A$).

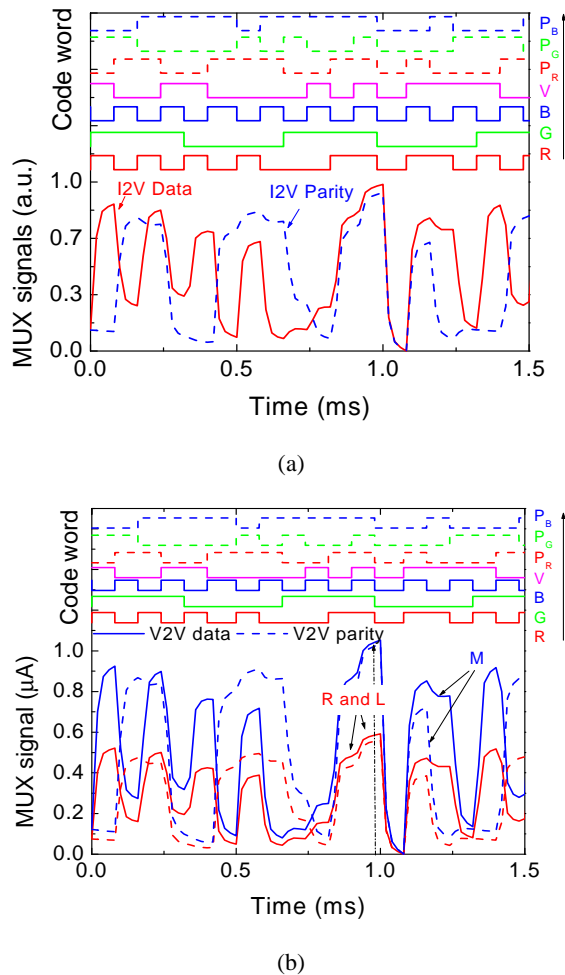


Fig. 12. Proof of concept: (a) Signals acquired in a I2V communication, MUX (solid line) and parity (dash line) signals; (b) Signals acquired by the R (right); L (Left); and M (middle) receivers in a V2V communication, MUX (solid line) and parity (dash line) signals.

5. Conclusion

In this paper, a VLC system, for vehicle safety applications, was presented. The system is composed of a VLC transmitter that modulates the light produced by white RGB-LEDs, and by VLC receivers based on photosensitive elements (a-SiC:H pinpin photodiodes) that code and decode the modulated signals. A scenario for the VLC system was tested and analyzed and a traffic scenario was simulated. By reading out in the receivers the magnitude of the multiplexed signal, it was possible, concurrently, to decode a transmitted message and to infer the driving distance between the transmitter and the receiver.

Acknowledgements

This work was sponsored by FCT – Fundação para a Ciência e a Tecnologia, within the Research Unit CTS – Center of Technology and systems, reference UID/EEA/00066/2013 and by the

IPL project VLC_MIMO, 2016 and IPL/2017/SMART_VeDa/ISEL

References


- [1]. S. Yousefi, E. Altman, R. El-Azouzi, Fathy, M., Analytical model for connectivity in vehicular Ad Hoc networks, *IEEE Transactions on Vehicular Technology*, Vol. 57, No. 6, 2008, pp. 3341-3356.
- [2]. N. Kumar, N. Lourenço, D. Terra, L. N. Alves, R. L. Aguiar, Visible Light Communications in intelligent transportation systems, in *Proceedings of the IEEE Intelligent Vehicles Symposium*, 2012, pp. 748-753.
- [3]. C. Liu, B. Sadeghi, E. W. Knightly, Enabling vehicular visible light communication (V2LC) networks, in *Proceedings of the Eighth ACM International Workshop on Vehicular Inter-networking (VANET'11)*, ACM, New York, NY, USA, 2011, pp. 41-50.
- [4]. P. Papadimitratos, A. La Fortelle, K. Evenssen, R. Brignolo, S. Cosenza, Vehicular communication systems: Enabling technologies, applications, and future outlook on intelligent transportation, *IEEE Communications Magazine*, Vol. 47, No. 11, November 2009, pp. 84-95.
- [5]. S. Schmid, G. Corbellini, S. Mangold, T. R. Gross, An LED-to-LED Visible Light Communication system with software-based synchronization, in *Proceedings of the IEEE Globecom Workshops*, 2012, pp. 1264-1268.
- [6]. D. O'Brien, H. L. Minh, L. Zeng, G. Faulkner, K. Lee, D. Jung, Y. Oh, E. T. Won, Indoor visible light communications: challenges and prospects, in *Proceedings SPIE 7091*, 2008, pp. 709106-1 – 709106-9.
- [7]. M. Vieira, P. Louro, M. Fernandes, M. A. Vieira, A. Fantoni, J. Costa, Three transducers embedded into one single SiC photodetector: LSP direct image sensor, optical amplifier and Demux device, *Advances in Photodiodes InTech*, Chap. 19, 2011, pp. 403-425.
- [8]. M. A. Vieira, P. Louro, M. Vieira, A. Fantoni, A. Steiger-Garção, Light-activated amplification in Si-C tandem devices: A capacitive active filter model, *IEEE Sensor Jornal*, Vol. 12, No. 6, 2012, pp. 1755-1762.
- [9]. I. L. Azevedo, M. G. Morgan, F. Morgan, The transition to solid-state lighting, in *Proceedings of the IEEE*, Vol. 97, No. 3, March 2009, pp. 481-510.
- [10]. M. A. Vieira, M. Vieira, P. Louro, V. Silva, Error detection on a spectral data using an optical processor based on a-SiC technology, *Sensors & Transducers*, Vol. 184, Issue 1, January 2015, pp. 116-122.
- [11]. R. W. Hamming, Error detecting and error correcting codes, *Bell Syst. Tech. J.*, Vol. 29, No. 2, 1960, pp. 147-160.
- [12]. M. A. Vieira, M. Vieira, V. Silva, P. Louro, J. Costa, Optical signal processing for data error detection and correction using a-SiCH technology, *Phys. Status Solidi C*, Vol. 12, No. 12, 2015, pp. 1393-1400.
- [13]. M. Vieira, M. A. Vieira, P. Louro, J. Costa, M. Fernandes, A. Fantoni, M. Barata, Multilayer architectures based on a-SiC:H material; Tunable wavelength filters in optical processing devices, *J. Nanosci. Nanotechnol.*, Vol. 11, No.6, 2011, pp. 5299-5304.

- [14]. M. A. Vieira, M. Vieira, V. Silva, P. Louro, M. Barata, Optoelectronic logic functions using optical bias controlled SiC multilayer devices, *MRS Proceedings*, Vol. 1536, 2013, pp. 91-96.
- [15]. M. A. Vieira, M. Vieira, P. Louro, V. Silva, J. Costa, A. Fantoni, SiC multilayer structures as light controlled photonic active filters, *Plasmonics*, Vol. 8, No. 1, 2013, pp. 63-70.
- [16]. I. Raza, S. Jabeen, S. R. Chaudhry, S. A. Hussain, M. S. Bhatti, M. H. Raza, Optical wireless channel characterization for indoor Visible Light Communication, *Indian Journal of Science and Technology*, Vol. 8, No. 22, 2015, pp. 1-9.
- [17]. M. A. Vieira, M. Vieira, P. Louro, P. Vieira, Smart Vehicle Lighting System in the Visible Range: Vehicle-to-Vehicle Communication, in *Proceedings of the Eighth International Conference on Sensor Device Technologies and Applications (SENSORDEVICES'17)*, Rome, Italy, 10-14 September, 2017, pp. 57-62.



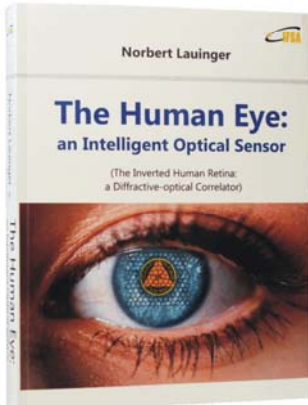
Published by International Frequency Sensor Association (IFSA) Publishing, S. L., 2017
(<http://www.sensorsportal.com>).

Norbert Lauinger



The Human Eye: an Intelligent Optical Sensor

(The Inverted Human Retina: a Diffractive-optical Correlator)





Hardcover: ISBN 978-84-617-2934-0
e-Book: ISBN 978-84-617-2955-5

The Human Eye: an intelligent optical sensor (The inverted retina: a diffractive - optical correlator) shows that the human eye from the prenatal structuring of the inverted retina hardware on up to the design of the central cortical visual pathway is not only different from but also radically more intelligent than a camera.

Many paradoxes in color vision (RGB peak positioning in the visible spectrum, overlapping of the RGB channels, relating local color to the whole scene, paradoxically colored shadows, Purkinje phenomenon etc.) are becoming intelligent solutions.

A fascinating book for all those wondering that the brightness of a scene is not cut in half and that the visible world doesn't collapse into a flat 2D-image when closing one eye. It should be a great of interest for students, scientists and engineers in eye-, vision- and brain-research, neuroscience, psychophysics, ophthalmology, psychology, optical sensor and diffractive optical engineering. Practical applications are the search for a retinal implant of the next generation and a helpful strategy against myopia in early childhood.



Order: http://www.sensorsportal.com/HTML/BOOKSTORE/Human_Eye.htm

A Wireless Sensor Networks Management Strategy for the Small and Medium Sized Manufacturing Enterprises

¹ Pedro CHAVES, ² Omar BRANQUINHO and ¹ Fabiano FRUETT

¹ Unicamp, FEEC, Av. Albert Einstein, 400 - Campinas - SP, zip code 13083-852, Brazil

² PUC Campinas, CEATEC, Pq. das Universidades - Campinas - SP, zip code 13086-900, Brazil

E-mail: pedrochaves@hotmail.co.uk, branquinho@puc-campinas.edu.br,
fabiano@dsif.fee.unicamp.br

Received: 10 November 2017 /Accepted: 10 December 2017 /Published: 29 December 2017

Abstract: The demand for Wireless Sensor Networks (WSN) applied to industrial process monitoring and control is increasing as the forth industrial revolution (Industry 4.0) gathers pace. Flexibility and low cost make WSN the perfect choice for these modern 21st century manufacturing plants. Small and Medium Sized Enterprises (SMEs) have an important role in the growth of developing economies as they account for approximately 60 % of all private sector employment, but are currently finding it difficult to take advantage of new sensor technologies. This paper describes the tests carried out with a WSN in order to ascertain the relationship between the Received Signal Strength Indicator (RSSI) and the Packet Error Rate (PER). Subsequently, a new RSSI based network management strategy is presented; it includes two RSSI tracking indices that guarantee an early warning in case of radio signal deterioration. Both indices are generated in real time; the first estimates the RSSI tendency allowing for the mapping of a sample position in the set and its value, while the second compares the current RSSI to a preconfigured reference value. This article ends with the implementation and testing of the strategy on the ScadaBR Supervisory System.

Keywords: Wireless sensor networks, WSN, PER, RSSI, Network management.

1. Introduction

Small and Medium Sized Enterprises (SMEs) contribute decisively for the advancement of developing countries. Worldwide, SMEs account for about 52 % of private sector value added, varying from 16 % of the gross domestic product (GDP) in low-income countries to 51 % of GDP in high-income ones. SMEs dominate the world business stage; estimates suggest that more than 95 % of enterprises across the world are SMEs, accounting for approximately 60 % of all private sector employment [1].

With the advent of the fourth industrial revolution (Industry 4.0), automation with the use of industrial WSN should intensify since one of the main characteristics of these networks is their great flexibility in terms of installation, which meets the needs of the modern 21st century manufacturing plants, regarding the flexibilization of the general arrangement of equipment [2]. Due to its inherent flexibility, it would be natural for control and not just process monitoring to be done with the use of WSN [3].

Smart factories will allow machines and materials to communicate while on the assembly line. At the

beginning of the process, each product will bring with it a chip with the necessary information for its assembly, and, as it advances in the line, it will communicate with the equipment by means of Identification by Frequency of Radio (RFID).

If compared to wired networks, WSN offer substantial advantages in terms of installation, commissioning and maintenance [4]. They can cover areas that were previously out of physical or economic reach, thus allowing the improvement of processes. Remote areas and physical obstructions are no longer a barrier.

The signal tends to be degraded by the type of processes executed in the area and by the infrastructure density, which can be estimated by mapping the areas where the sensor nodes will be installed, classifying them as low, medium and high.

A WSN is composed of a group of transceivers that monitor processes and environments and control

actuators. Commonly monitored parameters include temperature, humidity, pressure, flow, liquid level, luminosity, vibrations, voltage and concentration of pollutants. These networks are composed of several monitoring stations called sensor nodes that should be small, light and portable, a sink node and a central with enough processing power to receive and handle the data. Each sensor node should be equipped with a transducer, a microprocessor, a transceiver, a power source and, optionally, an actuator. The transducer generates an electrical signal based on physical effects, the microprocessor processes and saves the data while the transceiver sends and receives it to the monitoring centre.

Fig. 1 shows a diagram of a WSN. The Subsystem A can be considered as the client and is characterized by databases and network managers that request information from the Subsystem B.

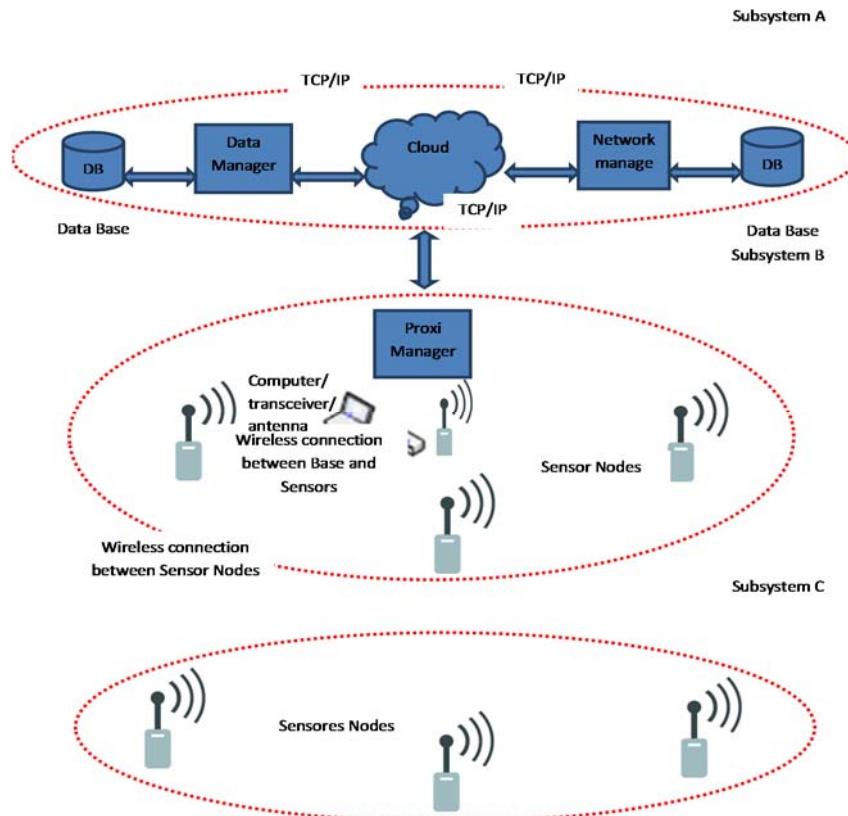


Fig. 1. Typical WSN Diagram.

The Subsystem B consists of a proxy manager, with the possibility of insertion of a database at this level. The proxy manager requests the data being monitored and converts it to the cloud protocol, Transmission Control Protocol/Internet Protocol (TCP/IP). This subsystem is complemented by the sink node (computer/transceiver/antenna) and sensor nodes (sensor/transceiver/antenna) which in turn, depending on the topology, route the packets to the sensor nodes of the Subsystem C.

The Subsystem C is composed primarily by the managed agents, sensor nodes that communicate wirelessly with the Subsystem B.

The *raison d'être* of a WSN is to monitor and control processes and environments [5], while a manufacturing process can be defined as a systematic series of operations executed to produce something. The management of a WSN must define a set of functions that will integrate configuration, monitoring, operation and maintenance of the network services and

devices [6]. Table 1 compiles the service classes for industrial environments, according to the International Society of Automation (ISA).

Table 1. Service Classes (ISA).

Use	Class	Description	Characteristic
Safety	0	Emergency Action	Always Critical
	1	Control	Usually Critical
Control	2	Supervision Control (Closed Loop)	Usually not Critical
	3	Open Control (Open Loop)	Human Action
Monitoring	4	Alert	Few Consequences
	5	Logging, up e download	No immediate Consequences

Currently in industrial environments, WSN are usually employed in monitoring processes, Classes 4 and 5, but not so commonly in control, Classes 1, 2 and 3 [4].

Network traffic, when used in monitoring and process control, includes continuous, asymmetric and spontaneous data transmission [7].

Some of the biggest challenges in the development of WSN are:

- Device limitations: battery capacity, size and weight;
- Topologies: Dynamic routing is subject to changes over time due to different processes and activities;
- Adverse conditions: problems with the propagation of radio waves, multipath, noise and interference caused by equipment and machines;
- Aggressive environment: environments with great thermal variation, vibrations, humidity, condensation and pollutants;
- Quality of service (QoS): WSN will attend processes with different demands;
- Security: WSN must have strategies to deal with internal and external attacks;
- Scalability: growth or changes in network topology;
- Integration: need to be compatible with existing infrastructure [8].

The transmissions of the process state readings (downlink) and the actuators control commands (uplink) use half-duplex as they occur in different time slots and must meet the requirements of the processes round trip times (RTT) [9].

For use in process control classes one, two, or three, timing is an essential parameter. The WSN must have low jitter and low delay. In [10] it is defended the use of the point-to-multipoint (star) topology, as this dispenses with routing between sensor nodes, reducing jitter and delay. This strategy, however, may limit the reach of WSN, a difficulty that can be minimized by the use of high-power transceivers.

Point-to-multipoint routing, if not well planned, can also cause reliability difficulties in the communication due to the lack of path redundancy between sink and sensor nodes.

A mesh topology with static or even dynamic multi-hop routing offers the possibility of path redundancy, but may compromise timing. Thus, the choice of network topology depends on the particularities of the project; distance between sensor nodes, density, processes criticality, equipment position, plant size, etc. [10], requiring careful planning.

With the use of devices and paths redundancies, a WSN may have greater availability than a wired network, however to ensure system reliability, network availability and data reliability must be assured. In wireless communications, the received signal strength is medium dependent [6]. The signal, when crossing the environment, suffers fading, caused by the degradation, absorption and attenuation of the radio signal. Interference in the same frequency band as the WSN can corrupt or even disable the signal [7].

The processes criticality and the characterization of the signal and medium generate subsidies to the network management system. The more critical the process is, the more reliable the link needs to be [11]. The International Organization for Standardization (ISO) divides the network management into five distinct areas. This classification was developed for the Open System Interconnection (OSI) model:

- Configuration management - controls, identifies and collects data from and supplies data to managed objects;
- Performance management - evaluates the behavior of managed objects and the effectiveness of the communication;
- Fault management - enables the detection, isolation and correction of abnormal operation of the OSI environment;
- Security management - addresses aspects essential to the safe operation and protection of managed objects;
- Account management - enables charges to be established and costs to be identified [12].

A strategy that assists in estimating the Received Signal Strength Indicator (RSSI) tendency with relation to a threshold would be relevant to the performance and configuration managements, as actions could be taken before that threshold is reached.

Supervisory Data Acquisition and Control Systems (SCADA) are industrial control systems used in the monitoring and control of remote devices. These systems collect data from remote sensor nodes in real time in order to monitor and control communication networks, including alarm monitoring, data processing, and equipment and conditions control. Based on the information from remote sensor nodes, manual or automatic commands can be executed on remote devices [13].

The WSN solutions currently offered by large solution providers tend to be complex, non-centralized

and expensive [3] putting these solutions out of the reach of most SMEs, considering that, differently from large corporations, these companies have neither the capital to acquire nor the dedicated departments to manage these new communication technologies [13].

Big WSN suppliers tend to offer solutions for the needs of large enterprisers, with prices that can reach millions of dollars. These suppliers offer large, noncentralized networks that grant the routing decisions to the nodes [14-16], effectively rendering the network hostage of the topology, impacting in its control. This reality does not really attend the necessities of SMEs regarding cost, control and complexity. Usually, these plants are small in area, demanding cheaper, less complex network solutions. Centralized solutions also allow for full network control.

For the tests in this paper, we used a low cost, centralized WSN approach geared towards SMEs, where the network manager has total control over its running.

We also identified a shortage of low-complexity network summarization solutions that can be used by non-technical operators working in SMEs. For that reason, in this paper, we present a management strategy that uses the RSSI as the main metric.

This paper is organized into eleven sections: in Section 2 we compare different WSN solutions, in Section 3 we explain the relation between RSSI and Packet Error Rate (PER), in Section 4 we present the Radiuino Platform, in Section 5 we specify the testing set up, in Section 6 we show the benchmarking test results, in Section 7 we introduce the indices management strategy, in Section 8 we describe the tests done with the strategy, in Section 9 we show the strategy implementation on a supervisory system, in Section 10 we show the tests done and in Section 11 we present our conclusions and future work.

2. WSN in the Industry

Since WLANs, Bluetooth, Wi-Fi, Wireless Hart and ZigBee, to mention just some, were introduced, a lot of the effort was focused on the non-licensed Industrial, Scientific and Medical (ISM) band of 2.4 GHz as some systems can require higher data rates. However, in some cases, this band may get overcrowded, degrading the signal. There are, however, other non-licensed bands reserved for ISM applications that can be used for wireless communication [17].

The 915 MHz ISM band is narrow and limits the maximum data rates. Applications such as SCADA, where the data requirements are lower than applications found in the 2.4 GHz frequency band, can use the 915 MHz band.

In this paper, we use a platform which operates on the 915 MHz band as there are no restrictions for the use of this ISM band regarding the application type [17].

3. The RSSI-PER Relation

The RSSI was chosen as the main metric in this study since link quality monitoring methods based on hardware, e.g., Link Quality Indicator (LQI), Signal to Noise Ratio (SNR) and RSSI, make use of basic metrics provided by the chip that, if compared to software solutions, require far less overhead allowing for a better response to changes on the link [18].

As indicated by [19], for a given scenario, there is a clear relation between the RSSI and the PER as the latter tends to go up as the former goes down. In this paper, we propose a strategy that takes advantage of this relation.

4. The Radiuino Platform

All measurements in this work were done using the low cost, open software, open hardware Radiuino platform [20]. The firmware used in the transceivers was developed using the Radiuino Integrated Development Environment (IDE). The Radiuino platform is structured in layers of protocol akin to the TCP/IP.

The RSSI and PER monitoring applications were developed in Python 2.6 [21] and the supervisory system used for the management was the open software ScadaBR [22].

The transceiver used was the BE990 radio module, with dimensions of 32.0 mm×24.4 mm×1.5 mm, as shown in the top of Fig. 2. It operates in the ISM band of 915 MHz and uses FSK modulation. The module was configured with a baud rate of 38.38 kbps. The BE990 complies with the regulations of the Brazilian National Telecommunications Agency (ANATEL), features an Atmega 328 micro controller, a Texas CC1101 transceiver and a Texas CC1190 RF amplifier [23].

At the sensor nodes, the module was mounted on the DK104 development board [20].



Fig. 2. BE990 and UartSBee.

This board has a voltage regulator that allows the use of power sources between 5 V and 14 V as shown in Fig. 3. The sensor nodes used in this study were always powered by 12-volt batteries.



Fig. 3. DK104 Development Board.

The DK104 does not have serial USB output for communication with the computer and therefore could not be used as the sink node. For this purpose, we employed the UartSBee module as it has a mini USB output, shown in bottom of Fig. 2.

The transceiver provides the parameter used in this study, the RSSI. It represents the signal strength observed at the transceiver at the time of reception in dBm [24]. The RSSI may suffer noise interference from other transmissions [25]. However [26] proves that the RSSI can be a good indicator of link quality, as long as this value is above the sensitivity limit of the device, which in the case of CC1190 is -112 dBm [23]. The RSSI is measured as an integer and then converted to dBm by subtracting a constant [25].

Through tests, it was validated that the BE990 presents up and downlink RSSI symmetry and for this reason, in this work, only the downlink RSSI values, that is to say, the perceived power in the sensor node, was used.

5. Benchmarking and Set Up

Benchmarking tests were carried out on all modules before any tests with the strategy were carried out.

For the benchmarking tests, the wireless communication link between the sink node and each remote sensor node was emulated using a coaxial cable.

To avoid saturation, Mini-Circuit attenuators were placed between the module in the sink node and the modules in each sensor node, as indicated in Fig. 4.

In turn, the modules of each sensor node were placed in a sealed RF test chamber, so to check their normalization and assess their PER and RSSI results with minimum electromagnetic interference (EMI).

6. Benchmarking and Correlation Tests

The results of the benchmarking tests are summarized in Table 2. It shows that all modules were conforming, returning very similar values of RSSI and

PER for the same attenuation scenario, in this case 90 dB. The highest standard deviation was just 0.13 dBm and the highest PER only 1.6 %, indicating good stability of all modules. The results indicated that the modules could be considered normalized and could be used in the correlation tests.

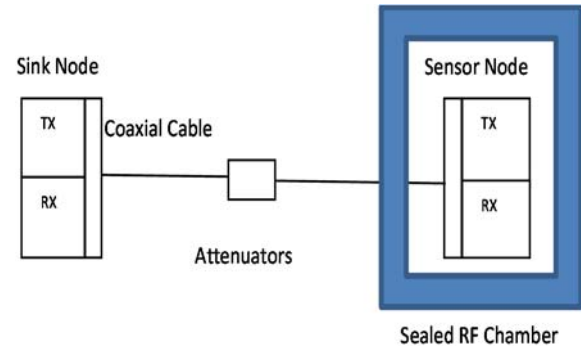


Fig. 4. Emulation Setup Diagram.

Table 2. Benchmarking results.

Sensor	SSI (average)	S.D. (dBm)	PER (%)
S1	- 42.50 dBm	0	0
S2	- 42.50 dBm	0.13	1.6
S3	- 42.00 dBm	0	0

The same set up shown in Fig. 4 was used again to collect the information that allowed correlating the RSSI to the PER. This time, the attenuation was gradually increased, thus reducing the RSSI level at the sensor node and consequently increasing the PER, so to find the RSSI level corresponding to the 5 % PER reference level (R_v) suggested by [27]. To guarantee the reliability of the results, three series of 200 packets each were sent to each sensor node. The data presented in Table 3 shows the average results of the three-test series.

Table 3. Correlation RSSI – PER.

RSSI Average (dBm)	PER (%)	RSSI St. Dev. (dBm)
-45.0	0	0.11
-52.0	0	0.31
-63.0	0	0.38
-69.5	0	0.64
-70.0	2.0	0.57
-71.5	2.5	0.69
-72.0	4.5	0.76
-75.0	5.0	0.57
-77.5	12.5	1.15
-80.0	38	4.41

The results indicate that -72 dBm is the maximum RSSI before the PER reaches the 5 % reference level R_v .

7. Indices Zr and Zt

Indices aid in the monitoring work since they simplify the comparison of a current state with a past or predefined one.

This paper presents a management strategy that includes two indices, both generated in real time. The first estimates the trend of RSSI allowing for the mapping of a sample position in the set and its value, while the second compares the current RSSI to a preconfigured reference one.

These indices are loosely based on the Box Plot diagram and therefore present benefits such as the low complexity calculations required to obtain them, thus ensuring their easy implementation in supervisory systems.

In order to evaluate the trend of the RSSI based on the signal dispersion, we propose the index Zr that is composed by the ratio of the average RSSI values of a large, configurable, sliding time window (Zb) expressed by (1), that can also be understood as the historical average, by the average of the RSSI values of a small, configurable, sliding time window (Zs) expressed by (2).

$$Zb = \bar{x} = \frac{x_1 + x_2 + \dots + x_m}{m}, \quad (1)$$

$$Zs = \bar{x} = \frac{x_1 + x_2 + \dots + x_n}{n}, \quad (2)$$

where $m > n$.

The index Zr, expressed by (3), shows how far Zs departs from the historical average Zb indicating the dispersion and, more importantly, the RSSI trend, with the advantage of returning values around 1. This index is independent of the signal strength in which the sensor node operates. This feature allows for its easy implementation in the monitoring of wireless sensor networks; since these sensor nodes are usually positioned in different areas, they tend to present different RSSI levels.

The index Zr will tend to 1 as Zs approaches Zb.

$$Zr = Zb / Zs \quad (3)$$

The second index, Zt, expressed by (4) tracks the value of Zs in relation to a reference level Rv value correlated to a PER threshold and tends to 1 as Zs approaches this reference value. This index is dependent on the signal strength at which the sensor node operates.

$$Zt = Rv / Zs \quad (4)$$

The observation of these two indices gives the operative in charge of the network a clear vision of the sensor nodes current situation with respect to the RSSI and, consequently, the PER.

8. Indices Testing

For the preliminary tests of the strategy, a WSN as specified in Section 5, comprising a sink node and a single sensor node was setup with the sensor node operating with a RSSI level above the reference level Rv of -72 dBm, as established in Section 6, allowing for the mapping of the RSSI variation to the increase of the PER. From this data, the indices Zr and Zt were extracted and compared to the RSSI behavior. The choice of the sliding time window for the tests was based on the Quality of Service (QoS) we expect industrial processes will demand from a WSN, so the sliding time window used for Zb was 60 minutes, and for Zs, it was 1 minute. However, these values are still subject of research. To validate the results, graphical comparisons between the variation of the RSSI and Zr, RSSI and Zt and Zr and PER were done.

Fig. 5 shows the RSSI with values in dBm on the primary vertical axis against the index Zr with values on the secondary vertical axis and the number of packets on the horizontal axis.

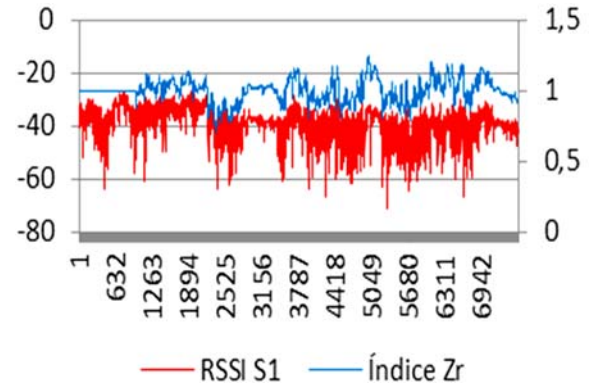


Fig. 5. RSSI x Index Zr.

The graph shows that the index Zr was equal to 1 up to approximately the packet 1000, which is equivalent to the 60 minutes required for Zb to be established. From that point on, the index tracks the variation of RSSI, always centered on 1 and differs from the RSSI as it considers the averages of the last 1 and 60 minutes sliding windows. This feature dilutes the impact of possible extreme and discrepant samples.

The graphs in Fig. 6 show the RSSI with values in dBm on the primary vertical axis against the index Zt with values on the secondary vertical axis, and the number of packets on the horizontal axis. The index Zt tracked the RSSI variation with respect to the reference level of -72 dBm that was never reached.

The index Zt acts as an alarm that is triggered whenever the RSSI reaches the pre-defined reference value, since its permanence at or below this threshold indicates an increase in the PER.

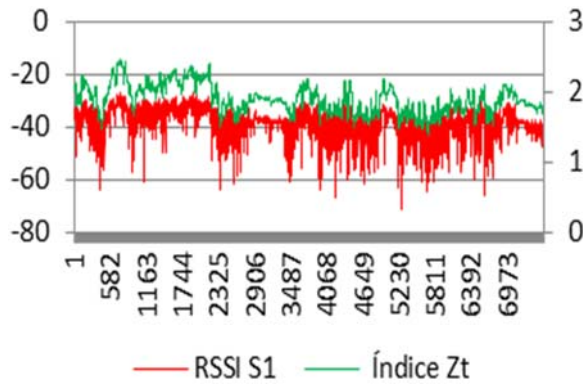


Fig. 6. R SSI x Index Zt.

Fig. 7 presents the index Zr with values on the primary vertical axis against the PER with values on the secondary vertical axis and the number of packets on the horizontal axis.

The graphs show that although the PER was consistently very low, it was higher at the times when the index Zr was below 1, that is, when the RSSI was below its historical average. It is important to observe that the graph of the PER is shown as the hourly average of its values.

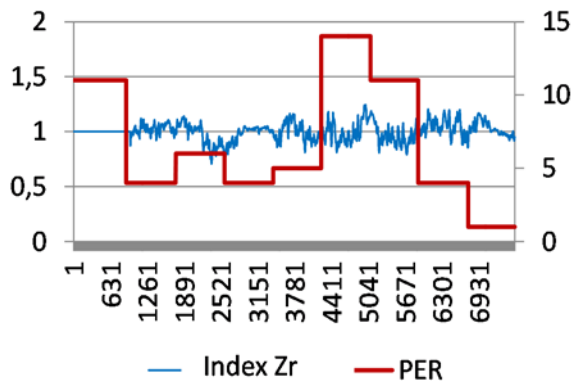


Fig. 7. Index Zr x PER.

The results shown on the graphs confirm the robustness of the indices Zr and Zt and their applicability as a wireless network management strategy.

9. Implementation on Supervisory

The strategy was implemented on the ScadaBR Supervisory System. For the tests, a WSN as specified in Section 5, consisting of a sink node and three sensor nodes using a point-to-multipoint topology was set up, as shown in Fig. 8. The supervisory system was configured to collect the downlink RSSI data from each sensor node, calculate Zs for the last minute and Zb for the last 60 minutes.

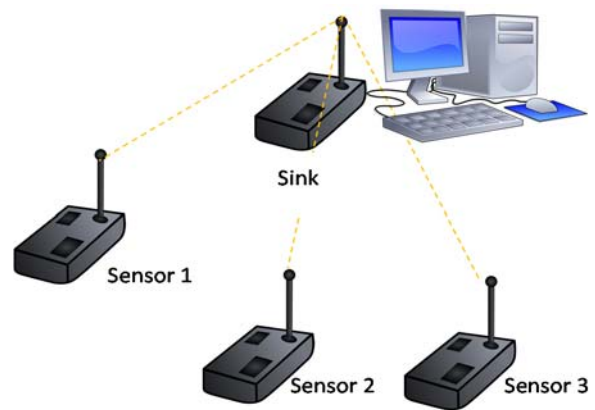


Fig. 8. Point-to-Multipoint Topology.

Monitoring via supervisory system allows the construction of graphical interfaces in which different levels of information can be presented, contemplating different levels of knowledge [5]. Figs. 9, 10, 11 and 12 show the ScadaBR screen. In each figure, the bottom chart on the right, "RSSI Sensors 1, 2 and 3" brings information that will be appreciated by a technically qualified person, the network manager, for example. The upper chart on the right, "Indices Sensors 1, 2 and 3" will be of great value for a person that is interested in the network but not necessarily technical, such as the production manager. The most concise information appears on the left side of the dashboard, with the Limit and Tendency light emitting diodes (LEDs) that are intended to alert a person that is not necessarily interested in the network, but dependent on it, such as a machine operator. Fig. 9 shows a snapshot of the graphs obtained with sensor nodes 1, 2 and 3.

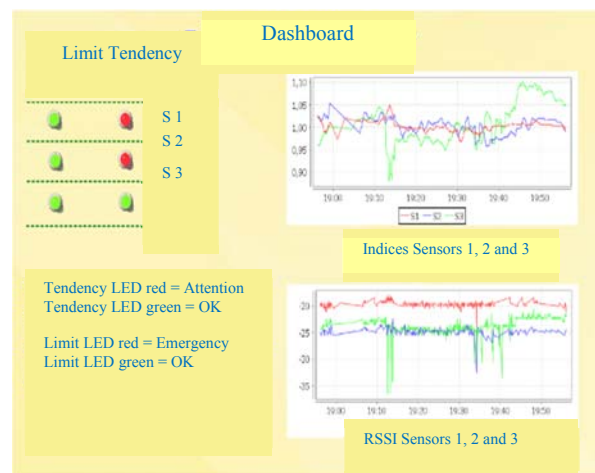


Fig. 9. Supervisory System Dashboard.

The chart "Indices Sensors 1, 2 and 3" shows the variation of the index Zr for each sensor node while the chart "RSSI Sensors 1, 2 and 3" brings the variation of RSSI.

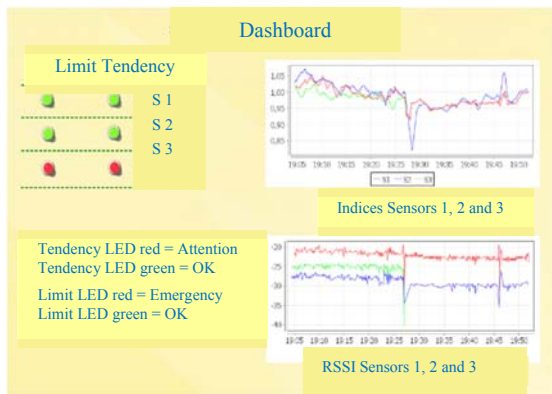


Fig. 10. Supervisory System Dashboard – First Test.

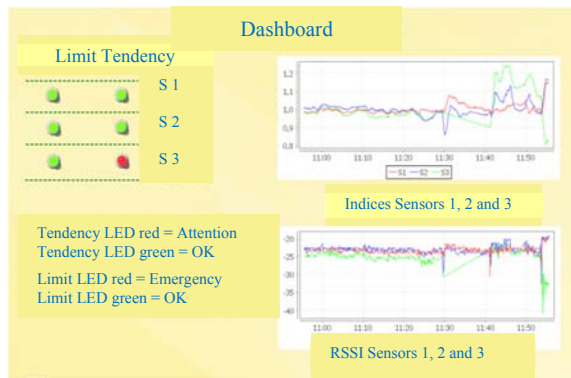


Fig. 11. Supervisory System Dashboard – Second Test.

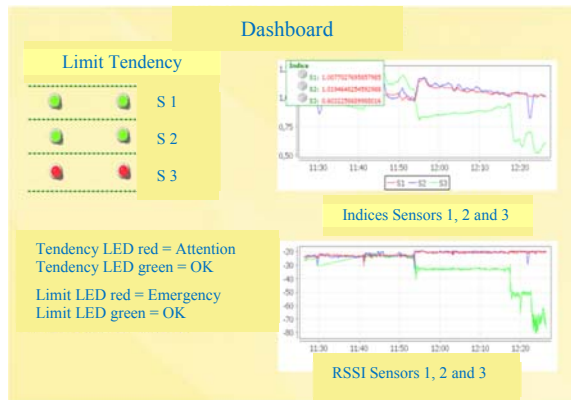


Fig. 12. Supervisory System Dashboard – Third Test.

On the left, the Limit LEDs flash green while the index Z_t is above the reference value, in this case -72 dBm, and red when Z_t is at or below it, and the Tendency LEDs that indicate the position of the index Z_r , flashing green while it is above 1 or red when it's below. For the sake of screen simplicity, we chose not to present graphs with the Z_t index variation. It can be seen that the Tendency LEDs for sensor nodes 1 and 2 were red indicating that RSSI on these two nodes were in a downward trend. This fact can be confirmed by the graph "Indices Sensor nodes 1, 2 and 3" as the trend lines for sensor nodes 1 and 2 (red and blue lines) end below 1.

10. Stress Testing

To validate the use of the indices strategy on the ScadaBR Supervisory System, we extended the use of the test setup described in Section 8. Tests introducing unexpected situations of use were carried out. These tests were useful to reveal any potential problems with the strategy on the supervisory system, such as performance or behavior issues, errors on startup, shutdown or on the interface.

The first test, shown in Fig. 10, was done in order to ascertain what would be the supervisory system behavior in case one of the sensor nodes became unavailable.

The network was started, and the 60 minutes needed for Z_b to be established were observed. To simulate unavailability, the sensor node 3 was purposely disconnected from power.

The Limit and Tendency LEDs for the sensor node 3 immediately lit up in red and the green trend lines for the sensor node 3 on graphs "Indices Sensors 1, 2 and 3" and "RSSI Sensors 1, 2 and 3" disappeared. We conclude that the strategy in the supervisory system behaved as expected.

The second test, shown in Fig. 11, investigated the behavior of the indices strategy on a supervisory system in case of sudden signal deterioration. For this test, the sensor node 3 was distanced from the sink node, simulating signal deterioration. Again, it can be seen that the Tendency LED for sensor node 3 lights up in red and the green line in the "RSSI Sensors 1, 2 and 3" graph reaches values below -40 dBm, reflecting accurately the node situation.

The third test, shown in Fig. 12, investigated the supervisory system behavior in case of acute signal deterioration.

For this test, the sensor node 3 was moved even further away from the sink node to a point where the RSSI reached and exceeded the reference value R_v of -72 dBm, established in Section 6.

In this test, the dashboard shows the sensor node 3 Limit LED in red, indicating that the RSSI on that sensor node was below the reference value, which can lead to a PER above 5 %. This condition was confirmed by the graph "RSSI Sensors 1, 2 and 3" as the green trend line for sensor node 3 reaches values below -80 dBm. The Tendency LED for that node also lights up in red indicating a RSSI deterioration which can be confirmed by the graph "Indices Sensors 1, 2 and 3" where the sensor node 3 green trend line shows the drop of the index Z_r .

In order to carry out the last and most extensive test, all nodes were connected to mains power, in order to guarantee the uninterrupted supply of power. The test consisted of a continuous and uninterrupted use of the indices strategy on the ScadaBR for a whole week, in order to ascertain any possible system locking. At the end of that period, the tests pointed out that the system did not present any faults. The tests results with the indices strategy on the ScadaBR Supervisory System confirm the robustness of the solution.

11. Conclusions and Future Work

This paper objective was to demonstrate the feasibility of employing a new network management strategy based on indices that use the RSSI as the only metric, as this solution requires far less overhead allowing for a better response to changes on the link. For that, a testing set up using the Radiuino platform was assembled so data could be collected.

The preliminary tests with the indices strategy indicated that, when compared to the RSSI readings, the strategy presents an easier interpretation of the data as the impact of extreme and discrepant samples were diluted by it.

The strategy was also implemented on the ScadaBR Supervisory System where an interface that attended the needs of different levels of network expertise was created. The stress tests carried out then returned results that also confirmed that the strategy was stable and robust enough to be employed in the monitoring of WSN in SMEs and thus help these companies to take full advantage of the Industry 4.0 possibilities.

There are still a number of topics following from our findings that would benefit from more research, including the further development of the supervisory system, as other open source network and application monitoring software like the Zabbix could be tested and evaluated, and the development of a methodology for the choice of the sliding time window for the indices Zb and Zs, according to the different industrial plant environments and requirement settings.

Also, the deployment of the indices strategy in a real SME environment with sensors distributed across the plant, where adverse conditions like propagation issues and interferences in the spectrum are the norm, would allow for a better understanding of the real capabilities of the strategy

References

- [1]. Growing the global economy through SMEs, *The Edinburgh Group*, Dec. 2017, http://edinburgh-group.org/media/2776/edinburgh_group_research_-_growing_the_global_economy_through_smes.pdf Accessed May 2017.
- [2]. Industry 4.0: The Next Industrial Revolution, *The Engineer*, May 2015, <http://www.theengineer.co.uk/manufacturing/automation/industry-40-the-next-industrial-revolution/1016696.article>. Accessed May 2015.
- [3]. O. Branquinho, Wireless Networks Technologies, October 2016, <http://pt.scribd.com/doc/206659698/Tecnologias-de-Redes-sem-Fio#>. Accessed October 2016.
- [4]. ISA 100 Wireless, Control Over Wireless: Current Applications and Future Opportunities, May 2016, http://www.nivis.com/resources/WCI_auto_Week_2012_%20Paper_v18Sep.pdf. Accessed May 2016.
- [5]. Pedro Chaves, Omar Branquinho, Fabiano Fruett, A Management Strategy for Centralized Wireless Sensor Networks Applied to Small and Medium Sized Manufacturing Enterprises, in *Proceedings of the 11th International Conference on Sensor Technologies and Applications (SENSORCOMM 2017)*, 10-14 September 2017, Rome, Italy, pp. 1-7. https://www.thinkmind.org/download_full.php?instance=SENSORCOMM+2017. Accessed November 2017.
- [6]. Wireless Training, *Emerson Process Management*, December 2015, <http://www2.emersonprocess.com/enUS/plantweb/wireless/WirelessTraining/Pages/index.asp>. December 2015.
- [7]. Gang Zhao, Wireless Sensor Networks for Industrial Process Monitoring and Control: A Survey, *Network Protocols and Algorithms*, Vol. 3, No. 3, December 2015, <http://macrothink.org/journal/index.php/npa/article/viewFile/580/533>. Accessed December 2015.
- [8]. Konstantin Mikhaylov, Jouni Tervonen, Joni Heikkilä, Janne Käsäkoski, Wireless Sensor Networks in Industrial Environment: Real-Life Evaluation Results, December 2015, http://cc.oulu.fi/~kmikhayl/site-assets/pdfs/2012_BCFIC.pdf, Accessed December 2015.
- [9]. Stefano Savazzi, Sergio Guardiano, Umberto Spagnolini, Wireless Critical Process Control in oil and gas refinery plants, in *Proceedings of the IEEE International Conference on Industrial Technology*, 2012, pp. 1003-1008. <http://home.deib.polimi.it/savazzi/articles/KF-006297.pdf>, Accessed December 2015.
- [10]. Ignace Verhamme, Wireless Control for Process Automation Using ISA100.11a, *Honeywell Process Solutions*, 2015. <https://www.honeywellprocess.com/library/marketing/article-reprints/wireless-control-for-process-automation-using-isa100.pdf>, Accessed December 2015.
- [11]. International Society of Automation, December 2016, <https://www.isa.org/isa100/> Accessed December 2016.
- [12]. W. Stallings, SNMP, SNMPv2, SNMPv3, and RMON 1 and 2, (3rd Edition), 1999.
- [13]. W. Peres, G. Stumpo, Small and medium-sized manufacturing enterprises in Latin America and the Caribbean under the new economic model, *World Development*, Vol. 28, No. 9, 2000, pp. 1643-1655.
- [14]. Emerson Process Management, Wireless Training, 2015. <http://www2.emersonprocess.com/enUS/plantweb/wireless/WirelessTraining/Pages/index.aspx>, Accessed December 2015.
- [15]. Banner Web Page, 2017, <https://www.bannerengineering.com/us/en/products/wireless-sensor-networks.html>. Accessed July 2017.
- [16]. Siemens Web Page, July 2017. <http://w3.siemens.com/mcms/industrial-communication/en/industrial-wireless-communication/iwlan-industrial-wireless-lan/Pages/iwlan.aspx>. Accessed July 2017.
- [17]. J. Shandle, Unlicensed 915-MHz Band Fits Many Applications and Allows Higher Transmit Power, *Digi-Key Electronics*, August 2015, <http://www.digikey.com/en/articles/techzone/2011/may/unlicensed-915-mhz-band-fits-many-applications-and-allows-higher-transmit-power>, Accessed August 2015.
- [18]. C. Wei, L. Jian, An Improved LQI-based Link Quality Estimation Mechanism for Wireless Sensor Networks, *Atlantis Press*, 2014, <http://www.atlantispress.com/php/pub.php?publication=csss14&frame=http%3A//www.atlantispress.com/>

- php/paperdetails.php%3Ffrom%3Dsession+results%26id%3D12655%26querystr%3Ddid%253D222, Accessed July 2016.
- [19]. V. Pereira, PER Estimate, RSSI Reading Protocol and WSN Best Routes Determination, <http://tede.bibliotecadigital.puc-campinas.edu.br:8080/jspui/handle/tede/889>, Accessed September 2016.
- [20]. Radiumino Site, <http://radiuino.cc/>, Accessed August 2015.
- [21]. Python Software Foundation, <https://www.python.org/downloads/>, Accessed May 2015.
- [22]. ScadaBR Forum, <http://www.scadabr.com.br>, Accessed August 2016.
- [23]. CC1101 Low-Power Sub-1 GHz RF Transceiver, <http://www.ti.com/lit/ds/symlink/cc1101.pdf>, Accessed July 2016.
- [24]. Texas Instruments, Calculation and usage of LQI and RSSI, https://e2e.ti.com/support/wireless_connectivity/wireless_notes/calculation-and-usage-of-lqi-and-rssi, Accessed June 2015.
- [25]. Ambili Thottam Parameswaran, Mohammad Iftexhar Husain, Shambhu Upadhyaya, Is RSSI a Reliable Parameter in Sensor Localization Algorithms? – An Experimental Study, *Semantic Scholar*, 2009, http://www.cse.buffalo.edu/srds2009/F2DA/f2da09_RSSI_Parameswaran.pdf, Accessed November 2015.
- [26]. Kannan Srinivasan, Philip Levis, RSSI is Under Appreciated, *International Journal of Sensor Networks and Data Communication*, 2006, <https://sing.stanford.edu/site/publications/14>, Accessed April 2015.
- [27]. H. Karl, A. Hillig, Protocols and Architectures for Wireless Sensor Networks, Hoboken, *John Wiley & Sons Inc.*, NJ, 2005.



Published by International Frequency Sensor Association (IFSA) Publishing, S. L., 2017 (<http://www.sensorsportal.com>).



Online Experimentation: Emerging Technologies and IoT

Maria Teresa Restivo, Alberto Cardoso, António Mendes Lopes (Editors)

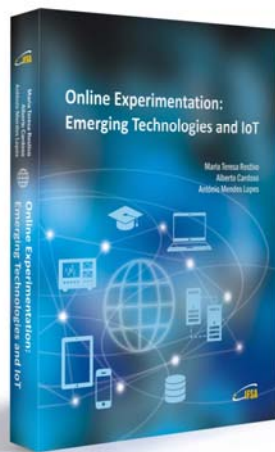
Online Experimentation: Emerging Technologies and IoT describes online experimentation, using fundamentally emergent technologies to build the resources and considering the context of IoT.

In this context, each online experimentation (OE) resource can be viewed as a "thing" in IoT, uniquely identifiable through its embedded computing system, and considered as an object to be sensed and controlled or remotely operated across the existing network infrastructure, allowing a more effective integration between the experiments and computer-based systems.

The various examples of OE can involve experiments of different type (remote, virtual or hybrid) but all are IoT devices connected to the Internet, sending information about the experiments (e.g. information sensed by connected sensors or cameras) over a network, to other devices or servers, or allowing remote actuation upon physical instruments or their virtual representations.

The contributions of this book show the effectiveness of the use of emergent technologies to develop and build a wide range of experiments and to make them available online, integrating the universe of the IoT, spreading its application in different academic and training contexts, offering an opportunity to break barriers and overcome differences in development all over the world.

Online Experimentation: Emerging Technologies and IoT is suitable for all who is involved in the development design and building of the domain of remote experiments.



Hardcover: ISBN 978-84-608-5977-2
e-Book: ISBN 978-84-608-6128-7

Order: http://www.sensorsportal.com/HTML/BOOKSTORE/Online_Experimentation.htm

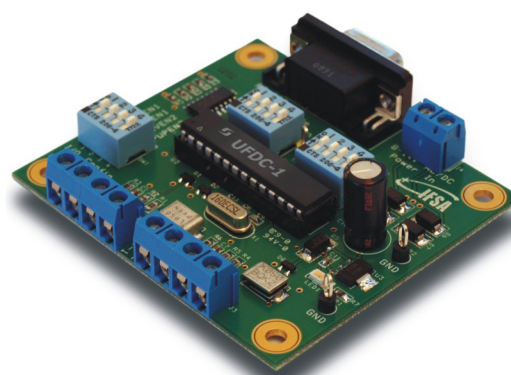
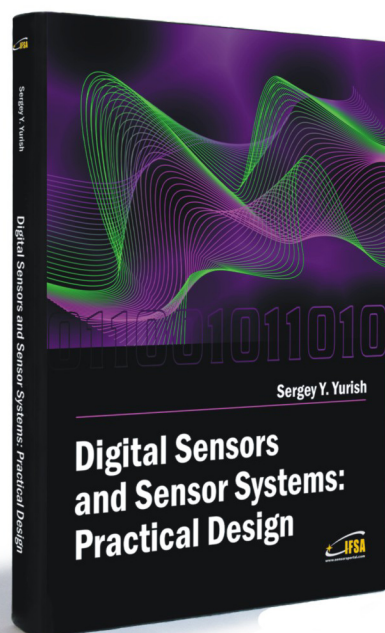
Theory:

Digital Sensors and Sensor Systems: Practical Design

and

Practice:

Development Board EVAL UFDC-1/UFDC-1M-16



Buy book and Evaluation board together. **Save 30.00 EUR**

Development Board EVAL UFDC-1 / UFDC-1M-16

Full-featured development kit for the Universal Frequency-to-Digital Converters UFDC-1 and UFDC-1M-16. 2 channel, 16 measuring modes, high metrological performance, RS232/USB interface, master and slave communication modes. On-board frequency reference (quartz crystal oscillator). Operation from 8 to 14 V AC/DC. Development board software is included.

All existing frequency, period, duty-cycle, time interval, pulse-width modulated, pulse number and phase-shift output sensors and transducers can be directly connected to this 2-channel DAQ system. The user can connect TTL-compatible sensors' outputs to the Development Board, measure any output frequency-time parameters, and test out the sensor systems functions.

Applications:

- Digital sensors and sensor systems
- Smart sensors systems
- Data Acquisition for frequency-time parameters of electric signals
- Frequency counters
- Tachometers and tachometric systems
- Virtual instruments
- Educational process in sensors and measurements
- Remote laboratories and distance education

Order online:

http://www.sensorsportal.com/HTML/BOOKSTORE/Digital_Sensors_and_Board.htm



International Frequency Sensor Association Publishing



www.sensorsportal.com

ISSN 1726- 5479



9 771726 547001